STUDIA

UNIVERSITATIS BABEŞ-BOLYAI

PHYSICA

1

1978

CLUJ-NAPOCA

ANUL XXIII 1978

STUDIA
UNIVERSITATIS BABEŞ-BOLYAI

PHYSICA
1

Redacţia: 3400 CLUJ-NAPOCA, str. M. Kogălniceanu, 1 ● Telefon 1 34 50

SUMAR — CONTENTS — SOMMAIRE

F. BOTA, R. V. BUCUR, I. COVACI, The hydrogen and deuterium transfer through the palladium-solution interface at constant current ● Transferul hidrogenului şi deuteriului prin interfaţa paladiu-soluţie, la curent constant 3

O. COZAR, V. ZNAMIROVSCHI, I. HAIDUC, Solvent dependent E P R spectra of Copper (II) — monoethanolamine complexes in water-ethanol mixtures ● Dependenţa de solvent a spectrelor R E S pentru complecşii Cu(II) — monoetanolamină în amestecurile apă-etanol 6

C. ŞERBAN, I. MACAVEI, D. AUSLANDER, ŞT. MAZUR, Une méthode ultrasonique d'agglomération des particules des suspensions ● Aglomerarea ultrasonică a particulelor din suspensii 10

C. ŞERBAN, D. AUSLÂNDER, Détermination de la solvatation de quelques électrolytes par une méthode ultrasonique ● Determinarea solvatării unor electroliţi printr-o metodă ultrasonică 16

S. COLDEA, Calculation of shear and bulk viscosity coefficients in simple liquid metals ● Calculul coeficienţilor de viscozitate laminară şi de volum în metale lichide simple 20

M. ILUŢIU C. STEŢIU, Determinarea ultrasonică a unor constante de material pentru toluen şi m-xilen ● Ultrasonic détermination of some characteristic coefficients of toluol and m-xylol 25

M. IUGA, Spectrul electronic al fluorclorbenzenilor în matrice de ciclohexan la temperatura de 77 K ● Electronic Spectra of fluoro-cloro-benzenes in cyclohexane at 77 K 28

I. NICULA, L. COCIU, I. MILEA, AL. NICULA, UV transmission of borate glasses ● Transmisia în UV a sticlelor pe bază de bor 32

M. CRISTEA, The Korteweg-de Vries equation for a two ion species plasma ● Ecuaţia Korteweg-de Vries pentru o plasmă cu două specii de ioni 35

AL. ANGHEL, M. CRIŞAN, Dynamical symmetry breaking due to radiative corrections in the scalar $\lambda\varphi^4 + g\varphi^3$ — theory ● Ruperea dinamică spontană a simetriei datorită corecţiilor radiative în modelul scalar $\lambda\varphi^4 + g\varphi^3$ 41

D. DĂDÎRLAT, M. CRIŞAN, Critical behaviour of the specific heat in inhomogeneous bidimensional superconductors ● Comportarea critică a căldurii specifice în supraconductori neomogeni bidimensionali 49

AL. NICULA, E. CULEA, L. STĂNESCU, E.S.R. and optical spectra of V^{4+} in borate glasses ● R.E.S. şi spectre optice ale ionului V^{4+} în sticle borate 55

I. ARDELEAN, V SEVIANU, D. C. conductivity of $xFe_2O_3 \cdot (1 - x)$ [$3B_2O_3 \cdot PbO$] glasses ● Conductibilitatea în curent continuu a sticlelor din sistemul $xFe_2O_3 \cdot (1 - x)$ [$3B_2O_3 \cdot PbO$] 59
GULÁCSI ZS , M. POPESCU, I RUS, Comportarea magnetică a compuşilor intermetalici $Ho_2Fe_{17-x}Al_x$ ● Magnetic behaviour of intermetallic compounds $HO_2Fe_{17-x}Al_x$ 63
T. FIAT, L. DĂRĂBAN, Studiul determinării litiului-6 prin metoda activării indirecte ● The lithium-6 determination study by indirect activation method 71

Note— Notes

F KOCH, Image of some radioactive granules with solid-state track detectors ● Imaginea unor granule radioactive înregistrate cu detectori de corp solid . . 77
O COZAR, GH. ILONCA, Studiu R.E.S. al $(NH_4)_3AlF_6 \cdot Ca$ ● E.S.R study of $(NH_4)_3AlF_6 : Ca$ 79

STUDIA UNIV. BABEŞ—BOLYAI, PHYSICA, 1, 1978

THE HYDROGEN AND DEUTERIUM TRANSFER THROUGH THE PALLADIUM-SOLUTION INTERFACE AT CONSTANT CURRENT*

F. BOTA, R. V. BUCUR, I. COVACI

The possibility of the interference between adsorption and absorbtion process in a Pd—H system has been suggested by C. Wagner [1]. Wicke and Meyer [2] experimentally made obvious the surface process contibution to the determination of overall process rate in a gas phase. The role of this layer was not generally taken into account in electrochemical measurements.

It seems that in measurements at constant current [3], the adsorption layer has a much more important role than in measurements at constant potential [4]. In the paper above mentioned [3], the problem was presented only qualitatively, therefore we want to present here some of the quantitative aspects.

In a recent work it has been shown [5] that the presence of adsorbed hydrogen is equivalent to a change of diffusion coefficient, an idea pointed out by Wicke and Meyer for the gas phase. This way, the great scattering of diffusion coefficient values could be explained.

In the present paper the overall oxidation reaction of hydrogen and deuterium in a thin palladium layer is studied, by taking into account the existence of adsorption layer. The experimental verification of the theory is presented, and also some constants are calculated, making obvious some isotope effects.

The mathematical treatment of the dependence potential — time, leads to a linear dependence ΔE vs $\log(\tau - t)$ ·

$$\Delta E = \frac{RT}{Z\mathcal{F}} \ln\left[\left(\frac{l + K}{K k_a^{\circ}}\right)^{1/\alpha} \cdot \frac{KC^{\circ}}{[H^+]}\right] - \frac{RT}{\alpha Z\mathcal{F}} \ln(\tau - t)$$

Fig. 1, 2, 3 and 4 show the experimental values obtained for hydrogen. The dependence is linear, as the theory predicts.

The slope is negative, so the process is irreversible They notice that for four different initial concentrations of hydrogen in palladium, the slope is constant, and it means that the slope is not depending on it.

Fig 5 shows the dependence of ΔE vs $\log(\tau - t)$ for deuterium, for the same initial concentration as the hydrogen (fig. 2). The slope for deuterium is bigger than for hydrogen. Therefore, the transfer coefficient has different values for the two isotopes:

$$\alpha_H = 0{,}74 \quad \text{and} \quad \alpha_D = 0{,}67.$$

In conclusion, the experimental data are in good agreement with the theory, and it is also possible to determine other data, concerning this system.

(Received January 29, 1977)

* This work was presented at the International Meeting on isotope effects in physical and chemical processes (1973).

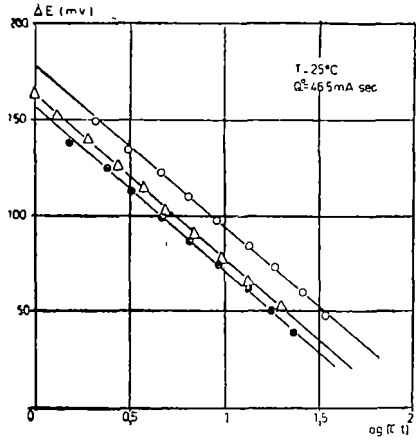

Fig. 1.

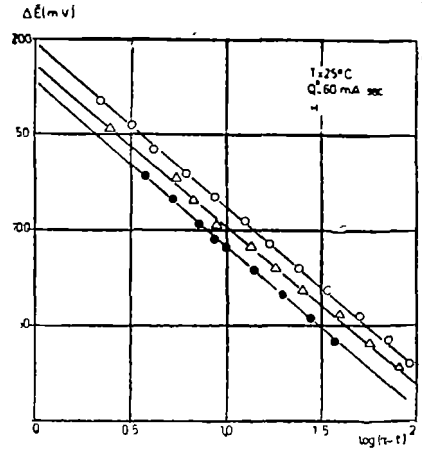

Fig. 2.

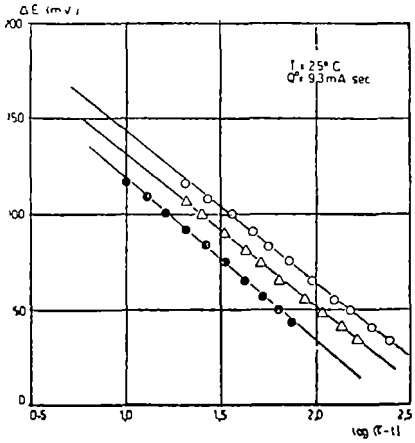

Fig. 3.

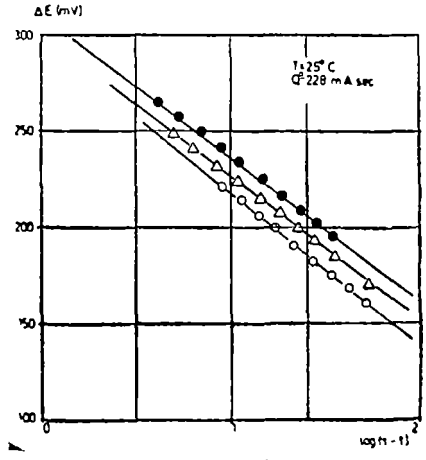

Fig. 4.

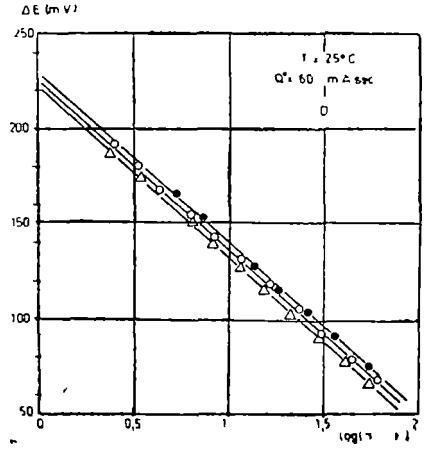

Fig. 5.

REFERENCES

1 C. Wagner, Z Phys Chem, **159**, 459 (1932)
2 E. Wicke, K Meyer, Z Physik Chem, **64**, 225 (1969)
3. R. V Bucur, Rev Phys, Bucharest, **7**, 91 (1962)
4. V. Breger, E Gileadi, Electrochim. Acta, **16**, 177 (1971)
5. F. Bota, R V. Bucur, I. Covaci, Studia Univ Babeş-Bolyai, Phys., f, 2, 91 (1972)
6. F. Bota, R. V. Bucur, I Covaci, *National Conference of Pure and Applied Physical Chemistry*, Bucharest, p 177 (1970), p 286 (1972).

TRANSFERUL HIDROGENULUI ŞI DEUTERIULUI PRIN INTERFAŢA PALADIU-SOLUŢIE, LA CURENT CONSTANT

(Rezumat)

Se verifică teoria stabilită într-o lucrare anterioară pentru sistemul [$Pd - H$], [$Pd - D$] în care se studiază dependenţa ΔE vs $\log(\tau - t)$ Se constată că dependenţa este liniară, cu panta negativă, independentă de concentraţia iniţială Se pune în evidenţă efectul izotopic prin determinarea coeficienţilor de transfer pentru hidrogen şi deuteriu.

STUDIA UNIV. BABEŞ—BOLYAI, PHYSICA, 1, 1978

SOLVENT DEPENDENT E.P.R SPECTRA OF COPPER (II)—MONOETHANOLAMINE COMPLEXES IN WATER — ETHANOL MIXTURES.

O. COZAR, V. ZNAMIROVSCHI, I. HAIDUC

1. **Introduction.** It was shown [1—2] that EPR spectra of Cu(II) complexes in water-ethanol mixtures of various concentrations are strongly dependent on the ethanol concentration This fact was explained in terms of a matrix effect and coordination of water molecules

As an extension of our investigation of Cu(II) complexes containing various ligands [2—3] we have investigated some $CuCl_2$-monoethanolamine complexes. Copper(II) chloride reacts with monoethanolamine to form several complexes [4] depending upon the reaction condition, particularly on the molar ratio of the reagents.

We have chosen for our study the blue compound $[Cu(H_2NCH_2CH_2OH)_4]Cl_2$ and the emerald-green compound $[Cu(H_2NCH_2CH_2OH)_3]Cl_2$ In the blue compound (A) the four molecules of monoethanolamine are coordinated only through nitrogen, whereas in the compound (B) the ligands are coordinated both through oxygen and nitrogen as:

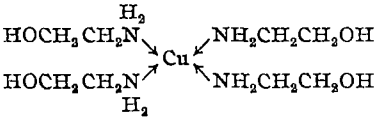

(A)

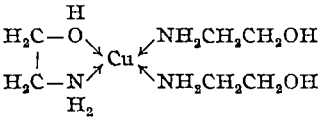

(B)

2. **Experimental.** The two compounds investigated were prepared according to the literature data [4] EPR spectra were recorded at room temperature (liquid solutions) and at 77 K (frozen solutions) with a JES—3B spectrometer in the X band, with a field modulation of 100 Kc/s Electronic spectra were recorded with a Specord UV—VIS (Carl Zeiss, Jena) spectrophotometer. The complexes were studied in ethanol-water solutions, the concentration being 4 mg/ml for compound (A) and 10 mg/ml for compound (B). The ethanol-water ratio in the solvent is shown in Tables 1 and 2.

3 **Results and discussion.** The EPR spectra obtained for liquid solutions, at room temperature, show four well resolved components of the hyperfine structure due to the nuclear spin $I = 3/2$ of the copper(II) ion. At 77 K, a modification of the symmetry of complexes is noticed, which depends upon the ethanol content of the solution. In water, the spectrum of compound (A) shows a slight anisotropy (Fig. 1), the signals in the parallel band ($g_{||}$) being practically unnoticeable, except the signal corresponding to $m_I = -3/2$, situated on the right hand of the perpendicular absorption ($g_{\perp}$). On addition of only 2% ethanol to water, complete resolution of the hyperfine structure in parallel absorbtion is obtained.

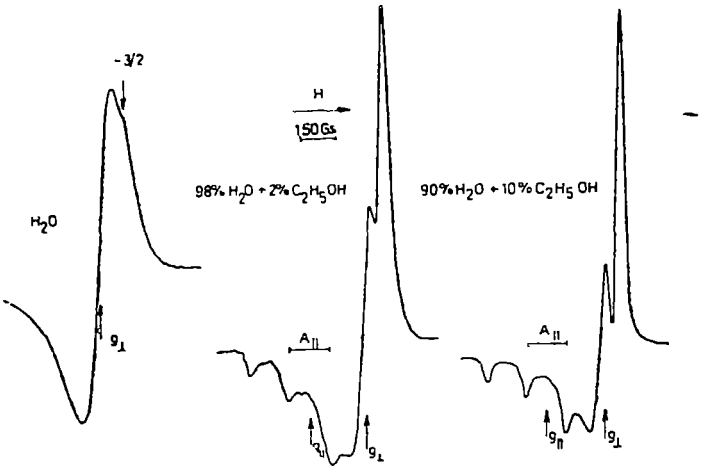

Fig. 1. Influence of the ethanol concentration upon the EPR spectra of the blue Cu(II)-monoethanolamine in water-ethanol mixture at 77K.

Compound (B) exhibits a resolved hyperfine structure in the parallel band even in water solution (Fig. 2) An improvement in the hyperfine structure resolution is noticed with increasing concentration of ethanol in solution, the spectra becoming almost identical with those of compound (A). The g and A parameters characteristic of the two compounds investigated, are listed in Tables 1 and 2.

The electronic spectra of the two complexes, in water and in a 35%EtOH+ + 65% H_2O mixture, show a single absorption band in the visible range at 15000 cm^{-1}. This band can be assigned to nonresolved $|E_g, B_{2g}\rangle - |B_{1g}\rangle$ transitions, as found in other copper(II) complexes [5, 6].

The antibonding molecular orbitals, corresponding to the ground and excited states of the *3d* electron, responsible for the paramagnetism of the compounds investigated are [7]:

$$|B_{1g}\rangle = \alpha d_{x^2-y^2} - \alpha' \Phi_\sigma(x^2 - y^2)$$

$$|B_{2g}\rangle = \beta d_{xy} - (1 - \beta^2)^{1/2} \Phi_\pi(xy)$$

$$|E_g\rangle = \begin{cases} \delta d_{xz} - (1 - \delta^2)^{1/2} \Phi_\pi(xz) \\ \delta d_{yz} - (1 - \delta^2)^{1/2} \Phi_\pi(yz) \end{cases}$$

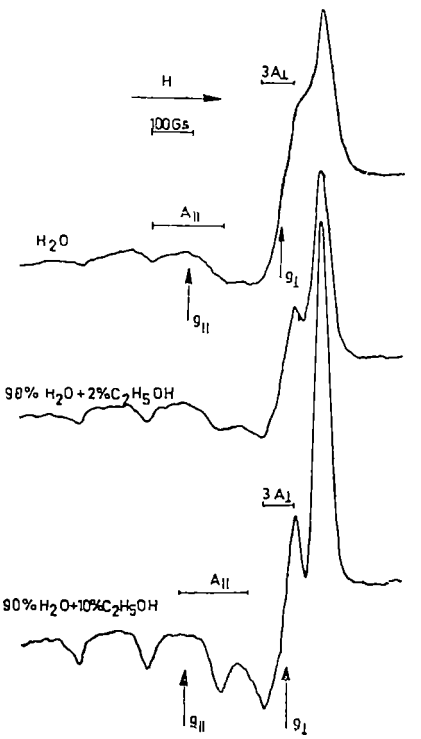

Fig. 2. Influence of the ethanol concentration upon the EPR spectra of the emerald-green Cu(II)-monoethanolamine in water-ethanol mixture at 77 K.

The parameters involved in these equations can be determined by using the following approximate relations [7]:

$$\alpha^2 = |A_{||}|/P + (g_{||} - 2.002) + 3/7(g_{\perp} - 2.002) + 0\ 04$$

$$g_{||} = 2.002 - 8\lambda\alpha^2\beta^2/\Delta_{xy}$$

$$g_{\perp} = 2.002 - 2\lambda\alpha^2\delta^2/\Delta_{xz}$$

where $P = 0.036$ cm^{-1}, $\lambda = -828$ cm^{-1}, Δ_{xy} and Δ_{xz} represent the electronic transitions $|B_{1g}\rangle \rightarrow |B_{2g}\rangle$ and $|B_{1g}\rangle \rightarrow |E_g\rangle$ respectively. For both transitions the experimental value of 15000 cm^{-1} is taken. The α^2, β^2 and δ^2 parameters are listed in tables 1 and 2.

Table 1

The EPR parameters and MO coefficients for complex (A)

Solvent	$g_{||}$	$g_{\perp}$	$\|A_{||}\|$ (10^{-4} cm^{-1})	$\|A_{\perp}\|$ (10^{-4} cm^{-1})	α^2	β^2	δ^2
H_2O	—	2.084	—	—	—	—	—
98% H_2O+ 2% EtOH	2.216	2 056	183.6	30.2	0,79	0 61	0 62
80% H_2O + 20% EtOH	2,223	2 050	188.0	25.2	0 80	0 62	0,54
EtOH	2.226	2.049	188 3	21 6	0,81	0,63	0.53

Table 2

The EPR parameters and MO coefficients for complex (B)

Solvent	$g_{||}$	$g_{\perp}$	$\|A_{||}\|$ (10^{-4} cm^{-1})	$\|A_{\perp}\|$ (10^{-4} cm^{-1})	α^2	β^2	δ^2
H_2O	2 195	2 050	175 3	25.0	0.74	0 59	0 59
98% H_2O + 2% EtOH	2 201	2 046	175 8	24 3	0 75	0 60	0 53
80% H_2O + 20% EtOH	2.212	2.044	181.3	23.0	0,77	0 62	0.49
60% H_2O + 40% EtOH	2.216	2.044	186.3	23.0	0 79	0.61	0.48

The experimental results suggest a decrease in symmetry of complexes with increasing ethanol concentration, which is due to the action of the vitreous matrix formed by freezing the ethanol-water mixture [1, 2, 8].

In water the symmetry of the complexes is higher, due to the coordination of two water molecules on the Oz axis, with formation of six-coordinate octahedral complexes with a less pronounced component of axial symmetry [2, 5]. The compound (A) has a higher symmetry than the compound (B), similar to that observed for [Cu(trien)SCN]SCN [2]. This is explained by the presence of the same environment around copper (four nitrogen atoms). In the case of complex (B), the chromophore $CuON_3$ is less symmetrical and contains two different donors in the coordination sphere.

Since the solutions in pure water as solvent, by freezing form a polycrystalline matrix [9] with weak bonds in the structural network, the deforming action upon the complexes incorporated in this matrix is weak. Addition of ethanol results in the change of the matrix [1,2] determining a vitreous state of the frozen mixture; this results in a stronger deforming action of the matrix upon the complex.

It seems that in this case a slight extension of the distance between the Cu(II) ion and the ligands occurs This is supported by the observed increase (Tables 1 and 2) in the ionic character of the $\sigma(\alpha^2)$ and $\pi(\beta^2)$ bonds in the xOy plane. The π bonds, both in — plane ($\beta^2 \leqslant 0.63$) and out-of- plane ($\delta^2 \leqslant 0.62$) have a strong covalent character, and these are responsible for the stability of the complexes investigated.

In water and in a 98% H_2O + 2% EtOH mixture, the out-of-plane π bonds are more ionic, due to the coordination of water molecules on the Oz axis; this involves d_{xz} and d_{yz} orbitals, thus perturbing the π bond formed with the donor atoms of the ligands. By increasing the ethanol content in solution, water is fixed in the structural matrix, it becomes less available for coordination, and thus the covalency of the π bond increases.

(Received February 5, 1977)

REFERENCES

1. V. Znamirovschi, O. Cozar, Acta Phys Pol, A42, 33 (1972)
2. O. Cozar, V. Znamirovschi, I. Haiduc, J. Mol. Struct.,**31**, 153 (1976)
3. O. Cozar, V. Znamirovschi, I Haiduc, Studia Univ. Babeş-Bolyai, Phys, 29 (1975)
4 V. V Udovenko, M. V Artemenko, Zhur. Neorg. Khim, **4**, 352 (1959)
5. B. J Hathaway, C. E Lewis, J Chem Soc, A 2295 (1969)
6 S.C Rustagi, G. N Rao, J Inorg Nucl Chem, **36**, 1161 (1974)
7 D. Kivelson, R. Neiman, J Chem. Phys, **35**, 149 (1961)
8. V. Znamirovschi, O Cozar, Al. Nicula, Molec. Phys, **27**, 273 **(1974).**
9. L Burlamacchi, J, Chem Soc, Faraday II, 54 (1975)

DEPENDENŢA DE SOLVENT A SPECTRELOR R.E.S. PENTRU COMPLECŞII Cu(II)-MONOETANOLAMINĂ ÎN AMESTECURILE APĂ-ETANOL

(Rezumat)

Se face un studiu RES a doi complecşi de Cu(II)-monoetanolamină în amestecuri apă-etanol, observîndu-se o dependenţă a spectrelor RES de concentraţia de etanol în apă Acest fapt se explică prin acţiunea deformatoare a matricu vitroase apă-etanol la 77 K asupra complecşilor studiaţi.

STUDIA UNIV BABEŞ—BOLYAI, PHYSICA, 1, 1978

UNE MÉTHODE ULTRASONIQUE D'AGGLOMÉRATION DES PARTICULES DES SUSPENSIONS

CORINA ŞERBAN, IOANA MACAVEI, D. AUSLÄNDER, ŞT. MAZUR

Introduction. L'agglomération et la précipitation des particules solides suspendues dans un milieu gazeux constitue un problème de grande actualité, ayant en vue le combat contre la pollution du milieu ambiant et la récupération de certains matériaux [1, 2].

La méthode de précipitation à l'aide des ultrasons présente une série d'avantages par rapport aux méthodes électrostatiques : elle permet une purification avancée des gaz, elle est utilisable en cas des gaz inflammables et corrosifs, elle peut être adaptée pour retenir un large domaine de dimensions des particules, etc

Considérations théoriques. Le processus spontané d'agglomération est accéléré sous l'action des ultrasons par la croissance de la fréquence de heurt des particules La diminution relative du nombre des particules est donnée par le degré de coagulation

$$E = 100e^{-k} \tag{1}$$

où k dépend de la concentration des particules, de l'intensité et la fréquence de l'ultrason, du temps d'ultrasonorisation et du type de suspension.

La valeur optimale de la concentration est de 5—10 g/cm³. La concentration au-dessus de 15 g/cm³ a un effet négatif, dû à l'absorption de l'ultrason. Pour chaque fréquence il y a un rayon critique des particules $r_{cr} = \sqrt{\frac{9\eta}{4\pi\rho_p f}}$ pour laquelle l'absorption est maximale et qui doit, par conséquence, être évitée.

L'intensité acoustique minimale nécessaire à la coagulation est de 130 dB.

En ce qui concerne la fréquence, on préfère l'utilisation des ultrasons au-dessus de 16 kHz, afin d'éviter le caractère facheux des sons intenses et l'emploi d'un spectre large de fréquences pour pouvoir actionner sur un domaine étendu de dimensions [3]

Le prolongement du temps d'ultrasonorisation contribue aussi à l'augmentation du rendement ; la valeur minimale pour une fréquence et intensité optimales est de 2—3 sec.

Sous l'action de l'ultrason, les particules sont soumises à un mouvement supplémentaire qui augmente la probabilité du heurt, donc l'agglomération [4].

Les particules participent au mouvement oscillatoire du gaz dans une mesure qui dépend du rayon de la particule r, de la fréquence du champ

acoustique f, de la viscosité du gaz η et de la densité de la particule ρ_p. Le rapport des amplitudes du mouvement des particules et du gaz

$$\frac{X_p}{(X_g)} = \frac{1}{\sqrt{1 + \left(\frac{4\pi\rho_p r^2 f}{9\eta}\right)^2}} \tag{2}$$

exprime la mesure de la participation des particules aux oscillations du milieu sous l'action des ultrasons. Dans le cas des particules polydispersées, la condition optimale de participation aux oscillations qui déterminent l'agglomération est

$$0{,}2 < \frac{X_p}{(X_g)} < 0{,}8 \tag{3}$$

Des forces hydrodynamiques prennent naissance entre les particules, en fonction de leur position relative à la direction de propagation de l'onde. La force d'attraction maximale est donnée par

$$F = \frac{3\pi\rho_g r^6}{l^4}(V_g - V_p) \tag{4}$$

où l est la distance entre deux particules L'effet des forces hydrodynamiques se manifeste surtout dans le cas des suspensions concentrées.

Sous l'action de la pression de radiation, les particules sont soumises à des forces proportionnelles à leurs surfaces

$$F = \frac{10\pi^2 r^3 E}{3\lambda} \sin 2kx \tag{5}$$

qui se déplacent vers les ventres des ondes stationnaires (5). Dans la formule (5) E représente la densité d'énergie acoustique, λ — la longueur de l'onde, k — le nombre d'onde et x — la distance de la particule du noeud de l'onde stationnaire, à un moment du temps donné.

La probabilité des heurts résultés des mécanismes décrits est favorisée par le mouvement brownien des particules, qui a un rôle important surtout dans le cas de petites particules

Installation expérimentale. On a travaillé au moyen d'une sirène ultrasonique aérodynamique de type axial, avec des paramètres calculés par les auteurs, la projection et la construction étant réalisées par l'Institut Polytechnique de Cluj-Napoca La fréquence du son émis est donné par

$$\mathrm{f} = \frac{mn}{60} \tag{6}$$

où m est le nombre identique d'orifices du rotor et du stator et n — le tournage du rotor Les dimensions des orifices ont été calculées en fonction de la consommation d'air comprimé (75 N m³/h), limité afin d'éviter la dilution excessive du milieu. Pour pouvoir travailler à des fréquences variables, on a prévu le réglage du tournage jusqu'à 15 000 rotations/min.,

ce qui donne pour $m = 78$ f = 19 500 Hz. L'interstice rotor-stator de 0,1 mm a assuré un rendement acoustique élevé.

La sirène a été prévue d'un entonnoir exponentiel, qui permet de réaliser une impédance constante et réelle sur une surface donnée. Aussi a-t-il été nécessaire de réaliser un système de refroidissement rigoureux, étant donné que l'on travaillait dans un milieu gazeux, à une température élevée

Résultats et discussions. La sirène a été montée sur la chambre de dépoussièrage d'une station pilote par laquelle la suspension de particules dans les gaz passait à la température de 850 °C.

On a déterminé les paramètres de fonctionnement de la sirène au froid (la fréquence et l'intensité de l'ultrason en fonction du tournage et de la chute de pression), dans l'absence de la suspension, avec un decibelmètre prévu de filtres de fréquence et un oscillographe avec deux spots.

A la suite on a effectué des mesurages dans les conditions de fonctionnement du pilote On a déterminé le contenu de poudre en 50 l de gaz par filtrage, pour différents débits d'alimentation de la sirène et à différentes fréquences La poudre filtrée a été analysée granulométriquement et prenant pour base les données obtenues, on a tracé les courbes de distribution sur les dimensions des particules filtrées. Les courbes intégrales $n = f(\Phi)$ donnent le purcentage de particules à dimensions plus réduites qu'une certaine valeur La fig. 1. représente cette courbe pour l'épreuve témoin recueillie dans l'absence du champ ultrasonique.

Les fig 2 et 3 s'en réfèrent aux épreuves de poudre récoltées après le passage de la suspension à travers le champ acoustique de la sirène, à la fréquence de 12 100 Hz, respectivement 14 100 Hz.

Pour les mêmes épreuves ont été calculées les courbes différentielles de distribution $\frac{dn}{d\Phi} = f(\Phi)$, représentées dans les figures 4—6.

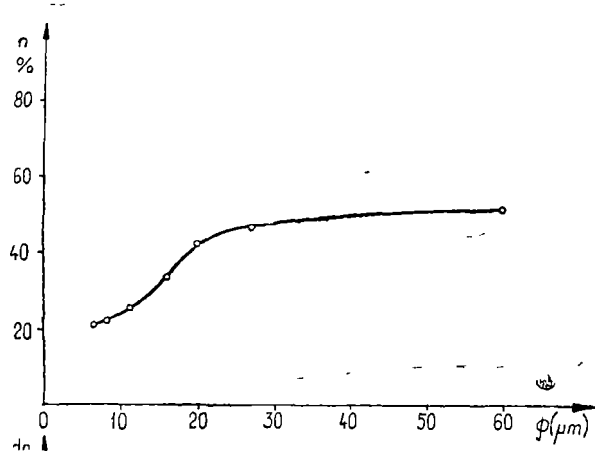

Fig. 1. Courbe intégrale de distribution des particules dans l'épreuve témoin.

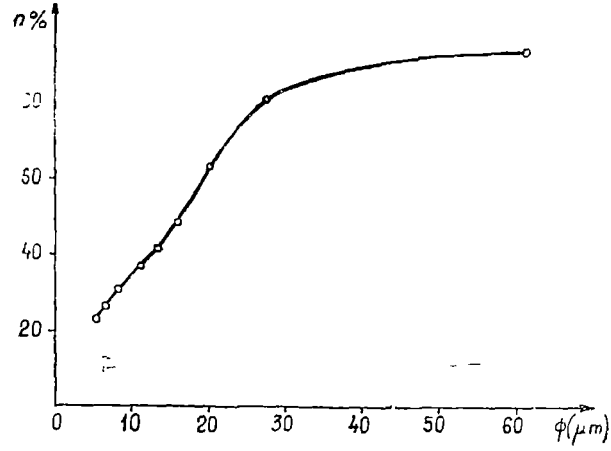

Fig. 2. Courbe intégrale de distribution des particules dans l'épreuve ultrasonorisée à $\nu = 12\,100$ Hz

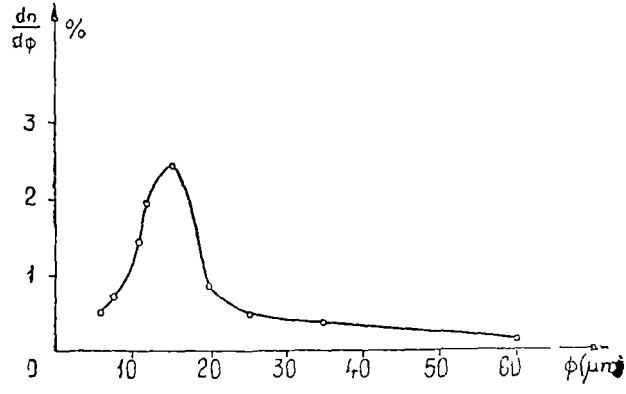

Fig. 4. Courbe différentielle de distribution dans l'épreuve témoin.

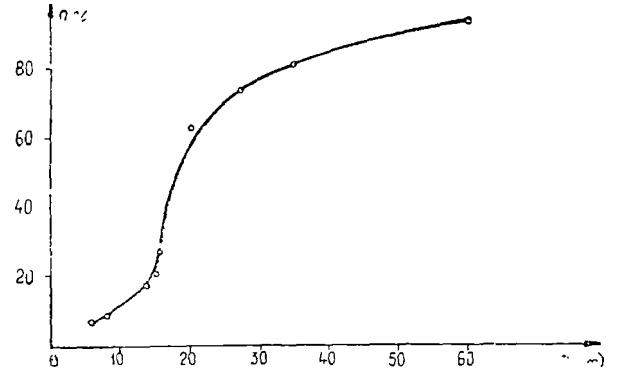

Fig 3 Courbe intégrale de distribution des particules dans l'épreuve ultrasonorisée à $\nu = 14\,100$ Hz

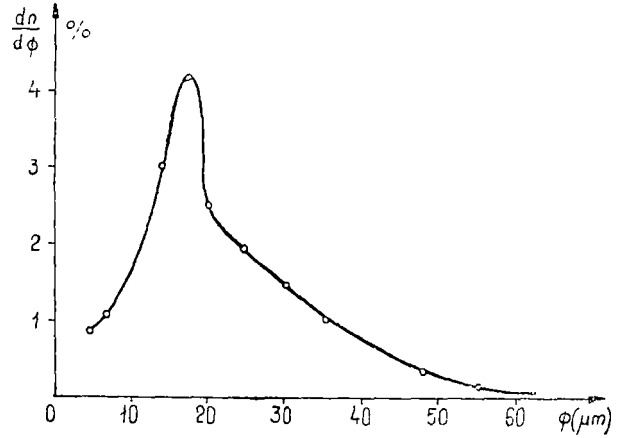

Fig 5 Courbe différentielle de distribution dans l'épreuve ultrasonorisée à $\nu = 12\,100$ Hz

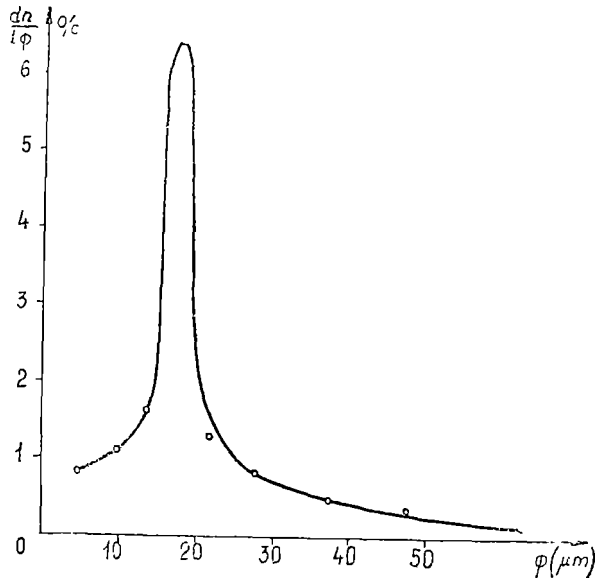

Fig. 6 Courbe différentielle de distribution dans l'épreuve ultrasonorisé à $\nu = 14\,100$ Hz.

Le pourcentage des particules aux diamètres compris entre les deux valeurs données Φ_1 et Φ_2, représente l'aire incluse entre la courbe et l'axe Φ, limitée par les valeurs respectives du diamètre : $\Delta n = \int_{\Phi_1}^{\Phi_2} \frac{dn}{d\Phi} d\Phi$

L'allure des courbes de distribution représentées sur les fig. 2, 3, 5, 6, en comparaison avec celles correspondant aux épreuves témoin des fig. 1 et 4, relèvent l'effet de l'ultrason. L'on constate que sous l'action du champ il y a une tendance nette de déplacement des dimensions vers une distribution à caractère de monodispersion qui s'accentue concomitamment avec l'augmentation de la fréquence. Par conséquence, si dans l'épreuve témoin au domaine des particules à dimensions entre 15—20 μm revient un pourcentage de 11%, sous l'action de l'ultrason, on obtient pour le même intervalle une valeur de 20% à 12 100 Hz et de 37% à 14 100 Hz.

Nous considérons que cet effet reflète le processus d'agglomération par l'augmentation de la fréquence de heurt des particules dans le champ ultrasonique. Le processus se manifeste de préférence sur les particules de moindre dimension.

(Manuscrit reçu le 31 janvier, 1977)

BIBLIOGRAFIE

1 V I, Nikitenko, V. I Turubarov, Akust. J., **8,** nr 3. 370 (1962).
2 D B. Dianov, L G Merkulov, V I Nikitenko, Akust J **8,** 1, 60 (1962)
3 W Schaaffs, Kolloid. Zts u Zts. fur Polymeren **235,** 1239 (1969).
4 E P. Mednikov, *Akusticeskaia Koagulatzia,* Uzd-vo AN SSSR, Moskva, 1963
5 E P Mednikov, A. .M. Sirotin., Akust. J. **13,** 3, 460 (1967).

AGLOMERAREA ULTRASONICĂ A PARTICULELOR DIN SUSPENSII

(Rezumat)

În lucrare sînt prezentate rezultatele cu privire la acţiunea ultrasunetului asupra procesului de aglomerare a particulelor din suspensii. Determinările experimentale efectuate cu o sirenă aerodinamică pun în evidenţă o creştere a randamentului aglomerării, sub acţiunea ultrasunetului Efectul se manifestă în alura curbelor de distribuţie granulometrică, integrale şi diferenţiale.

STUDIA UNIV. BABEŞ—BOLYAI, PHYSICA, 1, 1978

DÉTERMINATION DE LA SOLVATATION DE QUELQUES ÉLECTROLYTES PAR UNE METHODE ULTRASONIQUE

CORINA ŞERBAN, D. AUSLÄNDER

Considérations théoriques. Le phénomène de solvatation, causé par l'attraction coulombienne entre les ions et les molécules polaires du solvant, détermine des changements dans la structure de celui-ci. Analysant le processus, on distingue une solvatation primaire, dans laquelle les molécules du solvant étroitement liées â l'ion sont en mouvement avec celui-ci, ayant une énergie potentielle plus grande que l'énergie thermocinétique, les molécules du solvant perdant leurs degrés de liberté; et une solvatation secondaire, où les molécules de solvant, plus éloignées des ions solvatés primairement, subissent une attraction plus faible, le nombre de solvatation dépend de la température.

Des études existentes [1,2] il résulte que les ions sont solvatés par voies différentes; il semble que la solvatation des cations est réalisée au moyen des interactions électrostatiques, les molécules du solvant étant distorsionnées et les anions sont solvatés par des liaisons d'hydrogène. De même a-t-on constaté que les grands ions, tels que K^+, Rb^+, Cs^+, NO_3^-, J^- ont le rôle de désorganiser la structure, tandis que les ions fortement solvatés, comme Li^+, Be^{++}, Mg^{++}, Ca^{++} ont l'effet d'ordonner la structure du solvant.

Le nombre de solvatation est déterminée par une série de facteurs: la force d'attraction entre ions et dipôles; propriétés spécifiques du solvant; le nombre de coordination de l'ion dans le complexe solvaté; permitivité etc.

Méthode de travail. Les méthodes de déterminer les nombres de solvatation sont multiples et les résultas discordants [3]

Dans le présent travail nous avons appliqué une méthode ultrasonique, fondée sur des mesurages de vitesse de l'ultrason dans différentes solutions d'électrolytes, en calculant ensuite le nombre de solvatation Z pour une molécule, d'après la formule de Mihailov:

$$Z = \frac{\rho - \rho_0 \dfrac{\beta}{\beta_0} - c}{c} \cdot \frac{M}{M_0} \tag{1}$$

où ρ, ρ_0 — densité de la solution respectivement du solvant
c — concentration en g/cm^3
M, M_0 — masse molaire du soluté, respectivement du solvant
β, β_0 — compressibilité adiabatique de la solution et du solvant

$$\beta_{ad} = \frac{1}{a^2 \rho}$$

a — vitesse de l'ultrason.

Les molécules de la couche de solvatation étant fortement comprimées à cause de l'électrostriction, dans la déduction de la formule on a considéré le volume de la sphère de solvatation comme incompressible. De même dans l'approximation faite, le solvant est représenté comme un milieu diélectrique continu.

Résultats expérimentaux. Dans les recherches effectuées on a poursuivi l'action des sels monovalents et bivalents (LiCl, LiBr, LiJ, NaBr, NaJ, $MgCl_2$, $SrBr_2$) sur le méthanol, éthanol, butanol et glycol, et on a calculé le nombre de solvatation et leur variation en fonction de la température et de la concentration.

Analysant la dépendance de la solvatation de la température dans le domaine de 10°C—50°C, l'on constate l'indépendance de la température dans le cas des sels énumérés.

Les résultats obtenus ont été représentés graphiquement pour $t = 30$°C ; l'on constate dans tous les cas la reduction du nombre de solvatation avéc la croissance de la concentration, l'allure des courbes dépendant de la nature des ions et du solvant.

Sur les figures 1—4 on a mis en évidence la dépendance de la solvatation de la polarisabilité différente des ions et l'on a représenté comparativement le nombre de solvatation des différents ions dans le même solvant. Sur la figure 1 le solvant étudié est le méthanol, un alcool fortement associé, dans lequel se trouvent solutées quelques chlorures : LiCl, $SrCl_2$, $MgCl_2$. On remarque la diminution plus rapide avec la concentration du nombre de solvatation pour les sels bivalents vis-à-vis des sels monovalents Les molécules de $MgCl_2$ ayant un diamètre plus petit que $SrCl_2$ sont plus fortement solvatées. Le nombre de solvatation des molécules de LiCl a, généralement, des valeurs plus réduites. Des résultats similaires ont été obtenus aussi par A. Lindheumer et B. Brun pour des solutions de LiCl en méthanol, appliquant une méthode de résonance magnétique nucléaire.

De la figure 2, qui donne la variation des nombres de solvatation du $MgCl_2$, $SrBr_2$, $SrBr_2$ et LiCl en éthanol l'on constate un comportement analogue à celui décrit sur la figure 1.

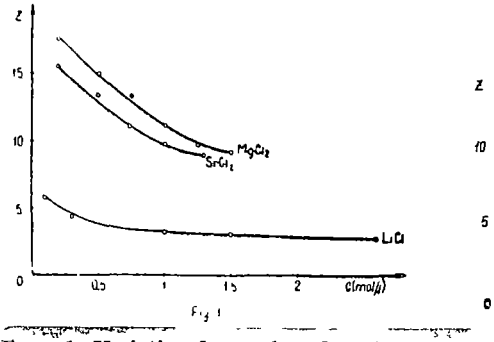

Fig 1 Variation du nombre de solvatation avec la concentration dans les solutions de $MgCl_2$, $SrCl_2$, LiCl en méthanol.

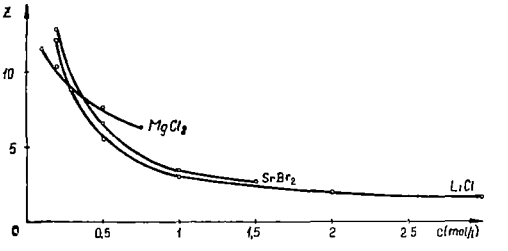

Fig 2. Variation du nombre de solvatation avec la concentration dans les solutions de $MgCl_2$, $SrBr_2$, LiCl en éthanol.

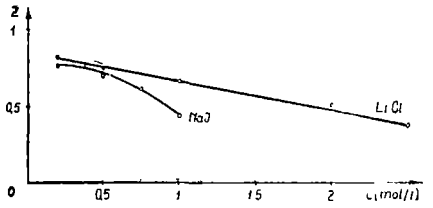

Fig 3. Variation du nombre de solvatation avec la concentration dans les solutions de LiCl et NaI en butanol

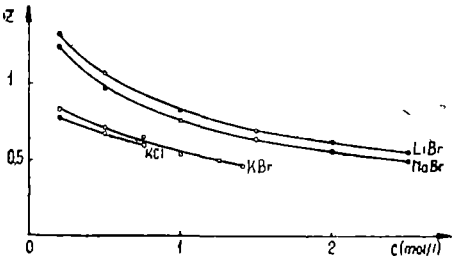

Fig 4 Variation du nombre de solvatation avec la concentration dans les solutions de quelques sels monovalents en glycol

Sur la figure 3 le solvant représenté est le butanol, dans lequel ont été soluté deux sels monovalents LiCl et NaCl L'on observe de même la diminution de la solvatation avec l'augmentation du diamètre moléculaire

Des effets semblables on été obtenus aussi dans les solutions de glycol des sels monovalents (fig. 4) A de petites concentrations l'effet en est réduit et avec l'augmentation de la concentration l'interaction ion-ion devient plus puissante Pour pouvoir apprécier l'influence du solvant sur le nombre de solvatation, on a représenté graphiquement la varaiation pour LiCl dans trois alcools différents · méthanol, éthanol et butanol (fig 5). On remarque que le nombre de solvatation le plus grand apparaît, dans les solutions d'éthanol, étant fortement affecté par la variation de la concentration, tandis que dans les solutions de butanol le Z est petit et presqu'indépendant de la concentration

Interprétations des résultats. La valeur du nombre de solvatation est en grande mesure déterminée par l'interaction ion-dipôle d'une part et-

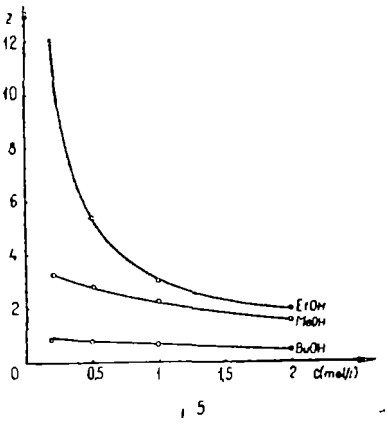

Fig 5 Variation du nombre de solvatation avec la concentration dans les solutions de LiCl en méthanol, éthanol et butanol.

Tableau 1

Énergie d'interaction ion — dipôle

Ion	Rayon Van der Waals Å	Solvant		
		Methanol	Ethanol	Butanol
Li^+	0,76	18,20	18,40	17,85
Na^+	1,01	7,25	7,34	7,23
K^+	1,34	3,70	3,74	3,63
Cl^-	1,81	1,91	2,02	1,90
Br^-	1,95	1,74	1,75	1,69
I^-	2,16	1,40	1,41	1,37
Mg^{++}	0,78	2,15	2,17	2,11
Sr^{++}	1,27	0,81	0,82	0,79
Energie d'interaction dipôle-dipôle *eV*		1,44	0,98	0,39

par l'interaction dipôle-dipôle d'autre part, ces interactions étant gouvernées par la permitivité de la solution.

L'interaction ion-ion mène à la diminution de la polarisabilité d'autant plus que le cation est plus petit et l'anion plus grand, la conséquence étant la diminution de l'interaction ion-dipôle. En cas de faibles concentrations l'effet est petit et avec l'augmentation de la concentration l'interaction ion-ion devient plus forte.

Pour interpréter les résultats obtenus on a calculé les valeurs de l'énergie d'interaction ion-dipôle, au moyen de la relation

$$E_{iD} = -\frac{e\mu}{r^2 KT}$$

où μ — moment dipolaire des molécules du solvant
r — distance entre le centre de la molécule de solvant et l'ion
et ces valeurs ont été comparées avec les énergies d'interaction dipôle-dipôle

$$E_{DD} = -\frac{2\mu^2}{r^3 KT}$$

Les résultats sont portés dans le tableau 1. Des calculs il s'ensuit que l'énergie d'interaction ion-dipôle des petits ions, tels que Li^+, Na^+ est 4—10 fois plus grande que l'interaction dipôle—dipôle, ce qui peut déterminer un ordre éloigné dans le liquide En poursuivant l'énergie d'interaction pour le même ion dans trois solvants, on remarque que la valeur la plus élevée correspond à l'éthanol. Analysant les autres valeurs du tableau, on voit que la disposition des courbes des graphiques est en grande partie confirmée.

Les ions négatifs sont toujours plus polarisables que les ions positifs de mêmes dimensions à cause de la charge positive de ces derniers qui établissent leur nuage électronique La polarisation étant dépendante de la densité de charge des ions, elle va augmenter avec le rayon des ions monovalents

Conclusions. Dans les solutions d'électrolytes il y a une tendance d'organisation, respectivement de désorganisation de la structure du solvant, sous l'influence des ions, ce qui détermine le changement des paramètres structurels. La contribution différencielle des ions détermine le renforcement du caractère d'organisation de la structure avec l'augmentation de la densité de charge de l'ion, respectivement d'atténuation de la tendance de désorganiser la structure du solvant, dû à l'accroissement de la sphère de solvatation.

(Manuscrit reçu le 7 février 1977)

BIBLIOGRAPHIE

1 G P Roscchina, A S Kaurostva, I D. Koşeleva, Zh. Struckt, Khim, **9**(1), 3—7 (1968)
2 PushtiPrakoshRostogi, Zeitsch Phys. Chem, Band 75, 3/4, 202—207 (1971)
3 Camelia Beldie, Stud Cercet. Chim, **15** (5), 349—380 (1967).
4. A Lindheimer, B Brun, J. Chim. Phsy, **69**(10) 1462—1470, (1972)

STUDIA UNIV BABEŞ—BOLYAI, PHYSICA, 1, 1978

CALCULATION OF SHEAR AND BULK VISCOSITY COEFFICIENTS IN SIMPLE LIQUID METALS

SPERANŢA COLDEA

1. **Introduction.** The problem of calculation of the ionic transport coefficients for liquid metals was recently developed [1] by generalisation of a previous method for self-diffusion, which was based on the Enskog theory of transport processes in dense fluids [2]. The basic assumption of the theory is that the viscosity coefficients of a simple liquid metal is equal to that of a hard-sphere fluid, under the same condition of temperature and density. The most important elements of this theory are: the way of estimating the hard sphere diameter of a metal atom as a function of temperature; the use of a correction factor to correct the errors in the Enskog theory [1], [3]. This correction factor is obtained from molecular dynamics calculations for dense gases [4].

The details of the theory will not be presented here and we will refer to the papers [1], [3].

2. **The shear viscosity.** The Enskog theory for dense hard-sphere gases and liquids gives [1]—[2]:

$$\mu_E = 0{,}3125\sigma^{-2}b\rho(mkT/\pi)^{1/2}\cdot\left(\frac{1}{b\rho\chi}+\frac{4}{5}+0{,}7614\ b\rho\chi\right) \tag{1}$$

where

$$b\rho = 2\pi n_T\sigma_T^3/3 = 4\eta_T \tag{2}$$

with n_T — the density, σ_T — the hard-sphere diameter and η_T — the packing fraction of the liquid metal; $\chi = g(\sigma)$ is the pair correlation function at contact for the hard-sphere fluid, or the Enskog correction factor An approximate formula for χ can be obtained from the Carnahan-Starling equation of state [5]·

$$\chi = g(\sigma_T) = \frac{Z-1}{4\eta_T} = \frac{2-\eta_T}{2(1-\eta_T)^3} \tag{3}$$

All these quantities are dependent on temperature T in the case of the melted metals We use the following equation for the effective diameter σ_T of a metal atom as a function of temperature [1]:

$$\sigma_T = \left(\frac{2{,}832\,M}{\rho_m N_A}\right)^{1/3}\cdot\frac{1-B\left(\frac{T}{T_m}\right)^{1/2}}{1-B} \tag{4}$$

where $B = 0{,}112$ is a constant for any metal and ρ_m is the mass density at the melting point [1].

Using the relations (1)—(4), we can obtain, after a simple algebra, the following expression for the shear viscosity of a hard sphere liquid metal [1]:

$$\mu'_E \cong (\pi RT/M)^{1/2}\rho_T \cdot \sigma_T\left(\frac{0{,}1056}{\eta_T}\cdot\frac{(1-\eta_T)^3}{(2-\eta_T)}+\right.$$

$$\left.+\,0{,}166+0{,}3218\eta_T\frac{(2-\eta_T)}{(1-\eta_T)^3}\right) \tag{5}$$

The physical quantities M (the atomic weight of the metal), R, T — the temperature, ρ_T, σ_T, and η_T in the previous relation (5) are known or can be calculated for the considered liquid metal and this expression can be used to estimate the numerical values of the corresponding shear viscosities, at the melting point or at higher temperatures. The result (5) for the shear viscosity coefficient of a liquid metal must be corrected by a correction factor, which is defined as:

$$C_{AW}(\eta) = \mu/\mu'_E \tag{6}$$

and then the real shear viscosity μ is:

$$\mu = C_{AW}(\eta)\cdot\mu'_E \tag{7}$$

We use the values of this factor $C_{AW}(\eta)$, which are deduced from molecular dynamics calculations for the dense gases (argon and kripton) [4]. The table 1 gives the correction factors $C_{AW}(\eta)$ as a function of density v/v_0 (v_0 being the corresponding packing volum of the metal atoms) and for various packing fractions. For the intermediate densities and various packing fractions the values of the correction factor can be directly obtained from the figure 1 of the paper [1]. (from a smooth interpolation using the molecular dynamics data of ref. [4]).

By using the expressions (5) and (7) for the shear viscosity of a liquid metal we can estimate the numerical values of this transport coefficient in some particular cases. We will compare the calculated results with the published experimental data of the shear viscosity for Na, K, Bi, and Hg. All these values are presented in table 2, together with the used data T, n_T, ρ_T, C_{AW} and with the corresponding references for the experimental values.

The theory was tested by comparison with the experimental results for the considered liquid metals, for which we could find published viscosity data [6]—[10], and we observed a good agreement between these data.

3. **The bulk viscosity.** The following expression for the bulk viscosity of the dense fluid was predicted from the Enskog theory [2]:

$$\mathcal{K}_E \cong 1{,}002\,\mu_0(b\rho)^2\chi \tag{8}$$

where

$$\mu_0 = 1{,}016\cdot\frac{5}{16}(mkT/\pi)^{1/2}\sigma^{-2} \tag{9}$$

Table 1

The values of the correction factor C_{AW} for various densities and various packing fractions η

v/v_0	$C_{AW}(\eta) = \mu/\mu'_E$	η	$C_{AW}(\eta)$	η	$C_{AW}(\eta)$
100	1,01±0,02	0,500	2,25	0,440	1,30
20	1,00±0,02	0,495	2,04	0,430	1,24
20	1,00±0,04	0,490	1,91	0,420	1,20
10	0,99±0,04	0,485	1,820	0,410	1,17
5	0,99±0,05	0,480	1,74	0,400	1,14
3	1,02±0,01	0,475	1,65	0,350	1,075
2	1,11±0,06	0,470	1,58	0,375	1,095
1,8	1,10±0,03	0,465	1,52	0,325	1,07
1,6	1,44±0,07	0,460	1,46	0,300	1,06
1,5	2,16±0,09	0,455	1,41	0,200	1,03

Table 2

The values of the calculated shear viscosity and the experimental data of these transport coefficients in liquid metals

Liquid Metal	$T_m(°K)$	$T(°K)$	$n_T \quad 10^{23}$	ρ_T (g/cm³)	C_{AW}	$\mu_E(P)$	$\mu_{corec}(P)$	$\mu_{exp}(P)$
Na	370,5	427	0,241	0,914	1,5	0,00343	0,00515	[6] 0,0045 [7] 0,00532
K	335	381	0,1257	0,817	1,38	0,0026	0,0036	[8] 0,0035 [6] 0,0042
Bi	551	681	0,2876	9,98	1,37	0,0137	0,0187	[9] 0 0164 [10] 0,0166
Hg	234,3	477	0,393	13,103	1,1125	0,001	0,0105	[11] 0,0105 [8], [10] 0,015

We assume that all the former considerations which were made for the self-diffusion and shear viscosity are valid in the case of bulk viscosity too.

By introducing the relations (2)—(3) and (9) in the relation (8) we obtain for the bulk viscosity of a simple liquid metal the following expression:

$$\mathcal{K}_E \cong 0{,}393\left(\frac{MkT}{N_A}\right)^{1/2} n_T^2 \cdot \sigma_T^4 \cdot \frac{(2-\eta_T)}{(1-\eta_T)^3} \tag{10}$$

The Enskog theory result for viscosity is of the right order of magnitude for all fluid densities, but it is not accurate enough for quantitative purposes Then we introduce a correction factor $V(\eta)$, analogous to that of the shear viscosity and which can be deduced from molecular dynamics data [4]:

$$K = V(\eta) \cdot \mathfrak{K}_E \tag{11}$$

where K is the real (or corrected) bulk viscosity coefficient of a liquid metal. The values of this correction factor, which depends on the packing fraction η, will be given in the table 3

Table 3

The values of the correction factor $V(\eta)$ of the bulk-viscosity at various densities v/v_0

$v/v_0 = \rho_0/\rho$	$V(\eta)$	$v/v_0 = \rho_0/\rho$	$V(\eta)$
100	0,9	2	0,9; 1,2
20	1,1, 1,0	1,8	1,1
5	0,9	1,6	1,1
3	0,98	1,5	0,6

By using the relations (10)—(11) we performed numerical calculations for several liquid metals as Na, K, Bi, and Pb The results are given in table 4.

Table 4

The values of the calculated and experimental results for bulk-viscosity for some liquid metals

Metal	$T_m(°K)$	$T(°K)$	$M\left(\frac{g}{\text{mol}}\right)$	η_T	$\rho_T\left(\frac{g}{\text{cm}^3}\right)$	$K_E(P)$	$V(\eta)$	$K(P)$	$K_{\text{exp}}(P)$
Na	370,5	377	23	0,47	0,926	0,00413	1,58	0,00653	<0,0179 [12]
K	335	423	39	0,466	0,824	0,00356	1,6	0,006	<0,007 [4], [12]
Pb	600	673	207,2	0,461	10,6	0,018	1,055	0,019	0,019 [6] [13]
Bi	551	578	209	0,47	10,02	0,017	1,58	0,027	<0,064 [13]

By a comparison of the calculated numerical values of the bulk viscosity with the corresponding experimental data for the considered liquid metals [6], [12]—[13], we observe a good agreement, but not so good as in the case of the shear viscosity. We must take into account the lack

of precision for determination of the correction factor $V(\eta)$ from the molecular dynamics calculations. Up to the present molecular dynamics calculations for bulk viscosity were not effectuated, apart from those for shear viscosity [4]. The experimental data for the bulk viscosity are in many cases inaccurate (for example the cases of Na, K and Bi). So much the more, the present theory for viscosity coefficients of liquid metals is remarkably accurate in predicting the absolute (numerical) values of these quantities. In a next paper another simple theoretical method for the calculation of the ionic transport coefficients (self-diffusion and viscosity) in the simple liquid metals will be developed and a comparison between the corresponding results of the two different methods will be made We must also re-examine the problem of the thermal conductivity in liquid metals, which is not a ionic transport coefficient [1], but it is an electronic one.

(Received January 31, 1977)

REFERENCES

1. S Coldea, Studia Univ. Babeş-Bolyai, ser. Phys 2, 28, (1974)
2. S Chapman and T. G. Cowling, *The Mathematical Theory of Non-uniform Gases*, Cambridge Univ Press, London-New York (1939).
3. P. Protopapas, Andersen H. C. and N. A. D., Parlee., J. Chem. Phys, **59**, 15 (1973)
4. B. J. Alder, D. M. Gas and T E Wainwright, J. Chem. Phys, **53**, 3813 (1970).
5 N. F. Carnahan and N. F. Starling, J Chem Phys., **51**, 635 (1969)
6. H Landolt and R Bornstein, Physikalische-Chemische Tabellen (1954).
7. Y. S Chiong, Proc. Roy. Soc. (London), A 157, 264 (1936).
8 A. Lodding, Zeitschr Naturfor, 16 a, 1252 (1961)
9. A. Budde and J Fischer., Z. Phys. Chem., **218**, 100 (1961)
10. I. Corsunskii, Izv vîş ucebn. zaved fiz., **3**, 145 (1975).
11. A. V. Grosse, J Chem Phys, **63**, 3419 (1964).
12 J Jarzynski, J. Chem. Phys, **41**, 1290 (1964).
13 J Jarzynski, Proc. Phys. Soc, **81**, 1745 (1963)

CALCULUL COEFICIENŢILOR DE VISCOZITATE LAMINARĂ ŞI DE VOLUM ÎN METALE LICHIDE SIMPLE

(Rezumat)

În prezenta lucrare este reluată problema calculării coeficienţilor de transport ionic în metale lichide, abordată de autor într-o lucrare anterioară, care se bazează pe utilizarea teoriei lui Enskog pentru procese de transport în fluide dense Folosindu-se aceleaşi consideraţii ca şi în cazul autodifuziei şi generalizînd metoda pentru coeficienţii de viscozitate se obţin, în urma calculelor efectuate, expresii ale acestor coeficienţi ce pot fi utilizate la evaluarea lor numerică Se compară datele calculate cu ajutorul acestor expresii teoretice cu rezultatele experimentale cunoscute în cîteva cazuri de metale lichide unicomponente Na, K, Bi, Pb şi Hg. Se găseşte o bună concordanţă a aceastor rezultate atît în cazul vîscozităţii laminare, cît şi în cazul celei de volum.

STUDIA UNIV. BABEŞ—BOLYAI, PHYSICA, 1, 1978

DETERMINAREA ULTRASONICĂ A UNOR CONSTANTE DE MATERIAL PENTRU TOLUEN ŞI m-XILEN

M. ILUŢIU şi C. STEŢIU

1. **Introducere.** Se ştie că factorul ce condiţionează mărimea constantelor fizice de material în lichide este structura lor moleculară Constantele de material fiind măsurabile experimental, în cursul timpului au existat o serie de încercări de a le lega prin relaţii empirice, semiempirice sau riguros demonstrate Dintre aceste relaţii ne vom referi în continuare la cele ce leagă viteza de propagare a undelor în lichide de densitate, coeficienţii de compresibilitate şi de coeficientul de dilatare volumică.

Între viteza de propagare a undelor v şi densitatea ρ a lichidelor s-a stabilit o relaţie de forma [1]

$$v = -A + B\rho \tag{1}$$

unde A şi B sînt constante ce depind de natura lichidului şi de presiune, fiind independente de temperatură.

Pe de altă parte, viteza de propagare a undelor este legată de coeficientul de compresibilitate adiabatică β_s a mediului lichid prin relaţia

$$\beta_s = \frac{1}{\rho v^2}, \tag{2}$$

relaţie ce reprezintă de fapt singura metodă directă de determinare a coeficientului de compresibilitate adiabatică Dacă se cunoaşte valoarea coeficientului de compresibilitate izotermă β_T (din măsurători piezometrice), se poate calcula exponentul adiabatic $\gamma = \beta_T/\beta_s$

Din termodinamică se cunoaşte relaţia

$$C_p = C_v + \frac{\alpha^2 T}{\rho \beta_T} \tag{3}$$

ce leagă căldurile specifice de coeficientul de dilatare termică α, temperatura T, densitatea ρ şi coeficientul de compresibilitate izotermă β_T.

2. **Prelucrarea datelor experimentale.** În scopul verificării ecuaţiilor (1) şi (3), ca lichide de studiu s-au folosit toluenul şi m-xilenul. Aparţinînd aceleiaşi serii, este de aşteptat ca proprietăţile lor fizice să se supună aceloraşi legi de interdependenţă

Dependenţa de densitate a vitezei de propagare a undelor în toluen şi m-xilen este reprezentată în fig. 1.

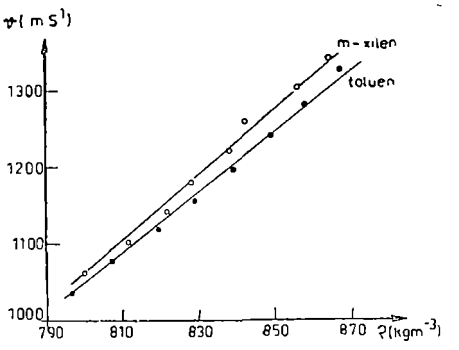

Fig 1 Dependenţa de densitate a vitezei de propagare a undelor ultrasonore în toluen şi m-xilen.

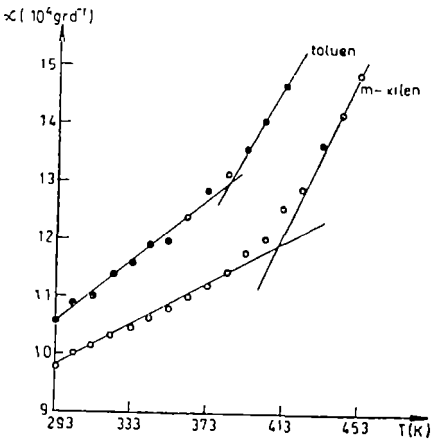

Fig 2 Dependența de temperatură a coeficientului de dilatare volumică a toluenului și m-xilenului

Tabel 1

	toluen		m-xilen	
T K	$v_{măs}$ ms^{-1}	v_{calc} ms^{-1}	$v_{măs}$ ms^{-1}	v_{calc} ms^{-1}
293	1328	1288	1344	1264
303	1284	1256	1303	1239
313	1241	1223	1262	1192
323	1199	1188	1222	1179
333	1157	1153	1182	1150
343	1117	1118	1143	1123
353	1076	1075	1104	1093
363	1036	1036	1066	1052
373		1004		1036
383		977		996
393		937		970
403		889		948
413		857		915
423		810		856
433		775		816
443		725		787

În ambele cazuri se obține o variație lineară a vitezei cu densitatea, variație conformă ecuației (1) Constantele ce intervin în ecuație au valorile A = 1 807, B = 3,57 pentru toluen, respectiv A = 1 612, B = 3,33 pentru m-xilen Folosind aceste constante, precum și date asupra densității luate din tabele [2], s-a calculat valoarea vitezei pentru un interval larg de temperaturi (tabel 1) Abaterea valorii calculate a vitezei din (1) față de valoarea măsurată a vitezei se încadrează în limitele erorilor de măsură. Ecuația (3) s-a verificat prin compararea datelor existente în literatură pentru coeficientul de dilatare al lichidelor cu cele calculate conform acestei ecuații Valorile căldurilor specifice au fost luate din [3]. Figura 2 ilustrează variația cu temperatura a coeficientului de dilatare Schimbarea de pantă ce apare indică temperatura corespunzătoare schimbării de fază În tabelele de constante fizice [2] coeficientul de dilatare volumică pentru toluen $\alpha = 1109 \cdot 10^{-6}$ grd^{-1} în intervalul 0—90 °C. În aceleași condiții, din (3) se obține $\alpha_{calc} = 1148 \cdot 10^{-6}$ grd^{-1} Pentru m-xilen după [2] $\alpha = 990 \cdot 10^{-6}$ grd^{-1} între 0—30 °C, iar din (3) rezultă în același interval de temperatură $\alpha_{calc} = 992 \cdot 10^{-6}$ grd^{-1} Concordanța datelor confirmă valabilitatea relației (3)

3 **Interpretarea rezultatelor obținute.** Existența unei dependențe lineare între viteza de propagarea a undelor prin lichide și densitatea acestora poate fi explicată ținînd cont de variația lor cu temperatura Atît viteza cît și densitatea scad linear la creșterea temperaturii. De aceea, în cazul lichidelor ale căror molecule prezintă o oarecare simetrie sferică și cînd nu intervine o asociație moleculară, verificarea unei relații simple de tipul ecuației (1) este posibilă, constantele A și B nu vor depinde de temperatură, ci numai de structura moleculară a lichidelor și de presiune

Relaţia (3) se cunoaşte din termodinamică, fiind obţinută prin folosirea metodei potenţialelor termodinamice [4] Verificarea ei experimentală confirmă utilitatea metodelor termodinamice în studiul fazei lichide

(Intrat în redacţie la 8 februarie 1977)

BIBLIOGRAFIE

1 A R Aziz, D H Bowman, C C Lim, Canad Journ. Phys, **50** 646 (1972)
2 Landolt-Bornstein, *Mechanisch — Thermische Zustandsgrossen*, II B, 1T, 1971
3 V V Zotov, I A Nerucev, Ultrazvuk i fizikohimiceskie svoistva vescestva, **54**, 3, 42 (1969)
4 I G Mihailov, V A Soloviev, I P Sîrnicov, *Osnovî molecuhiarnoi akustiki*, Izd Nauka, Moskva, 1964

ULTRASONIC DETERMINATION OF SOME CHARACTERISTIC COEFFICIENTS OF TOLUOL AND m-XYLOL

(Summary)

In this paper it was investigated the dependence between sound velocity and density. On the other side, it was proved a relationship between sound velocity and the volume coefficient of thermal expansion

STUDIA UNIV BABEŞ—BOLYAI, PHYSICA, 1, 1978

SPECTRUL ELECTRONIC AL FLUORCLORBENZENILOR ÎN MATRICE DE CICLOHEXAN LA TEMPERATURA DE 77 K

M. IUGA

Introducerea substanţelor, în special aromatice, în matrici cristaline de parafine normale liniare sau ciclice la temperaturi joase duce la apariţia unor spectre care constau din bande fine numite cvasilinii, efect cunoscut sub denumirea de efect Spolski [1]

Ca să se păstreze proprietăţile moleculei izolate, se alege o matrice a cărei interacţiune cu moleculele solvite să fie minimă.

În această lucrare se prezintă rezultatele pe care le-am obţinut din studiul spectrului de absorbţie al fluorclorbenzenilor în soluţie de ciclohexan la temperatura de 77 K, iar datele obţinute le-am comparat cu cele din spectrul de absorbţie al vaporilor.

Spectrele de absorbţie U. V. ale vaporilor acestor molecule au fost studiate de Ţintea [2], Krishnamachari [3] şi Varsány [4] iar spectrul I. R şi Raman de Nielsen [5].

Instalaţia experimentală a fost cea descrisă de Iliescu [6].

Fluorclorbenzenii şi ciclohexanul au fost purificate prin metodele clasice.

Îngheţarea probei s-a făcut lent, deoarece ciclohexanul prezintă două forme cristalografice: una monoclinică, care este stabilă sub 186 K şi alta cubică, care este stabilă deasupra temperaturii de 186 K. Prin răcirea probei la 77 K lent, predomină forma monoclinică

Spectrele sînt formate din bande fine pentru domeniul de concentraţii $5M^{-4} - 2M^{-2}$, ceea ce înseamnă că sistemul fluorclorbenzenul formează o soluţie substituţională cu locuri echivalente

Deplasarea bandei 0,0 pentru cei trei derivaţi este redată în tabelul 1.

Tabel 1

Molecula	$\nu_{0,0}$ cm^{-1} în vapori	$\nu_{0,0}$ cm^{-1} soluţie de ciclohexan	Deplasarea $\Delta\nu_{0,0}$ cm^{-1}
orto	37035	36668	367
meta	37027	36703	324
para	36297	35788	509

Rezultate. În figurile 1, 2 şi 3 sînt prezentate spectrele de absorbţie al fluorclorbenzenilor în matrice de ciclohexan la temperatura de 77 K.

Orto-fluorclorbenzenul. S-au măsurat 23 de bande de absorbţie cuprinse între 36668 şi 38741 cm^{-1}. Analiza electrono-vibraţională a spectrului s-a făcut cu frecvenţele prezentate în tabelul 2, făcîndu-se o comparaţie cu spectrul Raman şi I.R. în stare lichidă şi cu spectrul de absorbţie al vaporilor din U.V.

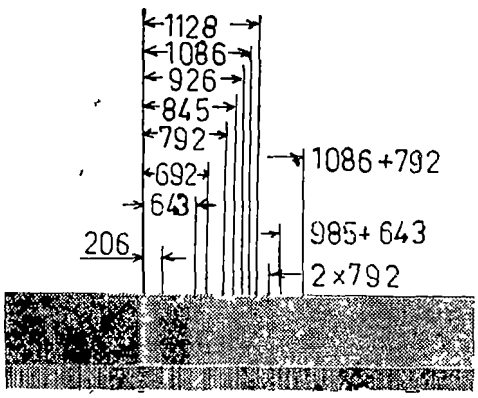

Fig 1 Spectrul de absorbţie al orto-fluorclorbenzenului în ciclohexan la 77 K, C = M^{-2}

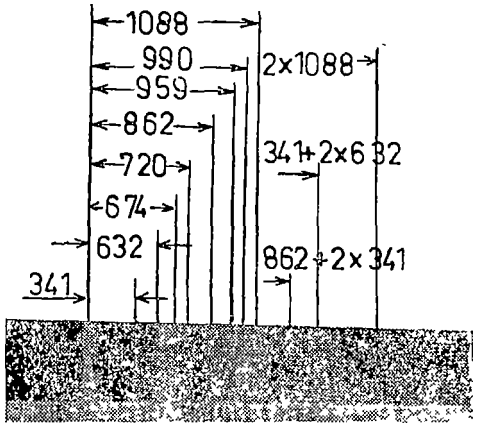

Fig 2 Spectrul de absorbţie al para-fluorclorbenzenului în ciclohexan la 77 K, C = 3,5 M^3

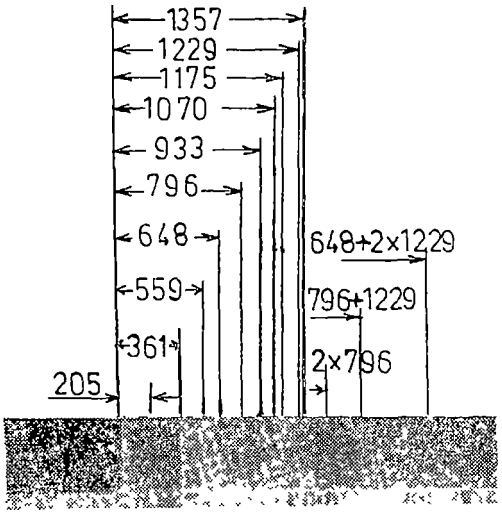

Fig 3 Spectrul de absorbţie al para-fluorclorbenzenului în ciclohexan la 77 K, C = M^{-3}

Se observă o bună concordanţă între valorile frecvenţelor din stare de vapori şi cele din soluţia de ciclohexan la 77 K

Meta-fluorclorbenzenul. S-au măsurat 21 benzi de absorbţie cuprinse între 36703 şi 39568 cm^{-1}.

Analiza electrono vibraţională a spectrului este prezentată în tabelul 3.

Para-fluorclorbenzen. S-au măsurat 27 de benzi de absorbţie cuprinse între 25788 şi 39642 cm^{-1}. Analiza electrono vibraţională e prezentată în tabelul 4.

Tabel 2

Nr. crt	Starea lichidă ω'' cm^{-1}		ω' cm^{-1} autorul	ω' cm^{-1} absorbția în vapori	Modul de vibrație
	I R	Raman			
1	—	167	154 s	147	10 b
2	—	231	206 s	—	10 a
3	679	679	643 i	639	6 a
4	698	698	692 i	692	4
5	804	804	792 i	794	11
6	844	850	845 i	—	17 a
7	934	925	936 i	940	17 b
8	992	991	985 i	—	5
9	1068	1071	1086 i	1076	9 b?
10	1126	1127	1128 i	1117	9 b
11	1239	1237	1234 fs	—	13
12	1288	1287	1286 fs	1182	3

Tabel 3

Nr crt	Starea lichidă ω'' cm^{-1}		ω' cm^{-1} autorul	ω' cm^{-1} absorbție în vapori	Modul de vibrație
	I R	Raman			
1	—	—	341 s	—	15
2	—	—	632 i	636	1
3	673	683	674 s	—	4
4	729	—	720 s	735	6 b
5	857	862	862 s	—	17 b
6	963	—	959 s	960	5
7	990	992	990 s	—	12
8	1080	1084	1088 s	1087	18 a
9	1220	1221	1218 s	1218	13
10	—	—	1379 s	1366	19 a

Tabel 4

Nr. crt	Starea lichidă ω'' cm^{-1}		ω' cm^{-1} autorul	ω' cm^{-1} absorbție în vapori	Modul de vibrație
	I R	Raman			
1	—	—	136 s	—	11
2	—	—	205 s	—	15
3	—	371	361 i	344	7 a
4	556	556	559 i	553	16 b
5	634	634	648 s	—	6 b
6	779	781	796 i	793	10 a
7	936	928	933 s	—	5
8	1069	1068	1070 i	1057	1
9	1182	—	1175 s	—	9 a
10	1233	1232	1229 s	1228	13
11	1361	—	1357 s	1372	14

Din aceste măsurători rezultă că s-a găsit o matrice potrivită pentru studiul spectrului de absorbţie al fluorclorbenzenilor care permite obţinerea de benzi fine iar analiza spectrelor s-a făcut cu un număr mai mare de frecvenţe decît cele găsite în spectrele de vapori

(Intrat în redacţie la 15 februarie 1977)

BIBLIOGRAFIE

1 E V Spolski, Uspeh Fiz Nauk, **68**, 51 (1959), **71**, 215 (1960), **80**, 255 (1963)
2 H Ţintea, Buletinul societăţii de ştiinţe din Cluj, X, 246—257 (1948)
3 S L N G Krishnamachari, Indian Journal of Physics, 447 (1957)
4 G Varsány, Acta chimica Acad, scientiarum Hungariae, vol 13, 347 (1958)
5 N A Navasimham, U. Z El Sabban şi J Rud Nielsen, The journal of Chemical Physics, **24** (6) 421, 431 şi 1232 (1956)
6 T Iliescu şi H Ţintea, Studia Univ Babeş-Bolyai, Phys , 24 (1976)
7 G Varsány, S Szoke, *Vibrational Spectra of benzene derivates*, Akademiai kiado Budapest, 1969

ELECTRONIC SPECTRA OF FLUORO — CLORO — BENZENES IN CYCLOHEXANE AT 77 K

(Summary)

We report the results which we have obtained studying the absorbtion spectra of fluorcolorobenzenes in cyclohexane solutions at 77 K

STUDIA UNIV. BABEŞ—BOLYAI, PHYSICA, 1, 1978

UV TRANSMISSION OF BORATE GLASSES

I. NICULA, LAVINIA COCIU, I. MILEA, AL. NICULA

1. **Introduction.** The importance of the UV radiations of 280—320 mμ, called biological rays, the high price and the technological difficulties in obtaining quartz glass (which has a great transmission up to 186 mμ), led to the seeking of new glasses, with moderate price and as great as possible transmission in this wavelength range. The results of these seekings are reviewed in [1], [2] and we mention here some of them:

— the Stevels' theory [3] extended to the case of pure oxide glasses (borates, silicates and phosphates) states that the absorption edge in all such glasses corresponds to the transition of electrons belonging to an oxygen ion to an excited state,

— a movement of the UV cut — off to longer wavelengths corresponds to a transition from the nonbridging oxygen which binds an excitable electron less tight than a bridging oxygen;

— the greater transmission of pure vitreous silicon and boric oxide in the UV has been attributed [3] to the absence of nonbridging oxygens which have lower excitable electronic levels in the UV than those of the bridging oxygens,

— McSwain, Borrelli and Su [4] studied the effect of the composition of the sodium borate glasses, on the UV absorption edge; at about 15 mole % of Na_2O, they found an important movement of the UV cut—off to longer wavelengths which was attributed to a) the appearance of nonbridging oxygens and b) to the change of boron coordination from 3 to 4 (the boron anomaly);

— Bishop reported [5] a high UV transmitance, especially at 253.3 mμ, of the ternary borate glass having molar composition of $1.0K_2O.1.0Al_2O_3.4\,5B_2O_3$ which does not favor the presence of nonbridging oxygens.

2. **Experimental and results.** The investigated glasses, formed by melt supercooling, contained B_2O_3, Li_2O, Al_2O_3 and ZnO in different concentrations. The glasses were melted in corundum crucibles in an electric furnace at the digestion temperature of 1150°C. The composition of the sample which presented a good UV transmission, as it is seen from figure 1, is $75\%B_2O_3$ $15\%Li_2O$ $10\%Al_2O_3$ (mole %). The optical absorbtion spectrum was obtained on an UV VIS Zeiss Jena spectrophotometer.

3. **Discussion.** We consider that besides the existence of nonbridging oxygens and the change of boron coordination the absorption edge is influenced by the distortion caused by the modifier ion, on the boron triangle. It is known [2, p 135), in glasses, boron usually shows a sp^2 hybridization and oxygen shows a sp^2 hybridization which tend towards sp. By introduction of a network modifier, oxygen may change the hybridization.

Using a model similar to that proposed by Griscom, Taylor, Ware and Bray [3] in order to explain the boron hole center, the molecular orbital scheme is that presented in fig. 2. It is observed: from fig. 2a,

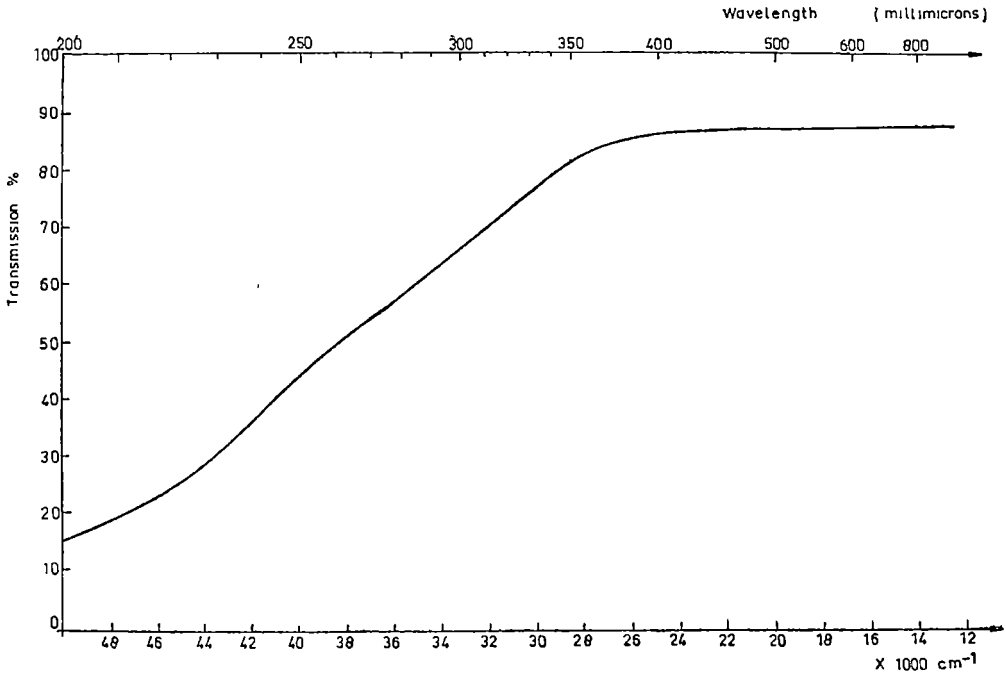

Fig 1. Transmission of 75 B_2O_3 15 Li_2O 10 Al_2O_3 glass (mole %) Thickness of sample: 1,6 mm.

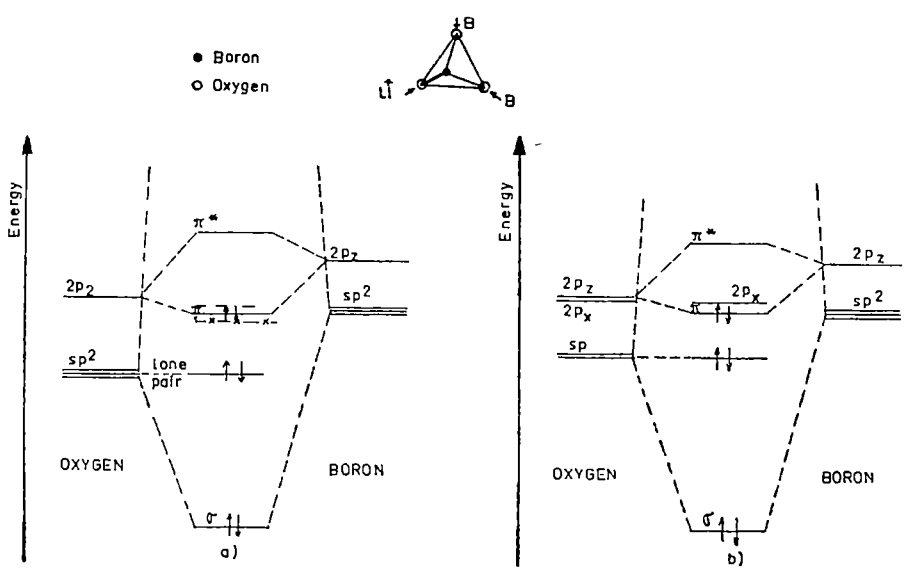

Fig. 2 Molecular orbital scheme: a) oxygen is sp^2 hybridized; b) oxygen is sp hybridized.

that in the case of the sp^2 hybridization, two electrons of oxygen form a π donor-acceptor bond with p_z orbital of boron. In the absence of the modifier the three bonds from the boron triangle are equivalent. The presence of the network modifier gives rise to a distortion of a boron triangle: a bond is shortened and the other two are lengthened. This means a better localization of a π bond. The energy level of the shorter bond is lowered, whereas the energy levels of the lengthened bonds are rised. In this way a movement of absorption edge to longer wavelengths appears.

In the case of sp hybridization of oxygen, besides the above aspect, there is an unparticipated p orbital of oxygen with a higher energy which favours the movement of the absorption edge to longer wavelengths.

The qualitative analysis carried out above imposes the necessity that the network modifier destroys as little as possible the boron triangle. We think aluminium satisfies this necessity.

(Received August 26, 1977)

REFERENCES

1. I Wong, C. A. Angell, Appl. Spectroscopy Revs, **4** (1), 97—154 (1970).
2. P. Baltă and E. Baltă, *Introduction to the physical chemistry of the vitreous state*, Ed. Acad. Bucureşti and Abacus Press — Tunbridge Wells, 1976.
3. J. M. Stevels, *Proc. IIth Intern Congr Pure Appl. Chem*, **5**, 519 (1953).
4 B. D. McSwain, N F. Borrelli and G. I. Su, Phys Chem Glasses, **4**, 1 (1963).
5. D. L. Griscom, P. C. Taylor, D. A Ware and P. I. Bray, J Chem. Phys., **48**, 11, 5158 (1968).

TRANSMISIA ÎN UV A STICLELOR PE BAZĂ DE BOR

(Rezumat)

S-a obţinut o sticlă cu transmisie satisfăcătoare în domeniul UV. Este dată o explicaţie calitativă a deplasării marginii de absorbţie în UV spre lungimi de undă mai mari, luîndu-se în considerare influenţa modificatorului de reţea asupra triunghiului de bor.

STUDIA UNIV. BABEŞ—BOLYAI, PHYSICA, 1, 1978

THE KORTEWEG—DE VRIES EQUATION FOR A TWO ION SPECIES PLASMA

MARIA CRISTEA

In the past decade there has been considerable interest in nonlinear effects in plasma. W a s h i m i and T a n i u t i [6] have shown that a weakly nonlinear description of one-dimensional ion sound wave disturbances travelling near the ion sound speed, is given by a Korteweg—de Vries (KdV) equation. The KdV equation has the form

$$\frac{\partial U}{\partial \tau} + aU\frac{\partial U}{\partial \xi} + b\frac{\partial^3 U}{\partial \xi^3} = 0 \tag{1}$$

where ξ and τ are independent variables and a and b are real, nonzero constants. Equation (1) is nonlinear through the convective term $U\partial U/\partial\xi$, and dispersive through the term $\partial^3 U/\partial\xi^3$ [1].

The KdV equation can be solved analytically as an initial value problem [2]. Its analytic solutions are solitary waves (solitons). If one seeks solutions to equation (1) into the form $U(\xi, \tau) = U(\xi - c\tau)$, where $c = \text{const.}$, one obtains

$$U(\xi, \tau) = \frac{3c}{a}\operatorname{sech}^2\left\{\frac{1}{2}\sqrt{\frac{c}{b}}\,[\xi - \xi_0 - c(\tau - \tau_0)]\right\} \tag{2}$$

where ξ_0 and τ_0 are integration constants.

The solitons, given by (2), interact nonlinearly and preserve their soliton identity [3], [7]. Z a b u s k y [8] demonstrated the correspondence between the soliton nonlinear asymptotic solutions of the time-dependent KdV equation and the bound states of the one-dimensional time-independent Schrodinger equation.

T r a n and H i r t [4] used a simple macroscopic model to derive a KdV equation for a two ion species plasma ($T_i = 0$ for both species) and found the dependence of the soliton's amplitude on the light ion concentration. They showed that the amplitude of the solitons is reduced drastically by a few percentages of light ions. Later, T r a n [5] studied the propagation of ion acoustic solitary waves in a two ion species plasma with $T_i \neq 0$,and found that two types of soliton can propagate.

The purpose of this paper is to derive the KdV equation for a two ion species plasma with nonzero temperature, and to establish the effect of the finite ion temperature on the amplitude of the solitons. We use a one-dimensional macroscopic description. Electron inertia effects are neglected and isothermal equations of state are adopted for electrons and for both ion species. In paper [5] an adiabatic equation of state is assumed for the heavy ions, whereas equation of state for the light ions depends on the phase velocity of the wave.

The basic equations can be written in the dimensionless form

$$\frac{\partial n_1}{\partial t} + \frac{\partial}{\partial x}(v_1 n_1) = 0 \tag{3}$$

$$A\left[\frac{\partial v_1}{\partial t} + v_1 \frac{\partial v_1}{\partial x}\right] = E - \frac{\sigma}{n_1}\frac{\partial n_1}{\partial x} \tag{4}$$

$$\frac{\partial n_2}{\partial t} + \frac{\partial}{\partial x}(v_2 n_2) = 0 \tag{5}$$

$$B\left[\frac{\partial v_2}{\partial t} + v_2 \frac{\partial v_2}{\partial x}\right] = E - \frac{\sigma}{n_2}\frac{\partial n_2}{\partial x} \tag{6}$$

$$\frac{\partial n_e}{\partial x} = -n_e E \tag{7}$$

$$\frac{\partial E}{\partial x} = n_1 + n_2 - n_e, \tag{8}$$

where 1, 2 and e denote the light ions, the heavy ions and the electrons, respectively. In equations (3)—(8) distances are normalized to the Debye electron length

$$\lambda_D^2 = \frac{\varepsilon_0 k_B T_e}{n_e q^2}, \tag{9}$$

densities are normalized to the unperturbed electron density n_e, time is normalized to the inverse of ion plasma frequency

$$\omega_p^2 = \frac{n_e q^2}{\varepsilon_0 m_2}(1 - \alpha + \mu\alpha), \tag{10}$$

velocity to ion sound velocity

$$c_s = \lambda_D \omega_p \tag{11}$$

and the electric field is normalized to the quantity $k_B T_e/q\lambda_D$. A and B are given by

$$A = \frac{1 - \alpha + \mu\alpha}{\mu}, \qquad B = 1 - \alpha + \mu\alpha, \tag{12}$$

where α is the concentration of light ions

$$\alpha = \frac{n_1}{n_1 + n_2} = \frac{n_1}{n_e} \tag{13}$$

and μ is the mass ratio

$$\mu = \frac{m_2}{m_1} > 1. \tag{14}$$

Assuming equal ion temperatures, we have noted

$$\sigma = T_i/T_e. \tag{15}$$

Let us make the coordinate transformation [6]

$$\xi = \varepsilon^{1/2}(x - t), \qquad \tau = \varepsilon^{3/2}x, \tag{16}$$

where ε is a small parameter ($0 < \varepsilon < 1$). The equations (3)—(8) become

$$-\frac{\partial n_1}{\partial \xi} + \frac{\partial}{\partial \xi}(n_1 v_1) + \varepsilon \frac{\partial}{\partial \tau}(n_1 v_1) = 0 \tag{17}$$

$$A\left[-\frac{\partial v_1}{\partial \xi} + v_1 \frac{\partial v_1}{\partial \xi} + \varepsilon v_1 \frac{\partial v_1}{\partial \tau}\right] = \tilde{E} - \frac{\sigma}{n_1}\frac{\partial n_1}{\partial \xi} - \varepsilon \frac{\sigma}{n_1}\frac{\partial n_1}{\partial \xi} \tag{18}$$

$$-\frac{\partial n_2}{\partial \xi} + \frac{\partial}{\partial \xi}(n_2 v_2) + \varepsilon \frac{\partial}{\partial \tau}(n_2 v_2) = 0 \tag{19}$$

$$B\left[-\frac{\partial v_2}{\partial \xi} + v_2 \frac{\partial v_2}{\partial \xi} + \varepsilon v_2 \frac{\partial v_2}{\partial \tau}\right] = \tilde{E} - \frac{\sigma}{n_2}\frac{\partial n_2}{\partial \xi} - \varepsilon \frac{\sigma}{n_2}\frac{\partial n_2}{\partial \tau} \tag{20}$$

$$\frac{\partial n_e}{\partial \xi} + \varepsilon \frac{\partial n_e}{\partial \tau} = -n_e \tilde{E} \tag{21}$$

$$\varepsilon \frac{\partial \tilde{E}}{\partial \xi} + \varepsilon^2 \frac{\partial \tilde{E}}{\partial \tau} = n_1 + n_2 - n_e, \tag{22}$$

where $\tilde{E} = \varepsilon^{-1/2}E$.

We assume that n_1, n_2, v_1, v_2, n_e and $\tilde{E}$ have power series expansions in ε about a homogeneous field-free equilibrium:

$$\begin{aligned}
n_1 &= \alpha + \varepsilon n_1^{(1)} + \varepsilon^2 n_1^{(2)} + \dots \\
n_2 &= (1 - \alpha) + \varepsilon n_2^{(1)} + \varepsilon^2 n_{22}^{(2)} + \dots \\
v_1 &= \varepsilon v_1^{(1)} + \varepsilon^2 v_1^{(2)} + \dots \\
v_2 &= \varepsilon v_2^{(1)} + \varepsilon^2 v_2^{(2)} + \dots \\
n_e &= 1 + \varepsilon n_e^{(1)} + \varepsilon^2 n_e^{(2)} + \dots \\
\tilde{E} &= \varepsilon \tilde{E}^{(1)} + \varepsilon^2 \tilde{E}^{(2)} + \dots
\end{aligned}$$

In lowest order, equations (17) — (22) become

$$\frac{\partial n_1^{(1)}}{\partial \xi} = \alpha \frac{\partial v_1^{(1)}}{\partial \xi} \tag{23}$$

$$-A\alpha \frac{\partial v_1^{(1)}}{\partial \xi} = \alpha \tilde{E}^{(1)} - \sigma \frac{\partial n_1^{(1)}}{\partial \xi} \tag{24}$$

$$\frac{\partial n_2^{(1)}}{\partial \xi} = (1 - \alpha)\frac{\partial v_2^{(1)}}{\partial \xi} \tag{25}$$

$$-B(1-\alpha)\frac{\partial v_2^{(1)}}{\partial \xi} = (1-\alpha)\tilde{E}^{(1)} - \sigma\frac{\partial n_2^{(1)}}{\partial \xi} \tag{26}$$

$$\frac{\partial n_e^{(1)}}{\partial \xi} = -\tilde{E}^{(1)} \tag{27}$$

$$n_1^{(1)} + n_2^{(1)} - n_e^{(1)} = 0. \tag{28}$$

To the next order in ε, equations (17) — (22) become

$$-\frac{\partial n_2^{(2)}}{\partial \xi} + \alpha\frac{\partial v_1^{(2)}}{\partial \xi} + \frac{\partial}{\partial \xi}\left(n_1^{(1)}v_1^{(1)}\right) + \alpha\frac{\partial v_1^{(1)}}{\partial \tau} = 0 \tag{29}$$

$$A\left[-\alpha\frac{\partial v_1^{(2)}}{\partial \xi} - n_1^{(1}\frac{\partial v_1^{(1)}}{\partial \xi} + \alpha v_1^{(1)}\frac{\partial v_1^{(1)}}{\partial \xi}\right] =$$

$$= \alpha\tilde{E}^{(2)} + n_1^{(1)}\tilde{E}^{(1)} - \sigma\frac{\partial n_1^{(2)}}{\partial \xi} - \sigma\frac{\partial n_1^{(1)}}{\partial \tau} \tag{30}$$

$$-\frac{\partial n_2^{(2)}}{\partial \xi} + (1-\alpha)\frac{\partial v_2^{(2)}}{\partial \xi} + \frac{\partial}{\partial \xi}\left(n_2^{(1)}v_2^{(1)}\right) + (1-\alpha)\frac{\partial v_2^{(1)}}{\partial \tau} = 0 \tag{31}$$

$$B\left[-(1-\alpha)\frac{\partial v_2^{(2)}}{\partial \xi} - n_2^{(1)}\frac{\partial v_2^{(1)}}{\partial \xi} + (1-\alpha)v_2^{(1)}\frac{\partial v_2^{(1)}}{\partial \xi}\right] =$$

$$= (1-\alpha)\tilde{E}^{(2)} + n_2^{(1)}\tilde{E}^{(1)} - \sigma\frac{\partial n_2^{(1)}}{\partial \xi} - \sigma\frac{\partial n_2^{(1)}}{\partial \tau} \tag{32}$$

$$\frac{\partial n_e^{(2)}}{\partial \xi} + \frac{\partial n_e^{(1)}}{\partial \tau} = -\tilde{E}^{(2)} - n_e^{(1)}\tilde{E}^{(1)} \tag{33}$$

$$\frac{\partial \tilde{E}}{\partial \xi} = n_1^{(2)} + n_2^{(2)} - n_e^{(2)}. \tag{34}$$

Integrating (23) — (28) with the boundary conditions

$$\left.\begin{array}{llllll} n_e \to 1, & n_1 \to \alpha, & n_2 \to 1-\alpha, & v_1 \to 0, & v_2 \to 0 & \\ n_e^{(1)} \to 0, & n_1^{(1)} \to 0, & n_2^{(1)} \to 0, & v_1^{(1)} \to 0, & v_2^{(1)} \to 0 & \end{array}\right\} \text{as } |\xi| \to \infty$$

we obtain

$$n_e^{(1)} = \frac{A-\sigma}{\alpha}n_1^{(1)} = (A-\sigma)v_1^{(1)} = \frac{B-\sigma}{1-\alpha}n_2^{(1)} = (B-\sigma)v_2^{(1)}. \tag{35}$$

From (28) and (35) it follows that

$$\frac{\alpha}{A-\sigma} + \frac{1-\alpha}{B-\sigma} = 1. \tag{36}$$

Hence, for a given light ion concentration, only two values of σ are permitted, namely

$$\sigma = 0 \quad \text{and} \quad \sigma = \frac{1 - \alpha + \mu^2\alpha}{\mu}. \tag{37}$$

The value $\sigma = 0$ corresponds to a plasma with cold ions. Substituting this value into our equations, they become identical with those from paper [4]. For our purpose, the nonzero value of σ is of interest. Using it the equalities (35) take the form

$$n_e^{(1)} = (1 - \mu)\, n_1^{(1)} = \alpha(1 - \mu)\, v_{11}^{(1)} = \frac{\mu - 1}{\mu}\, n_2^{(1)} = \frac{(\mu - 1)(1 - \alpha)}{\mu}\, v_2^{(1)}. \tag{38}$$

Eliminating the second order terms from equations (29) — (34) and making use of (38), we find that $n_e^{(1)}$ evolves according to

$$\frac{\partial n_e^{(1)}}{\partial \tau} + S n_e^{(1)} \frac{\partial n_e^{(1)}}{\partial \xi} + R \frac{\partial^3 n_e^{(1)}}{\partial \xi^3} = 0. \tag{39}$$

This is a KdV equation. But whereas in equation (1) a and b are constants, in (39) S and R depend on α and μ, their explicit expressison being

$$S = \frac{\mu(1 - \alpha + \mu\alpha)}{2(1 - \alpha + \mu^2\alpha)} \left[1 - 2 \frac{(1 - \alpha)^2 - \mu^4\alpha^2}{\mu\alpha(1 - \alpha)(\mu - 1)(1 - \alpha + \mu\alpha)} \right] \tag{40}$$

$$R = \frac{\alpha(1 - \alpha)(\mu - 1)^2}{2(1 - \alpha + \mu\alpha)(1 - \alpha + \mu^2\alpha)}. \tag{41}$$

We notice that for $\sigma = 0$, the following KdV equation is obtained

$$\frac{\partial n_e^{(1)}}{\partial \tau} + S_0 n_e^{(1)} \frac{\partial n_e^{(1)}}{\partial \xi} + R_0 \frac{\partial^3 n_e^{(1)}}{\partial \xi^3} = 0, \tag{42}$$

where

$$S_0 = \frac{1}{2} \left[\frac{3(1 - \alpha + \mu^2\alpha)}{(1 - \alpha + \mu\alpha)^2} - 1 \right], \qquad R_0 = \frac{1}{2}. \tag{43}$$

In this case only the amplitude of the soliton varies with α and μ, while its width remains unchanged. Equations (40) and (41) show that if $\sigma \neq 0$, both the amplitude and the width depend on α and μ.

Figure 1 illustrates the variation of S^{-1} (continuous lines) and S_0^{-1} (dotted lines) with α. We notice that the amplitude of soliton is proportional to one of these quantities, for $\sigma \neq 0$ and $\sigma = 0$, respectively. Two values of the mass ratio μ have been considered $\mu = 10$ and $\mu = 40$. For each curve the corresponding value of μ is indicated.

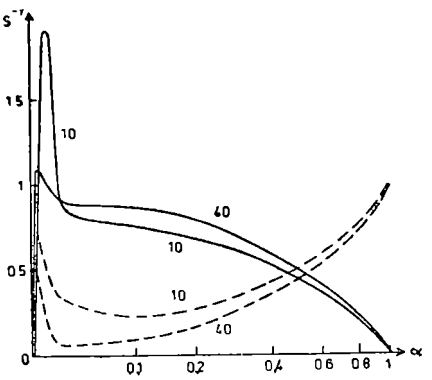

Fig. 1.

Figure 1 shows that for small values of α the amplitude is larger in the case of warm ions, while for large α values the soliton amplitude is smaller for warm ions than for cold ions. This result is in qualitative agreement with Tran's result [5]. A quantitative comparison is not possible, because the model used here, as well as the normalization of distances, velocities and time, are different.

In conclusion, a few percentages of light ions in a heavy ion plasma can play a significant role. If the ions are cold, the light ion impurities prevent the formation of solitons [4]. If, however, the ions have finite temperature, the solitons can easily arise, their amplitude being considerably larger.

(Received September 3, 1977)

REFERENCES

1. Davidson, R. C., *Methods in nonlinear plasma theory*, Academic Press, New York, 1972.
2. Gardner, C. S., Greene, S. M., Kruskal, M. D., Miura, R. M., Phys. Rev Lett., **19**, 1095 (1967).
3. Gorshkov, K. A., Ostrovsky, L. A, Papko, V. V., Zh Eksp Teor. Fiz, **71**, 585 (1976).
4. Tran, M. Q., Hirt, P. J., Plasma Phys., **16**, 617 (1974)
5. Tran, M. Q, Plasma Phys., **16**, 1167 (1974)
6. Washimi, M, Taniuti, T., Phys. Rev. Lett, **17**, 996 (1966).
7. Yajima, N., Outi, A., Progr. Theor. Phys., **45**, 1997 (1971).
8. Zabusky, N. J., Phys. Rev, **168**, 124 (1968).

ECUAŢIA KORTEWEG—DE VRIES PENTRU O PLASMĂ CU DOUĂ SPECII DE IONI

(Rezumat)

În lucrare se deduce o ecuaţie Korteweg—de Vries pentru o plasmă cu două specii de ioni, ale căror temperaturi sînt egale. Se găseşte că în cazul unei concentraţii mici a ionilor uşori formarea solitonilor este împiedicată dacă ionii sînt reci şi este favorizată dacă ionii au temperatură finită.

STUDIA UNIV. BABEŞ—BOLYAI, PHYSICA, 1, 1978

DYNAMICAL SYMMETRY BREAKING DUE TO RADIATIVE CORRECTIONS IN THE SCALAR $\lambda\varphi^4 + g\varphi^3$ — THEORY

AL. ANGHEL and M. CRIŞAN

I. **Introduction.** Quantum field theories with spontaneous broken symmetry were extensively studied in the literature, beginning with the works of Goldstone-Salam-Weinberg [1], Nambu-Jona Lasinio [2] and Vaks Larkin [3].

It was shown that even at the classical level the ground state of a scalar field with interaction has an assymmetric solution $\Phi = \text{const.} \neq 0$ if the bare mass of the theory: $m_0^2 < 0$. Radiative corrections when taken into account do not change this conclusion.

Recently some attempts [4—6] have been done in order to get solutions with dynamical broken symmetry, i e. the assymmetric solution is not a direct consequence of the starting lagrangian but appears when solving the exact quantum field equations.

In a scalar field theory this means the possibility of an assymmetric solution with $m_0^2 > 0$. In the work of Coleman and Weinberg [7] this possibility was investigated for the massless scalar field theory with self — interaction and for quantum electrodynamics with scalar fields interacting with pure Yaug — Mills fields. In the "one loop" approximation the so-called „effective potential" was calculated and the symmetry breaking effect was investigated. In the $\lambda\varphi^4$ — theory the symmetric solution disappears while in the quantum electrodynamics and non — Abelian gauge theories in a certain range of values for coupling constants, the symmetric solutions have remained unchanged.

Recently, Yoffe — Novikov — Shifman [8] have shown that the „effective potential method" is rather unadequate for the problem of dynamical breaking of symmetry.

Instead they have proposed a functional technique method which is an extension of the results of Boulware and Brown [9] and Salam, Stradthee [10].

In this paper we are going to study the problem of dynamical symmetry breaking for a scalar field with a self — interaction of the $\lambda\varphi^4 + g\varphi^3$ type. The paper is organized as follows. First we give a detailed account of the functional technique method we are going to use. Then the $\lambda\varphi^4 + g\varphi^3$ model is analysed in order to find solutions with broken symmetry. Conclusions and the discussion of the results obtained are given at the end of the paper.

II. **Functional technique method in the tree and one — loop approximation.** Let us start with a quantum field theory with a set of quantum fields $\Phi_a(x)$, $a = 1 \ldots N$, described by a local lagrangian

$$\mathfrak{L} = \mathfrak{L}\{\Phi_a(x);\ \partial_\mu \Phi_a(x)\}$$

The corresponding Euler — Lagrange equations are:

$$\mathfrak{F}\{\Phi\} = \partial_\mu \frac{\partial \mathfrak{L}}{\partial \Phi_{a,\mu}} - \frac{\partial \mathfrak{L}}{\partial \Phi_a} \tag{1}$$

The quantum nature of the fields $\Phi_a(x)$, which is not explicitly considered in eq. (1), is given by the following prescription: the canonicaly conjugated fields:

$$\Pi_a(x) = \frac{\partial \mathfrak{L}}{\partial \Phi_{a,0}} \tag{2}$$

satisfy the commutation $(\pm)$ or anticommutation relations'':

$$[\Phi_a(\vec{x},t),\ \Pi_b(\vec{y},t)]_{(\pm)} = i\hbar\,\delta_{a,b}\delta(\vec{x}-\vec{y}) \tag{3}$$

The vacuum average $\langle 0|\ |0\rangle$ of a time ordered product of exponentials containing a set of external sources $\xi_a(x)$ ·

$$\mathfrak{Z}(\xi) = \langle 0|\mathfrak{T}\left\{exp\left[\frac{\imath}{\hbar}\sum_a \int dx\ \ \xi_a(x)\ \ \Phi_a(x)\right]\right\}|0\rangle \tag{4}$$

is the generating functional of the Green functions of the theory

$$\left(\frac{\hbar}{\imath}\right)^n \frac{\delta^n}{\delta\xi_{a_1}(x_1)\ \ \ \delta\xi_{a_n}(x_n)}\,\mathfrak{Z}\{\xi\} = \langle O|\left\{\Phi_{a_1}(x_1)\ \cdot\right.$$

$$\left. \cdot\ \cdot\ \Phi_{a_n}(x_n)\ exp\left[\frac{\imath}{\hbar}\sum_a \int dx\ \xi_a(x)\ \Phi_a(x)\right]\right\}_+ |O\rangle \tag{5}$$

$$\langle 0|\{\Phi_{a_1}(x_1)\ \ldots\ \Phi_{a_n}(x_n)\}_+|0\rangle = \left(\frac{\hbar}{\imath}\right)^n \frac{\delta^n \mathfrak{Z}\{\xi\}}{\delta\xi_{a_1}(x_1)\ \ \ \delta\xi_{a_n}(x_n)}\Bigg| = 0 \tag{6}$$

In the standard way, we represent the quantum field $\Phi_a(x)$ as a functional derivative:

$$\Phi_a(x) \leftrightarrow \frac{\hbar}{\imath}\frac{\delta}{\delta\xi_a(x)} \tag{7}$$

This ,,trick'' can then be used to derive a functional — derivative equation for the generating functional of the Green functions. Acting on the right of $\mathfrak{Z}\{\xi\}$ with the differential operator:

$$\mathfrak{F}\left\{\frac{\hbar}{\imath}\frac{\delta}{\delta\xi(x)}\right\} \tag{8}$$

we get:

$$\mathfrak{F}\left\{\frac{\hbar}{\imath}\frac{\delta}{\delta\xi_a(x)}\right\}\mathfrak{Z}\{\xi\} = \partial_\mu\langle O|\left\{\frac{\partial\mathfrak{L}}{\partial\partial_\mu\Phi_a(x)}\cdot exp\left[\frac{\imath}{\hbar}\int dy\,\xi_b(y)\,\Phi_b(y)\right\}_+ |O\rangle -\right.$$

$$\left. - \langle O|\ \frac{\partial\mathfrak{L}}{\partial\Phi_a(x)}\ exp\left[\frac{\imath}{\hbar}\int dy\,\xi_b(y)\,\Phi_b(y)\right\}_+ |O\rangle \right. \tag{9}$$

After some straightforward calculations, eq. (9) gives:

$$\mathcal{F}\left\{\frac{\hbar}{i}\frac{\delta}{\delta\xi_a(x)}\right\}\mathcal{Z}\{\xi\} = \xi_a(x)\,\mathcal{Z}\{\xi\} \tag{10}$$

The generating functional of the connected Green's functions:

$$\mathcal{G}_n^{(c)}(x_1,\ x_2\ \ldots\ x_n)$$

is:

$$\frac{i}{\hbar}\,\mathcal{W}\{\xi\} = ln\,\mathcal{Z}\{\xi\} \tag{11}$$

and:

$$\mathcal{G}_n^{c}(x_1\ \ldots\ x_n) = \hbar^{n-1}\frac{\delta}{\delta\xi(x_1)}\ \ldots\ \frac{\delta}{\delta\xi(x_n)}\,\mathcal{W}\{\xi\} \tag{12}$$

From eq. (11) and (10) we simply get:

$$\xi_a(x) = exp\left[-\frac{i}{\hbar}\,\mathcal{W}\{\xi\}\right]\mathcal{F}\left\{\frac{\hbar}{i}\frac{\delta}{\delta\xi_a(x)}\right\}exp\left[\frac{i}{\hbar}\,\mathcal{W}\{\xi\}\right] \tag{13}$$

Expanding the right—hand side of eq. (13) in powers of $\frac{i}{\hbar}\,\mathcal{W}\{\xi\}$ we get the final result:

$$\xi_a(x) = \mathcal{F}\left\{\frac{\delta\mathcal{W}\{\xi\}}{\delta\xi_a(x)} + \frac{\hbar}{i}\frac{\delta}{\delta\xi_a(x)}\cdot 1\right\} \tag{14}$$

It will be useful in what follows to perform a Legendre transformation:

$$\mathcal{U}\{\Phi\} = \mathcal{W}\{\xi\} + \int dx\ \xi_a(x)\ \Phi_a(x) \tag{15}$$

such that:

$$\Phi_a(x) = -\frac{\delta\mathcal{W}\{\xi\}}{\delta\xi_a(x)} \tag{16}$$

and.

$$\xi_a(x) = \frac{\delta\mathcal{U}\{\Phi\}}{\delta\Phi_a(x)} \tag{17}$$

The new generating functional $\mathcal{U}(\Phi_a)$ when inserted in eq. (14) gives:

$$\frac{\delta\mathcal{U}\{\Phi\}}{\delta\Phi_a(x)} = \mathcal{F}\left[\Phi_a(x) + \frac{\hbar}{i}\int dy\ \mathcal{G}_{ab}(xy|\Phi)\frac{\delta}{\delta\Phi_b(y)}\right] \tag{18}$$

III. $\lambda\Phi^4 + g\Phi^3$ — **Model.** In this section we are going to study the problem of dynamically broken symmetry for the $\lambda\Phi^4 + g\Phi^3$ — model of quantum field theory as we claimed at the beginning of the present

paper For the sake of simplicity we have limited ourselves to a onecomponent scalar field Φ. The local lagrangian of the problem is:

$$\mathfrak{L} = \frac{1}{2}(\partial_\mu \Phi)^2 - \frac{m_0^2}{2}\Phi^2 - \frac{g}{3!}\Phi^3 - \frac{\lambda_0}{4!}\Phi^4 \tag{19}$$

and is obviously not invariant under the discret group of transformations: $\Phi \to -\Phi$.

A straightforward, but tedious calculation using eq. (1—18) together with the explicit form of the lagrangian (eq. (19)) gives:

$$\frac{\delta \mathcal{U}\{\Phi\}}{\delta \Phi(x)} = \Box\Phi(x) - \frac{g_0}{2}\left[\Phi^2(x) + 2\frac{\hbar}{i}\mathcal{G}(xx|\Phi)\right] -$$

$$-\frac{\lambda_0}{6}\left[\Phi^3(x) + 3\frac{\hbar}{i}\Phi(x)\ \mathcal{G}(xx|\Phi) + \left(\frac{\hbar}{i}\right)^2 \cdot \int dy_1\ dy_2\ dy_3\right.$$

$$\left.\mathcal{G}(xy_1|\Phi)\ \mathcal{G}(xy_2|\Phi)\ \mathcal{G}(xy_3|\Phi)\right].$$

$$\frac{\delta^3 \mathcal{U}\{\Phi\}}{\delta\Phi(y_1)\ \delta\Phi(y_2)\ y\delta\Phi(y_3)}. \tag{20}$$

and:

$$\mathcal{G}^{-1}(x,y|\Phi) = -\frac{\delta^2 \mathcal{U}\{\Phi\}}{\delta\Phi(x)\ \delta\Phi(y)} \tag{21}$$

In order to solve this equation we use an iteration procedure. To zero — — order in $\hbar$ the result is:

$$\frac{\delta \mathcal{U}_0\{\Phi\}}{\delta\Phi} = -\Box\ \Phi(x) - m^2\Phi(x) - \frac{g}{2};\ \Phi^2(x) - \frac{\lambda}{6}\Phi^3(x) \tag{22}$$

and:

$$\mathcal{G}^{-1}(x,y|\Phi) = -\Box\ \delta(x-y) - m^2\delta(x-y) - g\Phi(x)\ \delta(x-y) -$$

$$-\frac{\lambda}{2}\Phi^2(x)\ \delta(x-y) \tag{23}$$

which is the well—known „tree approximation".

To first order in $\hbar$ (one loop — approximation) we get:

$$\frac{\delta \mathcal{U}_1\{\Phi\}}{\delta\Phi(x)} = -\Box\ \Phi(x) - m_0^2\Phi(x) - \frac{g^0}{2}\Phi^2(x) -$$

$$-\frac{\lambda_0}{6}\Phi^3(x) - \frac{\hbar}{i}\left[g\,\mathcal{G}_0(xx|\Phi) + \frac{\lambda}{2}\Phi(x)\,\mathcal{G}_0(xx|\Phi)\right] \tag{24}$$

and:

$$\mathcal{G}^{-1}(xy \mid \Phi) = -\Box\ \delta(x-y) - m_0^2\ \delta(x-y) - \left[g_0\Phi(x) + \frac{\lambda_0}{2}\Phi^2(x)\right]\delta(x-y) -$$

$$-\frac{\hbar}{i}\left\{\left(g + \frac{\lambda}{2}\Phi\right)((g + \lambda\Phi)D_2(m_{ph}) + \frac{\lambda}{2}\delta(x-y)D_1(m_{ph}) \right. \tag{25}$$

where:

$$D_1(m_{ph}) = \int \frac{\delta^4 k}{(2\pi)^4} \frac{1}{m_{ph}^2 - k^2} \tag{26}$$

$$D_2(m_{ph}) = \int \frac{\delta^4 k}{(2\pi)^4} \int \frac{\delta^4 p}{(2\pi)^4} \frac{e^{ip(x-y)}}{(m_{ph}^2 - k^2)[m_{ph}^2 - (p-k)^2]} \tag{27}$$

and m_{ph} is the physical mass parameter:

$$m_{ph}^2 = m^2 + g\Phi + \frac{\lambda}{2}\Phi^2 \tag{28}$$

The symmetry breaking solution of the model is given by the real root Φ_c, of the following equation:

$$\frac{\delta^a U\{\Phi\}}{\delta\Phi(x)} = 0 \tag{29}$$

If such a symmetric solution exists then it must be the solution of:

$$m_0{}^2\ \Phi_c + \frac{1}{2}g_0\Phi_c^2 + \frac{1}{6}\lambda_0\Phi_c^2 + \frac{\hbar}{i}\left(g + \frac{1}{2}\lambda\ \Phi_c\right)D_1(m_{ph}) = 0 \tag{30}$$

in which case the physical mass m_{ph} is obtained from eq. (25) for $p^2 = 0$:

$$m_{ph}^2 = m_0^2 + \left(g_0\Phi_c + \frac{1}{2}\lambda_0\ \Phi_c^2\right) + \frac{1}{2}\lambda\left(\frac{\hbar}{i}\right)D_1(m_{ph}) -$$

$$-\left(g + \frac{1}{2}\lambda\Phi_c\right)(g + \lambda\ \Phi_c)\frac{\hbar}{i}\tilde{D}_2(m_{ph}) \tag{31}$$

where:

$$\tilde{D}_2(m_{ph}) = \int \frac{d^4 k}{(2\pi)^4} \frac{1}{(m_{hp}^2 - k^2)[m_{ph}^2 - (p-k)^2]}\Bigg|_{p^2=0} \tag{32}$$

IV. **The renormalization program.** In this section we are going to develop the renormalization program for the field theory with spontaneous symmetry breaking. Since developing the theory, we have encountered quantities which are not convergent in the limit of infinit momentum cut — off, we isolate within a systematic procedure and remove all divergences using convenient counterterms in the starting lagrangian and appropriate Z — factors.

The Z — factors we introduce in order to renormalize our theory are:

$$\Phi_{CR} = \mathfrak{Z}_{\Phi}^{-1/2}\,\Phi_c,\quad g = g_0\,\mathfrak{Z}_{\Phi}^{3/2}\,\mathfrak{Z}^{-1}$$
$$\lambda = \lambda_0\,\mathfrak{Z}_{\Phi}^{2}\,\mathfrak{Z}^{-1} \tag{33}$$

With a usual mass counterterm δm^2, the interaction term of the renormalized lagrangian reads:

$$\mathfrak{L}_1(x) = -\frac{g}{3}\,\Phi_R^3 - \frac{\lambda}{4}\,\Phi_R^4 + \frac{1}{2}\,\delta m^2\,\Phi_R^2 - \frac{g}{3!}(\mathfrak{Z}-1)\,\Phi_R^3$$
$$-\frac{\lambda}{4}(\mathfrak{Z}-1)\,\Phi_R^4 + \frac{1}{2}(\mathfrak{Z}_{\Phi}-1)(\partial_\mu \Phi_R)^2 \tag{34}$$

The additional counterterms are depicted in fig. 1.

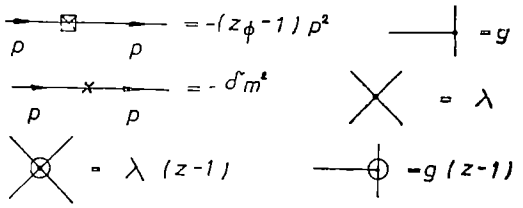

Fig. 1

The Z — factors $\mathfrak{Z}_{\Phi}$, $\mathfrak{Z}$ and the mass counter-term are determined from the conditions:

$$G_R^{-1}(p^2 = 0) = -m_{ph}^2 \tag{35}$$

$$\left.\frac{\partial G_R^{-1}(p^2)}{\partial p^2}\right|_{p^2=0} = 1 \tag{36}$$

$$\Gamma_R^{(3)}\,[\{p_i^2\} = 0] = g \tag{37}$$

In the "one — loop" approximation the Feynman diagrams contributing to (35—37) are depicted in fig. 2.

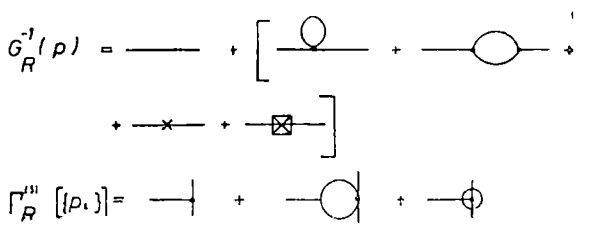

Fig 2

Adding the contributions we get:

$$Z_\Phi = 1 + \frac{g^2}{2} \cdot B'(O,\ m_{ph},\ \Lambda) \tag{38}$$

$$\delta m^2 = \frac{\lambda}{2} A(O,\ m_{ph}) + \frac{g^2}{2} B(O,\ m_{ph},\ \Lambda) \tag{39}$$

$$\mathfrak{Z} = 1 + \frac{3\lambda}{2}\left(\frac{\hbar}{i}\right) B(0,\ m_{ph},\ \Lambda) \tag{40}$$

where $B(p,m_{ph},\Lambda)$ is the following integral

$$B(p,\ m_{ph},\ \Lambda) = \int_0^{\hat{}} \frac{d^4k}{(2\pi)^4} \frac{1}{(m_{ph}^2 - k^2)\,[m_{ph}^2 - (p-k)^2]} \tag{41}$$

It is obvious then that $B(O,\ m_{ph},\ \Lambda)$ is the same with $\tilde{D}_2(m_{ph})$ defined by eq. (32).

We end this renormalization program by notting that the renormalization constant $\mathfrak{Z}_\Phi = 1 + O(g^2)$ and $\mathfrak{Z} = 1 + O(\lambda)$ so in the following calculations we will always put $\mathfrak{Z}_\Phi = 1$.

V. **The critical region.** At the critical point $m_{ph} = 0$ and since $\tilde{D}_2(O) = \infty$ if there is to be a critical point we must have:

$$\text{a)}\ \Phi_{CR} = -\frac{2g}{\lambda} \qquad \text{b)}\ \Phi_{CR} = -\frac{g}{\lambda} \tag{42}$$

in the renormalized version of eq. (31). In particular this is true only for a special combination of the parameters. Namely:

$$\frac{2g}{\lambda}\left[m_0^2 - \frac{\mathfrak{Z}}{3}\frac{g^2}{\lambda}\right] = 0 \tag{43}$$

for the case (a), and:

$$\frac{g}{\lambda}\left[m_0^2 - \frac{\mathfrak{Z}}{3}\frac{g^2}{\lambda} - \left(\frac{\hbar}{i}\right)\frac{\lambda}{2} D_1(0)\right] = 0 \tag{44}$$

for the case (b). These conditions are direct consequences of eq. (30).

Then it follows that at these points:

$$m_0^2 = -\frac{1}{2}\lambda\left(\frac{\hbar}{i}\right) D_1(0) = m_{0c}^2\ (a) \tag{45}$$

and:

$$m_0^2 = -\frac{\mathfrak{Z}}{2}\frac{g^2}{\lambda} = -\frac{1}{2}\lambda\left(\frac{\hbar}{i}\right) D_1(0) \equiv m_{0c}^2\ \text{(b)} \tag{46}$$

We disregard the trivial solution $g = 0$.

VI. **Conclusions and discussion.** We have shown that in a scalar field theory which has a $g\Phi^3$ interaction in addition to $\lambda\Phi^4$ there are two critical values for the parameter g below which there is no symmetry

breaking. At these critical points there is a second order phase transition i.e. $\langle 0|\ \Phi|0\rangle$ changes continuously from zero to a non — zero value, but there is no spontaneous symmetry breaking. For $g > g_c$ the transition is of first order i.e. there is an abrupt change in the value of $\langle 0|\ \Phi|0\rangle$ from zero to non — zero.

Our result, that there are two critical values for the coupling constant g, is in contrast with the result obtained by Alexander and Amit [11] who have found just one critical value. We believe that this discrepancy is due to our improved method which correctly takes into account the radiative corrections.

(Received October 13, 1977)

REFERENCES

1. I. Goldstone, A. Salam, S. Weinberg, Phys. Rev, **127**, 965 (1962).
2. Y. Nambu, G. Iona—Lasinio, Phys. Rev., **122**, 345 (1961).
3 B. G. Vaks, A. I. Larkin, JETF, **40**, 282 (1961).
4 I. Schwinger, Phys Rev., **125**, 397 (1962).
5 A. A. Migdal, A. M. Polyakov, JETF, **51**, 135 (1966).
6 R. Jackiw, K. Johnson, Phys. Rev., D**8**, 2386 (1973).
7. S. Coleman, E. Weinberg, Phys. Rev, D**7**, 1888 (1973).
8. B. L Yoffe, V. A. Novikov, M. A. Shifman, J. of. Nuclear Phys., T**22**, 401 (1975).
9. D Boulware, L. Brown, Phys Rev, **172**, 1628 (1968).
10. A Salam, J. Stradthee, Phys. Rev, **170**, 582 (1968).
11. S. Alexander, D. Amit, J. Phys., A **8**, 1988 (1975).

RUPEREA DINAMICĂ SPONTANĂ A SIMETRIEI DATORITĂ CORECȚIILOR RADIATIVE ÎN MODELUL SCALAR $\lambda\Phi^4 + g\Phi^3$

(Rezumat)

Folosind formalismul funcțional se analizează ruperea dinamică spontană a simetriei datorită corecțiilor radiative în modelul $\lambda\Phi^4 + g\Phi^3$. Sub o anumită valoare a constantei g nu există ruperea de simetrie, deci nu este posibilă tranziția de fază.

În punctul g_c apare o tranziție de speța a doua iar pentru $g > g_c$ tranziția este de speța întîia.

STUDIA UNIV. BABEŞ—BOLYAI, PHYSICA, 1, 1978

CRITICAL BEHAVIOUR OF THE SPECIFIC HEAT IN INHOMOGENEOUS BIDIMENSIONAL SUPERCONDUCTORS

D. DĂDÎRLAT, M. CRIŞAN

1. **Introduction.** The starting point in studying the specific heat of a dirty superconductor is the generalized Ginzburg-Landau free — energy, which considers the local fluctuations of the strength of the B.C.S. coupling because of the structural inhomogeneities of the film [1]

$$F(\psi) = d\int dx^2\left[A(\vec{x})\,|\psi|^2 + \frac{1}{2}B|\psi|^4 + C|\vec{\nabla}\psi|^2\right] \tag{1.1}$$

where $\psi(\vec{x})$ is the order parameter, d is the film thickness and $A(\vec{x}) = A_0 + \delta A(\vec{x}) \cdot \delta A(\vec{x})$ is proportional to the local fluctuations of Tc,

$$A_0 = N_0\left(\frac{T}{T_{c0}} - 1\right) = N_0\tau$$

$$B = \frac{0.106\ N_0}{T^2_{(0)}} \tag{1.2}$$

$$C = N_0\ \xi^2_{c0}$$

where $\zeta(0)$ is the amplitude of the correlation length and No is the density of states at the Fermi level for a bulk superconductor.

Using the generalized Ginzburg-Landau free-energy defined by (1.1) we calculate in the second section the selfenergy. In the sections 3 and 4 we calculate the specific heat in the following two limits: $\rho\xi \ll 1$ and $\rho\xi \gg 1$. The section 5 is devoted to the conclusions.

2. **The selfenergy of an inhomogeneous bidimensional superconducting system.**

Using Hartree-Fock approximation and treating $\delta A(\vec{x})$ like a small perturbation we obtain for the Green function the diagramatic expression

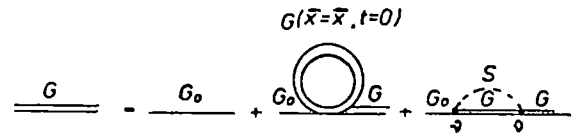

where G_0, in the Gaussian model ($B = 0$, $A = A_0$), is

$$G_0^{-1}(\vec{q}) = \frac{Cd}{T}\left(\vec{q}^2 + \frac{A_0}{C}\right) \tag{2.1}$$

and G has the analytical expression

$$G^{-1} = G_0^{-1} + \Sigma \tag{2.2}$$

The selfenergy Σ is given by:

$$\sum(\vec{q}) = \frac{d}{T} G(\vec{x} = \vec{x}',\ t = 0) - \frac{d^2}{T^2} \int \frac{d^2q'}{(2\pi)^2} \tilde{S}(\vec{q} - \vec{q}')\, G(\vec{q}') \qquad (2\,3)$$

In eq. (2.3) $\tilde{S}(\vec{q}) = S(q)\nu^2(q)$, where $S(q)$ is the Fourrier transform of the correlation function of $\delta A(\vec{x})$, and $\nu(q)$ is the vertex function

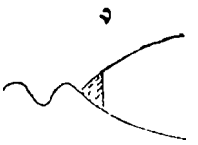

For bidimensional films, $\nu(q)$ is given by [2]

$$\nu^{-1}(q) = 1 + \frac{T}{T_{co}} \frac{w}{K^2 \xi^2_{(0)}} \frac{ln \left\{ \frac{q}{2K} + \left[1 + \left(\frac{q}{2K} \right)^2 \right]^{\frac{1}{2}} \right\}}{\frac{q}{2K} \left[1 + \left(\frac{q}{2K} \right)^2 \right]^{\frac{1}{2}}} \qquad (2.4)$$

where

$$w = \frac{0.106}{4\pi\ N_0 d \xi^2_{(0)} T_{c0}} \qquad (2\,5)$$

$$[K(T)]^2 = \frac{1}{\xi^2_{(0)}} \left[\tau + \frac{T}{N_0 \cdot d} \Sigma(0) \right]$$

Using (2.2) and (2.5)

$$G(\vec{x} = \vec{x}',\ t = 0) = \int_0^{q_0} \frac{q dq}{2\pi} G(q) = \frac{T}{4\pi C d} ln \left(1 + \frac{q_0^2}{K^2} \right) \qquad (2.6)$$

The specific heat for the general case of a n — component bidimensional system is given by [3]

$$C\infty = \frac{2}{n} \frac{\partial^2 F}{\partial \tau^2} \qquad (2.7)$$

Using also the Ward identity

$$-\frac{\partial F}{\partial \tau} = \frac{n}{2} G(0) \qquad (2.8)$$

we obtain for the specific heat:

$$C\infty = -\frac{\partial G_{(0)}}{\partial \tau} \qquad (2.9)$$

From (2.1)

$$G_0^{-1} = \frac{dN_0 \tau}{T} \qquad (2.10)$$

With (2.6) and (2.10) introduced in (2.3), we can express the selfenergy as:

$$\sum(0) = \frac{B}{4\pi C} ln\left(1 + \frac{q_0}{K^2}\right) - \tag{2.11}$$

$$- \frac{d^3}{T^3} N_0^2 \frac{\langle \delta T_c^2 \rangle}{T_{c0}^2} \int \frac{\frac{q}{2\alpha^2}\, dq\, exp\left(-\frac{q^2}{4\alpha^2}\right) v^2(q)}{\frac{Cd}{T}(q^2 + K^2)}$$

3. The case $q\xi \ll 1$

In this limit (2.11) becomes:

$$\sum(0) = \frac{d}{T} \frac{N_0^2}{C} \frac{\langle \delta T_C^2 \rangle}{T_{c0}^2} \frac{1}{[K(T)]^2} \tag{3.1}$$

From (2.5) and (3.1) we obtain a selfconsistent equation, which gives for Σ the expression:

$$\sum(0) = \frac{N_0 d}{2T}\left[\left(\tau^2 + 4\frac{\langle \delta T_c^2 \rangle}{T_{c0}^2}\right)^{\frac{1}{2}} - \tau\right] \tag{3.2}$$

In the following, we consider

$$\tau = \frac{T - T_c}{T_c} \ll 1 \tag{3.3}$$

and, in this approximation

$$\sum(0) = \frac{N_0 d}{2T}[\beta - \tau] \tag{3.4}$$

where

$$\beta = 2\frac{\langle \delta T_c^2 \rangle^{\frac{1}{2}}}{T_{c0}}$$

$$G_0^{-1} = \frac{dN_0}{2T}\tau + \frac{dN_0}{2T}\beta \tag{3.5}$$

From (2.9) and (3.5)

$$C_\infty = \frac{2T_c}{dN_0}[\tau + \beta]^{-2} \tag{3.6}$$

Eq. (3.6) shows a monotonic critical behaviour of C_∞ in the limit $q\xi \ll 1$. This behaviour is in agreement with the experiment [3], but the theory is not complete because we must consider the $O(1)$ terms, corresponding to "ring" diagrams. Summing up all ring diagrams means the first order in the screening-approximation.

The screening-correction to the selfenergy is

$$\delta Fs = \frac{1}{2}\int \frac{d^3q}{(2\pi)^3} ln \ [1 + \Pi_0(q,K)] \tag{3.7}$$

where

$$\Pi_0(q,K) = \int \frac{d^3q}{(2\pi)^3} g(p+q,K) \ g(p,K) \tag{3.8}$$

with

$$g(p,K) = \frac{1}{q^2+K^2} \tag{3.9}$$

Using (3.7)

$$\frac{\partial(\delta F_s)}{\partial\tau} = \frac{1}{2}\frac{dK}{d\tau}\int \frac{d^3q}{(2\pi)^3} \frac{\frac{\partial\pi_0}{\partial K}}{1+\pi_0} \tag{3.10}$$

In the limit $q \ll K, \Pi_0$ is given as:

$$\Pi_0 \cong \frac{1}{4\pi K^2}\left[1 - \frac{2}{3}\left(\frac{q}{2K}\right)^2\right] \cong \frac{1}{4\pi K^2} \tag{3.11}$$

$$\frac{\partial\Pi_0}{\partial K} = -\frac{1}{2\pi K^3} \tag{3.12}$$

Introducing (3.4) in (2.5) we obtain:

$$\frac{\partial K(T)}{\partial\tau} = \frac{1}{2\xi_{(0)}^3} \ \frac{1}{K(T)} \tag{3.13}$$

and for the correction to the free-energy

$$\frac{\partial(\delta F_s)}{\partial\tau} \sim \left(\frac{q_0}{K}\right)^2 \frac{1}{1+4\pi K^2} \to 0 \tag{3.14}$$

In conclusion, we have not a screening-correction, and in this limit the total specific heat is given by (3.6).

4. **The case** $q\xi \gg 1$

In this approximation

$$v(q)^{-1} = \frac{4Tw}{T_{c0}\,\xi_{(0)}^2} \frac{ln\left(\frac{q}{K}\right)}{q^2} \tag{4.1}$$

and the selfenergy is given as:

$$\Sigma(0) \cong \frac{B}{4\pi C} ln\left(\frac{q_0}{K^3}\right) \tag{4.2}$$

Using (4.2) in Dyson equation we obtain for G

$$G^{-1}(0) = \frac{dN_0}{T}\tau + \frac{B}{4\pi C} ln\left(\frac{q_0}{K^2}\right) \tag{4.3}$$

From (2.5) and (4.2)

$$\Sigma(0) \cong \gamma\left(1 - \frac{\tau}{q_0 \xi^2(0)}\right) \cong \gamma \tag{4.4}$$

where

$$\gamma = \frac{0.106}{4\pi\, T_{c0}^2 \xi_0^2(0)} \tag{4.5}$$

In the same limit $\tau \ll 1$

$$G^{-1}(0) = \frac{dN_0}{T_c}\tau + \gamma \tag{4.6}$$

and

$$C_\infty = \frac{T_c}{dN_0}\left[\tau + 0.008 \frac{T_c}{T_{c0}\, dN_0\, \xi^2(0)}\right]^{-2} \tag{4.7}$$

For the screening-correction we must reanalyse (3.10)

$$\Pi_0 = \frac{1}{\pi q^2} \; ; \quad \frac{\partial \Pi_0}{\partial K} \to 0 \tag{4.8}$$

The screening-correction being small in this case too, the total specific heat is given by (4.7).

In the following it is necessary to study the region with $\tau \geqslant 1$ because of two reasons:

— The screening-correction will not be zero in this case.

— The anomaly in the specific heat could be shifted from Tc because of the impurities.

Using the same method we obtain:

$$G(0) = \frac{T_c}{dN_0}\frac{\tau + 1}{\tau} \qquad q \ll K \tag{4.9}$$

$$G(0) = \frac{\tau + 1}{\gamma + \left(\frac{dN_0}{T_c} + \gamma\right)\tau} \qquad q \gg K$$

and

$$C_\infty = \frac{T_c}{dN_0}\frac{1}{\tau^2} \qquad q \ll K$$

$$C_\infty = \frac{dN_0}{T_c}\frac{1}{\left[\gamma + \left(\frac{dN_0}{T_c} + \gamma\right)\tau\right]^2} \qquad q \ll K \tag{4.10}$$

In order to develop the screening-correction, we approximate in (3.10)

$$\Pi_0 \ll 1 \tag{4 11}$$

$$ln\ (1+\Pi_0] \cong \Pi_0$$

and

$$\delta Fs = \frac{1}{2} G^2_{(0)} \tag{4 12}$$

Using (4.9) and (4.12), the screening-corrections are:

$$\begin{aligned} \delta C_s &= \left(\frac{T_c}{dN_0}\right)^2 \frac{1}{\tau^2}\left(3+\frac{4}{\tau}\right) \qquad q \ll K \\ \delta C_s &= \left[\gamma + \left(\gamma + \frac{dN_0}{T_c}\right)\tau\right]^{-4} \qquad q \ll K \end{aligned} \tag{4.13}$$

5. **Conclusions.** The main result of this paper is the monotonic behaviour of the specific heat in the critical region for $T \gtrsim Tc$. The screening-correction is zero for $\tau \ll 1$. For $\tau \geqslant 1$ the screening-correction is not zero, but it doesn't bring any divergence in the specific heat.

(Received October 13, 1977)

REFERENCES

1. S. Cremer, E. Simanek, Phys Rev. B. **14**, 1927 (1976).
2. G. Rickayzen, A. J. Bray, J. Phys, F **3**, L 134 (1973).
3. D. J. Scalapino, R. A Ferrell, A J Bray, Phys. Rev, Lett **31**, 292 (1973)

COMPORTAREA CRITICĂ A CĂLDURII SPECIFICE ÎN SUPRACONDUCTORI NEOMOGENI BIDIMENSIONALI

(Rezumat)

Se calculează căldura specifică a unui film supraconductor neomogen în aproximația de ecranare. În regiunea critică se obține o comportare fără singularități.

STUDIA UNIV. BABEŞ—BOLYAI, PHYSICA, 1, 1978

E.S.R AND OPTICAL SPECTRA OF V^{4+} IN BORATE GLASSES

AL. NICULA, E. CULEA, L. STĂNESCU

This paper presents the results of a study of some borate glasses internal structure, $(100-x)\%\ B_2O_3 - x\%\ V_2O_5$ with $x \leqslant 12$ and $(100-x)\%\ Na_2B_4O_7 - x\%V_2O_5$ with $x \leqslant 12$, using the ESR and optical spectra. The experimental results were interpreted by means of the molecular orbitals theory.

Experimental technique. The samples were obtained by melting some mixtures of boric acid and V_2O_5, respectively borax and V_2O_5, which were previously dehydrated 48 hours at 200°C. The mixtures were heated up to 1 100°C, respectively 1 000°C. The samples were allowed to fall in drops on a heated rust-proof steel plate.

The ESR spectra were registered by a JES—3B spectrometer, at room temperature. Optical spectra were registered on Beckman DK—2 and UV—VIS spectrophotometers

Experimental data and their discussion. The ESR spectra obtained by us (see fig 1) are characteristic ion which has a $3d^1(S = 1/2,\ I = 7/2)$ electronic configuration. The hiperfine structure which may be observed is due to the interaction of the unpaired electron with the V^{51} nucleus.

These spectra can be analysed by means of the spin hamiltonian of axial symmetry

$$H = \beta(g_{\|}\ H_z S_z + g_{\perp}\ H_x S_x + g_{\perp}\ H_y\ S_y) + A_{\|}\ S_z\ I_z + A_{\perp}\ S_x\ I_x + + A_{\perp}\ S_y I_y \qquad (1)$$

with the usual notation. This leads to the following resonance condition:

$$h\nu = g\beta H(m) + K(\theta)m \qquad (2)$$

where

$$g = \sqrt{g_{\|}^2 \cos^2\theta + g_{\top}^2 \sin^2\theta} \qquad (3)$$

$$K(\theta) = \sqrt{A_{\|}^2\ g_{\|}^2\ \cos^2\theta} + + \sqrt{A_{\perp}^2 g_{\perp}^2 \sin^2\theta} \qquad (4)$$

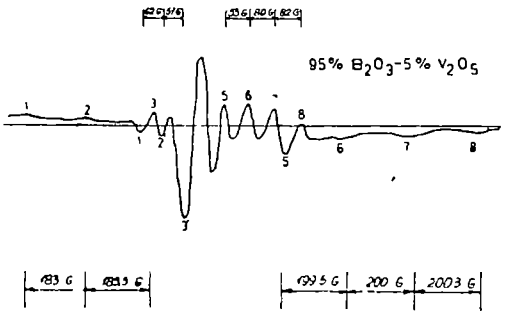

Fig 1a

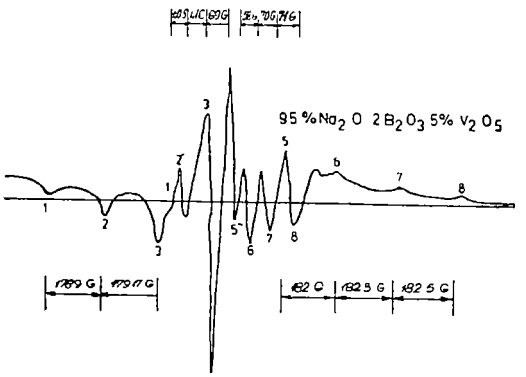

Fig. 1b

m = magnetic cuantic number,
θ = the angle between magnetic field axis and ligand field symmetry axis.

Though these ESR spectra represent the superposition of the spectra corresponding to the different possible values of $\theta \in \left[0, \frac{\pi}{2}\right]$, the strong anisotropy of the hiperfine coupling tensor A permits us to find $A_\perp$ and $A_\parallel$ easily.

The ESR parameters obtained by us are given in table 1.

Table 1

$B_2O_3(100-x)\% - V_2O_5\%$ glasses

	V_2O_5 %	$A_\parallel \cdot 10^4$ cm^{-1}	$A_\perp \cdot 10^4$ cm^{-1}	$g_\parallel$	$g_\perp$
1	5	194	69	1,938	1,982
2	9	194	69	1,938	1,982
3	12	194	69	1,939	1,983

Na_2B_4O $(100-x)\% - V_2O_5 x\%$ glasses

	V_2O_5 %	$A_\parallel \cdot 10^4$ cm^{-1}	$A_\perp \cdot 10^4$ cm^{-1}	$g_\parallel$	$g_\perp$
1	1	174	58	1,940	1,979
2	2,5	174	58	1,938	1,978
3	5	174	58	1,939	1,979
4	11	174	58	1,939	1,979
5	15	174	58	1,938	1,978
6	19	174	58	1,940	1,980

In previous works [1, 2, 3, 6] it was shown that the V^{4+} ion, in oxidic glasses with 1—5% V_2O_5, appears as vanadyl ion VO^{2+} and forms molecular complexes of octahedral symmetry (C_{v4}). The ESR data show that this tendency is also maintained in our glasses, having a greater content of V_2O_5. We have obtained $A_\parallel < A_\perp$ and $g_\parallel < g_\perp$ which means that the spectra are given by VO^{2+}, but in this case the spectra could be registered at room temperature only if the ligand field has an octahedral symmetry [4].

The ESR parameters variation indicate the variation of covalency degree of paramagnetic ion — ligand bonding. This is determined by the distorsion degree of the molecular complex, which differs if it is incorporated in $(100-x)\%$ $B_2O_3 - x\%$ V_2O_5 glasses matrix (where only BO_3 groups appear), or in $(100-x)\%$ $Na_2B_4O - x\%$ V_2O_5 glasses matrix (where BO_4 groups also appear).

It is known that the increase of the covalency degree of the paramagnetic ion — ligand bonding leads to the decrease of the hyperfine structure constant because at a $3d^1$ electronic configuration $A_{\parallel}$ and $A_{\perp}$ are essentialy dipolar ($A_{\parallel}$ and $A_{\perp} \sim \langle r^{-3} \rangle$, where r = electron — V^{51} nucleus distance).

ESR and optical data could be correlated using the simple expressions calculated by Kivelson and Lee [5] in the hypothesis that the unpaired electron of V^{4+} is located on b_2^* ($\beta_{22}^* \simeq 1$) orbital:

$$g_{\parallel} = g_e - \frac{4 g_e \lambda \beta_1^2}{\Delta_{\parallel}} \tag{5}$$

$$g_{\perp} = g_e - \frac{g_e \lambda \varepsilon_{\pi}^{*2}}{\Delta_{\perp}} \tag{6}$$

$$K_v = \frac{7}{2} \cdot \frac{A_{\parallel} + 2A_{\perp}}{A_{\parallel} - A_{\perp}} \tag{7}$$

$$\beta_2^{*2} P_v = \frac{A}{\frac{2}{7} - K_v} \tag{8}$$

where $\Delta_{\parallel} = E_{b_1^*} - E_{b_2^*}$, $\Delta_{\perp} = E_{e_{\pi}^*} - E_{b^2}^*$,

λ = spin — orbit coupling constant

K_v = Fermi contact interaction constant

$P_v = 2\ \gamma \mu_c\ \mu_v \langle b_2 | r^{-3} b_2 \rangle$,

β_1^*, β_2^*, ε_{π}^* molecular orbital coefficients.

Using (5), (6), (7), (8) relations and the ESR and optical absorption data it is easy to compute β_1^{*2}, ε_{π}^{*2}, K_v and P_v. The results thus obtained are presented in table 2.

Table 2

	$E_{b_1^*} - E_{b_2^*}$ cm^{-1}	$E_{a_{\pi}^*} - E_{b_2^*}$ cm^{-1}	$g_{\parallel}$	$g_{\perp}$	β_1^{*2}	ε_{π}^{*2}	$A_{\parallel cm} \cdot 10^4$	$A_{\perp cm} \cdot 10^4$	K_v	$\beta_2^{*2} P_v$
95% B_2O_3 — 5% V_2O_5	—	12900	1,938	1,982	—	0,769	194	69	0,759	146
95% Na_2B_4O — 5% V_2O_5	16700	10500	1,939	1,979	0,776	0,719	174	58	0,714	135

$\lambda = 170\ cm^{-1}$ has been used.

Conclusions. The ESR results indicate a decrease of the covalency degree of paramagnetic ion — ligand bonding from (100—x)% $Na_2B_4O_7$ — — x% V_2O_5 glasses to (100—x)% B_2O_3 — x% V_2O_5 glasses.

The variation of ε_{π}^{*2} indicates the decrease of covalency degree of π (out-of-plane) bonding from (100—x)% $Na_2B_4O_7$ — x% V_2O_5 to (100—x)% B_2O_3 — x% V_2O_5 glasses. The variation of K_v indicates the decrease of covalency of σ bondings (especially of those with vanadyl 0) in the same direction. This means that the molecular complex is less distortioned in the symmetry axis direction in (100—x)% B_2O_3 — x% V_2O_5 glasses than in (100—x)% $Na_2B_4O_7$ — x% V_2O_5 glasses.

The P_v values indicate the decrease of electron—V^{51} nucleus distance in (100—x)% B_2O_3 — x% V_2O_5 glasses (when the electron is situated on the b_2 orbit).

The increase of V_2O_5 concentration does not influence ESR parameters, but it increases the stability of samples in moist atmosphere. We have also obtained glasses with less than 5%PbO, more stable and more hard (the ESR parameters don't change)

(Received October 14, 1977)

REFERENCES

1 H G Hecht, T Johnston, J Chem Phys, **46** (1), 23 (1967)
2 L D Bogomolova, T F. Dolgolenko, V. N Lazukin, N V Petrovih, Dokladı Akad. Nauk SSSR, **208**, 580 (1973)
3 L D. Bogomolova, T. F Dolgolenko, V. N Lazukin, V A Iachkin, J Magn Resonance, **15**, 293 (1974).
4 I. Siegel, J Chem. Phys, **134** (1), 193 (1964)
5 D. Kivelson, S K Lee, J Chem Phys, **41**, 1896 (1964)
6 L D Bogomolova, V A. Iachkin, V N Lazukin, *XIX th Congress Ampère*, Heidelberg, 1976, p 235

RES ŞI SPECTRE OPTICE ALE IONULUI V^{4+} ÎN STICLE BORATE

(Rezumat)

Lucrarea de faţă prezintă rezultatele studiului structurii interne a unor sticle boiate (100—x)% B_2O_3 — x% V_2O_5 cu $x \leqslant 12$ şi (100—x)% $Na_2B_4O_5$ — x% V_2O_7 cu $x \leqslant 12$, utilizînd ca mijloace de investigare R.E S şi spectrele optice. Datele obţinute au fost interpretate prin prisma teoriei orbitalilor moleculari

STUDIA UNIV BABEŞ—BOLYAI, PHYSICA, 1, 1978

D.C. CONDUCTIVITY OF $xFe_2O_3 \cdot (1-x)\ [3B_2O_3 \cdot PbO]$ GLASSES

I. ARDELEAN and V. SEVIANU

It is already known that in semiconducting oxide glasses containing transition metal ions there exists electronic conduction due to the presence of transition metal ions in two valence states, for instance V^{4+} and V^{5+} in vanadium glasses and Fe^{2+} and Fe^{3+} in iron glasses [1—6]. However, the transport mechanism depends on the particular glass system; a fact which requires experimental studies to be undertaken in this field.

In the present piece of work we have attempted to study the d.c. conductivity of the $xFe_2O_3 \cdot (1-x)\ [3B_2O_3 \cdot PbO]$ glass system, with x increasing up to 50 mol · % of Fe_2O_3.

The Experimental Technique. The samples were prepared by melting H_3BO_3, PbO and Fe_2O_3 of analytical grade in sintercorund crucibles at 1250°C, for two hours, followed by cooling the glasses by pouring them onto a plate made of stainless steel.

The sample composition in molar percentages is given in Table 1.

Table 1

Sample number	1	2	3	4	5	6	7	8	9	10	11
$3B_2O_3PbO$ mol%	98	95	90	85	80	75	70	65	60	55	50
Fe_2O_3 mol%	2	5	10	15	20	25	30	35	40	45	50

The homogeneity of the $xFe_2O_3 \cdot (1-x)\ [3B_2O_3 \cdot PbO]$ glasses was confirmed by studying the IR absorbtion spectra, the X-ray diffraction patterns [7], the U.V. and visible absorption spectra [8], the Mossbauer effect [9] and by magnetic measurements [10] The measurements based on the Mossbauer effect demonstrated the presence of both the Fe^{2+} and Fe^{3+} ions.

For measurement purposes the samples were polished in parallelipipedic forms, of 0.5 — 3 mm thickness and 1 — 1 5 cm^2 contact area

The measuring equipment was similar to that described previously [11]. The meter was a T R 2201 megaohmeter

Results and Discussion. Figure 1 illustrates the dependence of log ρ (the resistivity) as a function of the reciprocal of the tempe rature, for all the samples of the $xFe_2O_3 \cdot (1-x)\ [3B_2O_3 \cdot PbO]$ system. The labels of the curves coincide with the numbering of the samples in Table 1. As it can be seen, the resistivity of the glasses of the $xFe_2O_3 \cdot (1-x)\ [3B_2O_3 \cdot PbO]$ system displays a temperature dependence which is characteristic to the semiconductor materials, that is: $\rho = \rho_0 \exp(q/kT)$, where q is the activation energy.

In the case of the sample with 50 mol % Fe_2O_3 the measurements were performed at both increasing (filled circles) and decreasing (empty circles) temperatures. It may be noticed that the results were reproducible within the temperature range studied (300 K — 700 K).

No polarisation of the samples was noticed during the measurements; the resistance remained constant in time at a given temperature and voltage. This observation infers the absence of the ionic component of the conductibility.

A change of the slope, belonging to the temperature range investigated, becomes obvious in Figure 1 for the samples with a molar percentage of Fe_2O_3 greater than 15%. A similar behaviour has been reported [4, 5] in the case of the phosphate glasses containing iron, but the cause responsible for this effect has not been elucidated. One may note that

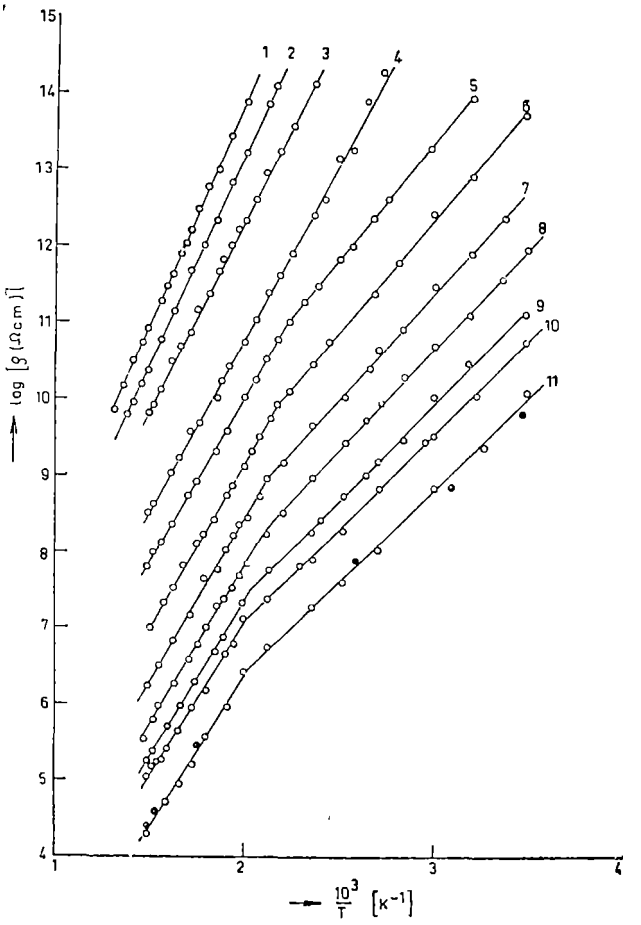

Fig. 1.

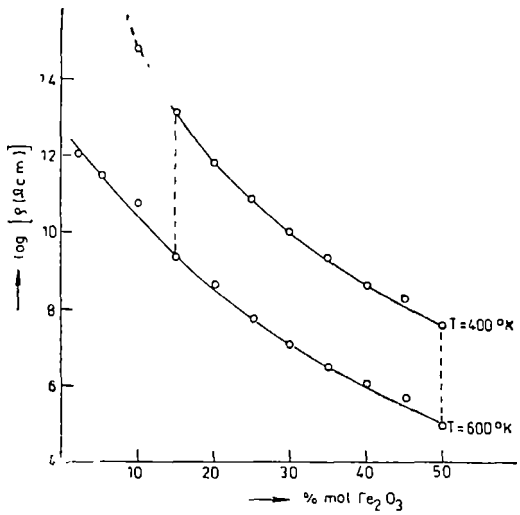

Fig. 2.

the magnetic, susceptibility measurements show that the samples with more than 15 mol % of Fe_2O_3 have a negative θ_p [10].

Figure 2 shows the dependence of log ρ on the Fe_2O_3, at two temperatures: 400 K and 600 K (taken on the two regions of different activation energies). The effect of inserting iron in the glass matrix becomes in this way evident. A similar behaviour has been reported for phosphate glasses with iron [5] and with vanadium [12]. One may notice the sudden resistivity increase at 400 K taking place in glasses with more than 15 mol % Fe_2O_3. It is noteworthy the fact that while the difference between the resistivities at the two temperatures is equal to 2.5 orders of magnitude in the case of the 50 mol % Fe_2O_3 sample, the same difference equals 4 orders of magnitude in the case of the 15 mol % Fe_2O_3 sample.

Conclusions. We may conclude that the glasses belonging to the $xFe_2O_3 \cdot (1-x)\ [3B_2O_3 \cdot PbO]$ system manifest a semiconducting behaviour in the temperature range 300 — 700 K and that their conductivity increases with increased Fe_2O_3 contents. Two activation energies are evidentiated in the case of the samples with a molar percentage of Fe_2O_3 greater than 15.

(Received October 15, 1977)

REFERENCES

1. N. F. Mott, J. Non-Crystalline Solids, 1 (1968).
2. M. Sayer and A. Mansingh, Phys. Rev. B 6, 12 (1972).
3. F. A. Wedgwood, J. Non-Crystalline Solids, 21 (1976).
4. A. W. Dozier et al., J. Amer. Cer. Soc., 55, 7 (1972).

5. K W. Hansen, J Electrochem. Soc., **112**, 10 (1965).
6 A. Mansingh, J M Reyes and M. Sayer, J. Non-Crystalline Solids, **7**, 12 (1972)
7 I Ardelean et al., Studia Univ. Babeş-Bolyai, Phys , 1, 53 (1977).
8 I. Ardelean and I. Milea, Studii şi Cercetări de Fizică, 8 (1977).
9 E. Burzo and I. Ardelean, *International Conference on Mossbauer spectroscopy*, 5—10 *September, Bucharest*, 1977, p. 245.
10 I. Ardelean, E. Burzo and I Pop, Solid State Comm , **23**, 211 (1977).
11. L. Stănescu et al, Buletin Ştiinţific IPC, **5**, 65 (1962)
12. I. I. Kitaigorodskii and V. G Karpechenko, Steklo i Keramika, **15**, 8 (1958).

CONDUCTIBILITATEA ÎN CURENT CONTINUU A STICLELOR DIN SISTEMUL $xFe_2O_3 \cdot (1-x)\ [3B_2O_3 \cdot PbO]$

(Rezumat)

În această lucrare se prezintă conductibilitatea sticlelor din sistemul $xFe_2O_3 \cdot (1-x)\ [3B_2O_3 \cdot PbO]$, unde x variază între 2 şi 50% mol, în funcţie de temperatură, în domeniul de 300—700 K

Sticlele din acest sistem sînt semiconductoare. Ele conţin ionii metalului tranziţional în două stări de valenţă, Fe^{2+} şi Fe^{3+}, transportul de curent realizîndu-se prin electroni.

Conductibilitatea probelor creşte odată cu creşterea conţinutului de Fe_2O_3

La probe cu conţinut mai mare de 15% mol Fe_2O_3 se pun în evidenţă două energii de activare

STUDIA UNIV. BABEŞ—BOLYAI, PHYSICA, 1, 1978

COMPORTAREA MAGNETICĂ A COMPUŞILOR INTERMETALICI $Ho_2Fe_{17-x}Al_x$

GULÁCSI ZSOLT, MIRCEA POPESCU, ILIE RUS

1. **Introducere.** Compuşii intermetalici $Ho_2Fe_{17-x}Al_x$ ($x = 2; 3; 4$) cu structura de tipul Th_2Ni_{17} prezintă interesante proprietăţi fizice, o parte din ei constituind materiale ce se utilizează la confecţionarea magneţilor permanenţi. În acest sens au fost studiaţi şi compuşii pseudobinari $Ho_2Fe_{17-x}Al_x$, în care o parte din atomii de fier au fost substituiţi prin atomi netranziţionali, cum sînt cei de aluminiu. Scopul unor asemenea substituţii este determinat de posibilitatea virtuală de modificare a densităţii de stări electronice şi implicit a interacţiunii de schimb, prin mărirea distanţei dintre atomii elementelor de tranziţie din compuşi. Realizarea unei asemenea modificări, ar conduce la consecinţe cu largi implicaţii practice.

2. **Prepararea probelor şi metodica experimentală.** Compuşii intermetalici $Ho_2Fe_{17-x}Al_x$ ($x = 2, 3, 4$) au fost preparaţi din metale de înaltă puritate provenite de la firma Fluka, utilizîndu-se un cuptor cu inducţie, în atmosferă neutră de argon, prin metoda suportului de cupru răcit. Prepararea compuşilor s-a făcut în laboratorul Departamentului de Chimie de la Universitatea din Pittsburgh, prin amabilitatea profesorului W. E. Wallace.

Susceptibilitatea magnetică şi intensitatea de magnetizare s-au măsurat cu o balanţă de susceptibilităţi de tip Weiss-Forrer, avînd o sensibilitate de 10^{-8} cm³/g, între 100 şi 800 K

3. **Rezultate experimentale şi discuţii.** Dependenţa de temperatură a susceptibilităţii magnetice reciproce între 400 şi 800 K este redată în figura 1.

După cum se poate vedea, dependenţa de temperatură $\chi^{-1} = f(T)$ este neliniară şi poate fi descrisă prin legea lui Néel pentru comportarea substanţelor ferimagnetice în domeniul paramagnetic:

$$\frac{1}{\chi} = \frac{1}{\chi_0} + \frac{T}{C} - \frac{\sigma}{T-\theta}$$

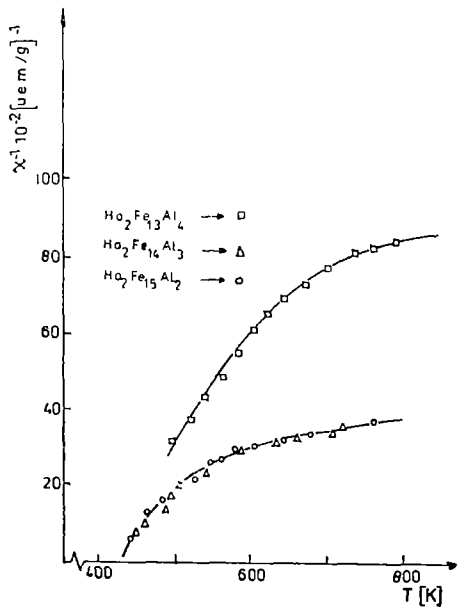

Fig. 1.

unde χ_0, σ şi θ sînt constante ce depind de coeficienţii cîmpului molecular, iar C constanta Curie-Weiss.

Valorile constantei Curie-Weiss determinate din curbele experimentale sînt redate în tabelul 1, în care mai sînt cuprinse şi valorile momentului magnetic efectiv, calculate din valorile constantei Curie-Weiss.

Tabel 1

Nr. crt.		$Ho_2Fe_{15}Al_2$	$Ho_2Fe_{14}Al_3$	$Ho_2Fe_{13}Al_4$
1	C $\frac{\text{T. gram}}{\text{u.e.m.}}$	0,3012	0,281	0,266
2	$\frac{\mu_{ef}}{\text{compus}} \cdot \mu_B$	54,47	52,05	50,03

Din tabel se constată o scădere sistematică a valorii momentului magnetic pe formula unitate a compusului, odată cu creşterea concentraţiei atomilor de aluminiu care substituie atomii de fier.

Dependenţa de temperatură a intensităţii de magnetizare în domeniul de ordine magnetică între 100 şi 500 K, la diverse intensităţi ale cîmpului magnetic pînă în apropierea cîmpului de saturaţie magnetică, este redată în figurile 2, 3 şi 4.

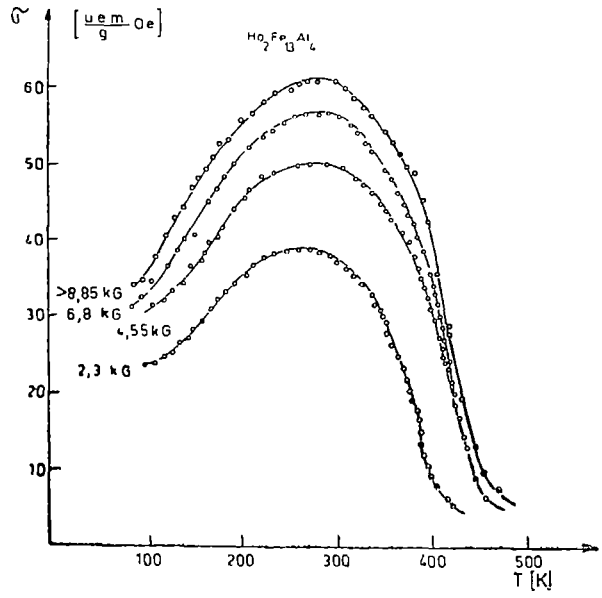

Fig. 2.

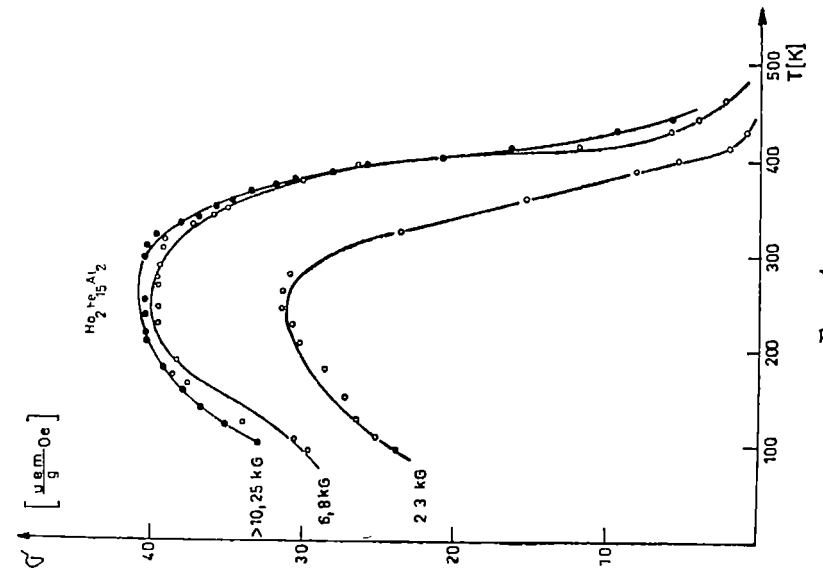
σ [μ g m Oe / g]
40
30
20
10
100
200
300
400
500
T[K]
>10,25 kG
6,8kG
2 3 kG
$Ho_2Fe_{15}Al_2$

Fig. 4.

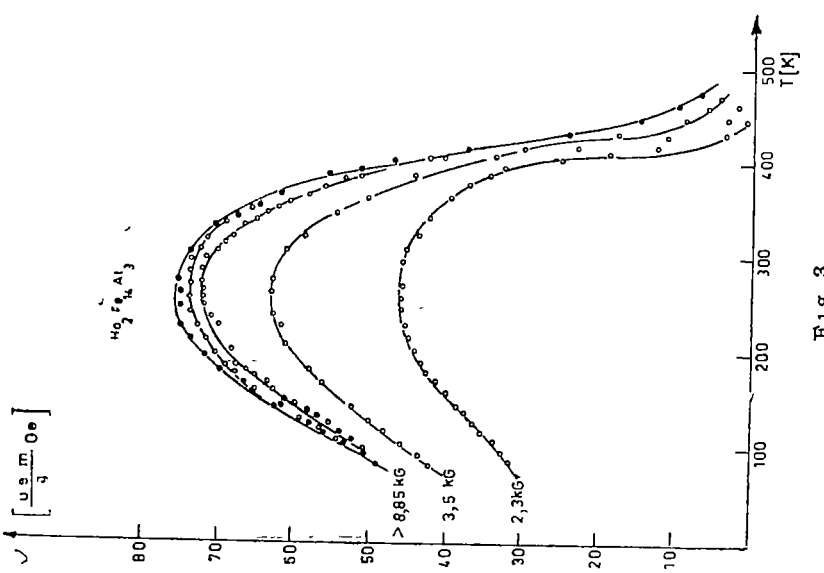
σ [μ g m Oe / g]
80
70
60
50
40
30
20
10
100
200
300
400
500
T[K]
> 8,85 kG
3,5 kG
2,3kG
$Ho_2Fe_{14}Al_3$

Fig 3.

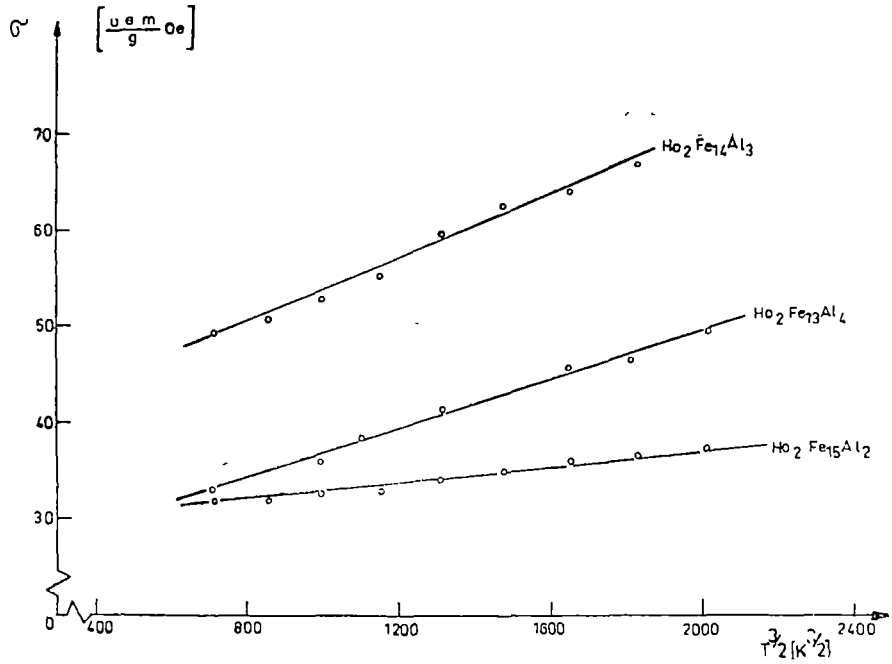
σ
[u e m / g Oe]
70
60
50
40
30
0
400
800
1200
1600
2000
2400
Ho2 Fe14 Al3
Ho2 Fe13 Al4
Ho2 Fe15 Al2
T2 [K2]

Fig 5.

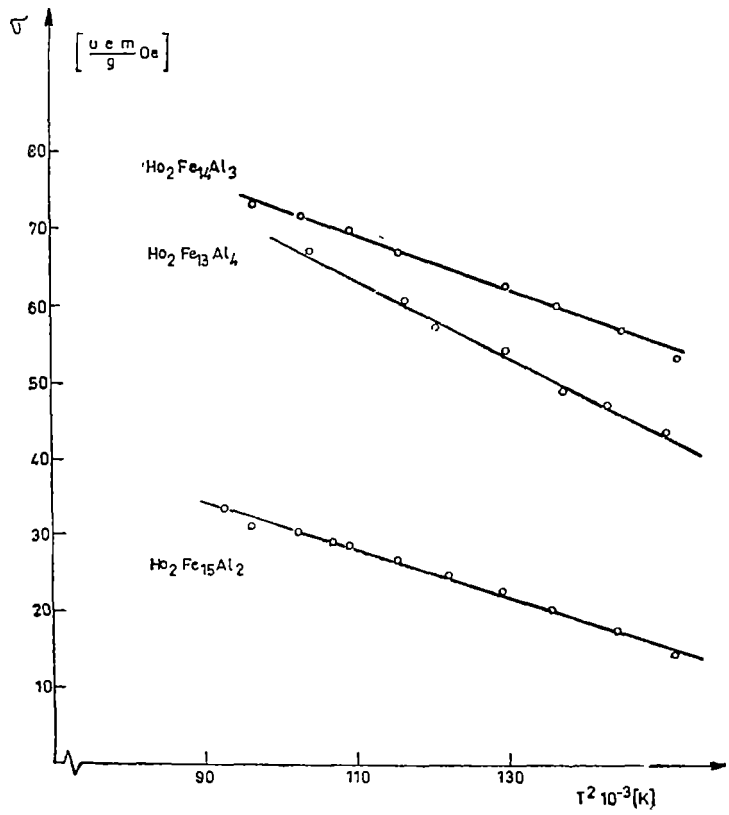
σ
[u e m / g Oe]
80
70
60
50
40
30
20
10
90
110
130
Ho2 Fe14 Al3
Ho2 Fe13 Al4
Ho2 Fe15 Al2
T2 10-3 [K]

Fig. 6.

Din figuri se constată o dependenţă specific ferimagnetică pentru compuşii studiaţi.

Pentru interpretarea curbelor experimentale au fost comparate, pe regiuni de temperatură, cu relaţiile teoretice de tipul: $\sigma = f(T^{3/2})$; $\sigma = f(T^2)$ şi $\sigma^2 = f(T)$, care reprezintă trei familii de drepte ce descriu corect rezultatele experimentale (fig. 5, 6, 7).

În prima regiune rezultatele sînt descrise prin modelul undelor de spin cu legea $T^{3/2}$ a lui Bloch. În regiunea a doua apare interacţiunea dintre undele de spin, care se descrie cu o lege pătratică de temperatură. În regiunea a treia, regiunea fenomenelor critice, descrierea se face cu o lege de forma: $\sigma = \text{const}\,(T^c - T)^{1/2}$. Aici are loc tranziţia de fază magnetică ferimagnetism-paramagnetism. Prin extrapolarea dreptelor pînă la inter-

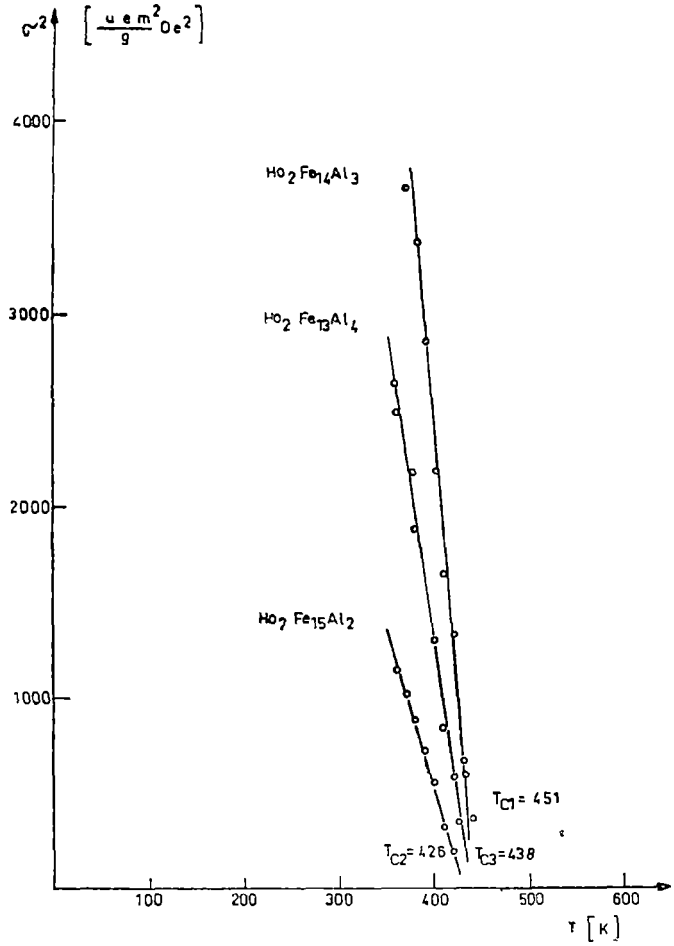

Fig 7.

secţia cu axa temperaturilor s-au obţinut valorile temperaturii critice T_c. Relaţiile de comparaţie a datelor experimentale sînt reprezentate în tabelul 2.

Tabel 2

Nr. crt.	Domeniul de temperatură, K	$\sigma = \sigma_{sat}(T)$
1	80—40	$\sigma = 40{,}5 + 0{,}013435\ T^{3/2}$
2	140—370	$\sigma = -0{,}000964\ T^2 + 0{,}4974\ T + 11{,}5328$
3	370—438	$\sigma = 157{,}8524\left(1 - \frac{T}{438}\right)^{1/2}$

În ipoteza că momentul magnetic al atomilor de pămînt rar se conservă prin aliere şi pe baza reprezentării teoretice a rezultatelor experimentale, s-a făcut analiza curbelor dependenţei de temperatură a intensităţii de magnetizare pe subreţele magnetice, pentru cazul compusului $Ho_2Fe_{14}Al_3$, aşa cum rezultă din figura 8.

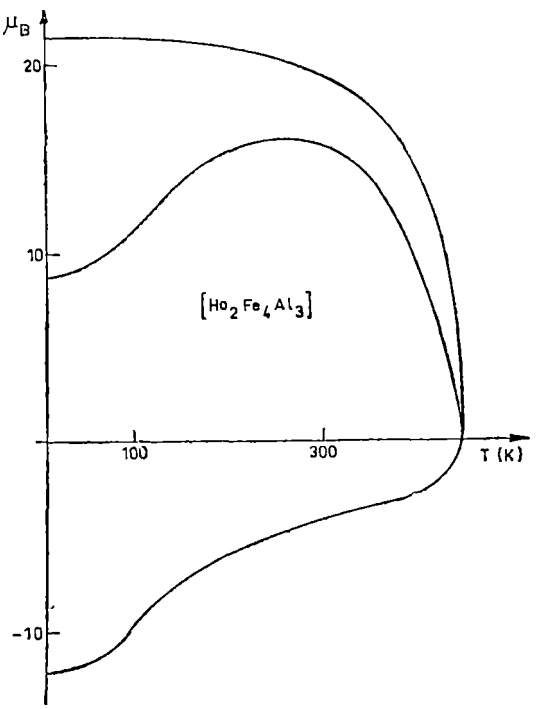

Fig. 8.

Relaţiile analitice pentru separarea intensităţii de magnetizare pe subreţele sînt redate în tabelul 3.

Tabel 3

T,K	Subreţea Ho	Subreţea Fe
80—140	$\sigma = 96{,}2 - 0{,}0124\ T^{3/2}$	$\sigma = 55{,}7 - 0{,}0258\ T^{3/2}$
140—370	$\sigma = -0{,}00076\ T^2 + 0{,}651T + 17{,}25$	$\sigma = 0{,}000204\ T^2 + 0{,}154\ T + 6{,}01$
370—438	$\sigma = 220{,}99 \left(1 - \frac{T}{438}\right)^{1/2}$	$\sigma = 63{,}14 \left(1 - \frac{T}{438}\right)^{1/2}$

Din extrapolarea curbelor experimentale pentru magnetizarea de saturaţie, la $T = 0$, s-au putut determina valorile momentului magnetic pe atom de fier, aşa cum este redat în tabelul 4.

Tabel 4

	$Ho_2Fe_1Al_2$	$Ho_2Fe_{14}Al_3$	$Ho_2Fe_{13}Al_4$
μ_{ef}, μ_B	0,99	0,92	1,02

În limita erorilor experimentale, mai mici de 10%, momentul magnetic păstrează o valoare aproximativ constantă, în jur de $1\mu_B$/Fe.

De aici rezultă că momentul magnetic al atomului de fier în compus este puternic afectat de prezenţa atomilor de aluminiu în reţea, mai cu seamă de către sistemul electronilor de conducţie.

Se constată de asemenea că efectul de substituţie prin atomi de aluminiu, care trebuie să mărească densitatea de stări electronice în banda de conducţie, constă în compensarea electronilor cu spinul necompensat din pătura „3d" a atomilor de fier.

*

Autorii sînt recunoscători prof. dr Iuliu Pop, lect. dr Mircea Crişan şi asist. dr Marin Coldea pentru propunerea temei, pentru indicaţiile şi discuţiile utile avute pe parcursul efectuării lucrării.

(Intrat în redacţie la 19 octombrie 1977)

BIBLIOGRAFIE

1. W. E. Wallace, *Rare Earth Intermetalics*, Academic Press, New York and London, 1973.
2. I. Pop, V. I. Cecernikov, Prib. i Tekh. Exper., 5, 180 (1964).

MAGNETIC BEHAVIOUR OF INTERMETALLIC COMPOUNDS $Ho_2Fe_{17-x}Al_x$

(S u m m a r y)

We have studied the magnetic behaviour of intermetallic compounds $Ho_2Fe_{17-x}Al_x$ ($x = 2, 3, 4$) in the 77—800 K temperature interval. The compounds have displayed a ferrimagnetic behaviour, the temperature dependency of magnetic susceptibility in the paramagnetic region being described by Néel law.

With respect to the magnetic order domain, the intensity of magnetization was compared in each of the three temperature regions with the following theoretical relationships $\sigma = f(T^{3/2})$, $\sigma = f(T^2)$, $\sigma^2 = f(T)$,

The experimental curves $\sigma = f(T)$ were also decomposed after the magnetization of undernetworks, assuming that the magnetic momentum of rare earth ions does not change under alloying conditions.

STUDIA UNIV BABEŞ—BOLYAI, PHYSICA, 1, 1978

STUDIUL DETERMINĂRII LITIULUI-6 PRIN METODA ACTIVĂRII INDIRECTE

T. FIAT şi L. DĂRĂBAN

1. **Introducere.** Pentru determinarea concentraţiilor izotopice de litiu-6 prin metoda transmisiei neutronilor termici sînt necesare cantităţi mari de probă [1]. O metodă mai avantajoasă ar fi cea a activării cu neutroni, deoarece activitatea indusă într-o probă în urma bombardării ei cu neutroni este proporţională şi cu abundenţa izotopului ţintă [2]. În cazul izotopilor litiului, litiul-6 nu se activează, dar litiul-7 se poate activa cu neutroni rapizi formînd în urma reacţiei $^{7}Li(n, \gamma)\ ^{8}Li$ un nucleu β^- activ cu $T_{1/2} = 0{,}84$ sec. Prin măsurarea radiaţiei β^- ($E_{max} = 13$ MeV) cu contoare Cerenkov [3—4] se poate determina ^{7}Li. Metoda nu prea este comodă din cauza perioadei de înjumătăţire foarte scurtă a nucleului de ^{8}Li.

Se pot produce, însă, nuclee radioactive în probe cu conţinut de ^{6}Li folosind produşii reacţiei:

$$^{6}Li + n = {}^{4}He + {}^{3}H + 4{,}80\ \text{MeV} \qquad (1)$$

şi în special tritonii cu energia de 2,74 MeV ca particule bombardante În literatură s-au studiat o serie de reacţii cu tritoni de acest fel [5—8]. Pentru determinarea litiului-6, pînă în prezent nu s-au folosit decît două reacţii: $^{18}O(t, \alpha)\ ^{17}N$ [9], unde se măsoară neutronul emişi de nucleul ^{17}N cu $T_{1/2} = 4{,}14$ sec şi ^{16}O (t, n) ^{18}F[10—17] în care se măsoară radiaţia gama de anihilare a pozitronilor emişi de nucleul ^{18}F cu $T_{1/2} = 112$ min Ultima reacţie este cea mai convenabilă din cauza secţiunii eficace foarte mari a reacţiei cu tritoni, de 0,5 barni [6], şi uşurinţei pregătirii probelor în care ^{6}Li trebuie să fie în contact intim cu $^{16}O(Li_2CO_3$ sau soluţii cu $H_2O)$.

La activarea cu particule încărcate, pe măsură ce acestea pătrund în probă, ele îşi micşorează energia datorită frînării, astfel încît secţiunea eficace a reacţiei ^{16}O (t, n) ^{18}F depinde de energia tritonilor în momentul impactului cu nucleul de ^{16}O. Funcţia $\sigma(E)$ se numeşte funcţia de excitare şi este reprezentată printr-o curbă de excitare [18—19]. O astfel de curbă nu poate fi obţinută sub o formă analitică ci se determină experimental pe baza unor etaloane Astfel, metoda activării indirecte primeşte un caracter relativ.

2. **Partea experimentală.** S-a urmărit aplicarea metodei la determinarea abundenţei de ^{6}Li din materia primă ce se vehiculează în instalaţiile de separare şi la determinarea unor impurităţi din probe prin activare cu neutroni.

Probele sub formă de Li_2CO_3 şi soluţii apoase cu LiCl în cantitate de 5 ml au fost închise ermetic în capsule cilindrice de polietilenă cu dimensiunea de 20 × 35 mm Iradierea s-a efectuat la reactorul nuclear de la

IFA-București în condiții de perfectă etanșeitate a capsulelor, timp de 43 ore, la un flux de neutroni termici $\Phi_n = 4 \cdot 10^9$ n/s.cm^2.

Ținînd cont de perioada de înjumătățire a ^{18}F, se observă că activarea indusă a fost la saturație.

După un timp de răcire de 2 ore s-au făcut măsurătorile pe un spectrometru gama echipat cu un detector Ge(Li) de tip 722X coaxial, cu un volum de 36 cm^3 și o rezoluție de 3,5 KeV. Eficiența maximă pentru picul de 1,33 MeV, la o distanță sursă-detector de 25 cm, era de 20%. În final, se obțin datele calculate referitoare la suprafața picului de 511 KeV, energiile celorlalte picuri precum și reprezentarea grafică a spectrului.

3. **Rezultate și concluzii.** S-au comparat abundențele naturale de ^6Li pentru două tipuri de carbonați de litiu și trei tipuri de cloruri de litiu din surse diferite, pe baza activității picului de anihilare, care este proporțională cu suprafața lui. S-au identificat impurități de Mn și Na în Li_2CO_3 livrat de firma Merck (fig. 1) și Br, Ca, Na, K în Li_2CO_3 de un alt tip (fig. 2).

În figura 3 se reprezintă spectrul gama al apei potabile cu ajutorul căreia s-au preparat soluțiile de LiCl.

S-au identificat de asemenea Ba, I, Mn, Na într-un tip de clorură (fig. 4) Mn, Ca, I, Na într-o clorură comercială de tip reactiv chimic pur (fig. 5) și I, Mn, Na în alt tip de clorură de litiu (fig. 6).

Se observă reacția nucleară de activare a clorului $^{37}Cl(n, \gamma)^{38}Cl$ și o substanțială activitate pe picul de anihilare datorată litiului-6.

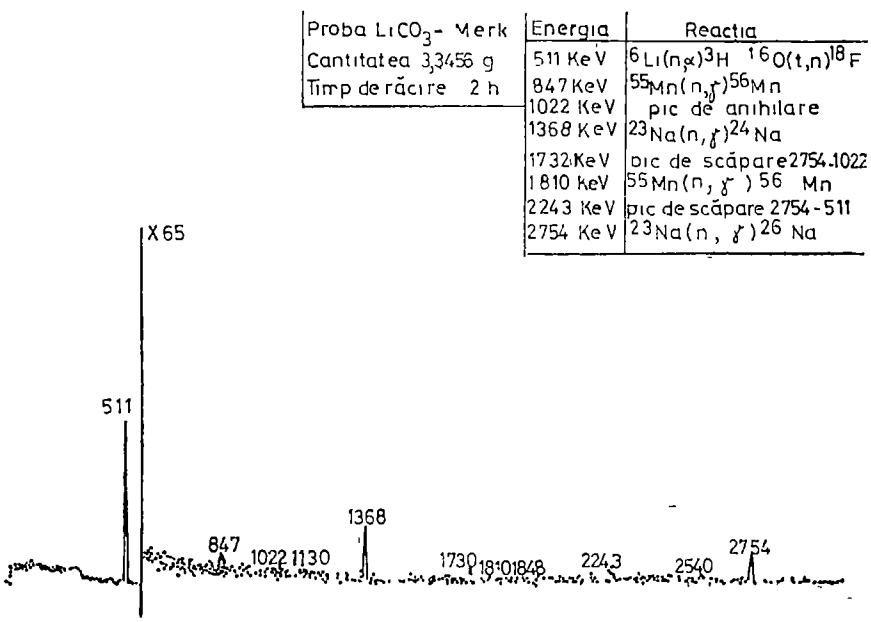

Fig. 1.

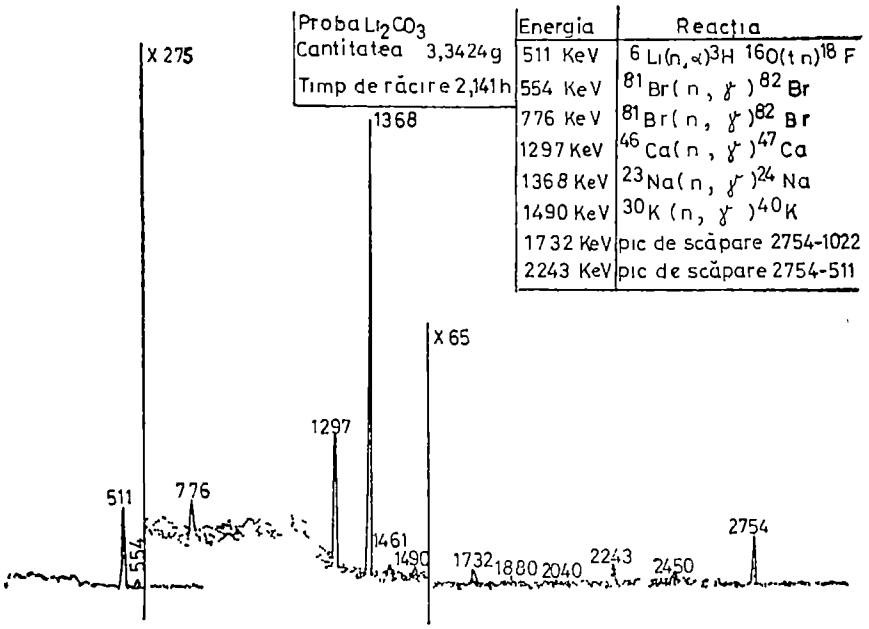

Energia	Reacția
511 KeV	$^6Li(n,\alpha)^3H$ $^{16}O(t,n)^{18}F$
554 KeV	$^{81}Br(n,\gamma)^{82}Br$
776 KeV	$^{81}Br(n,\gamma)^{82}Br$
1297 KeV	$^{46}Ca(n,\gamma)^{47}Ca$
1368 KeV	$^{23}Na(n,\gamma)^{24}Na$
1490 KeV	$^{30}K(n,\gamma)^{40}K$
1732 KeV	pic de scăpare 2754-1022
2243 KeV	pic de scăpare 2754-511

Fig. 2.

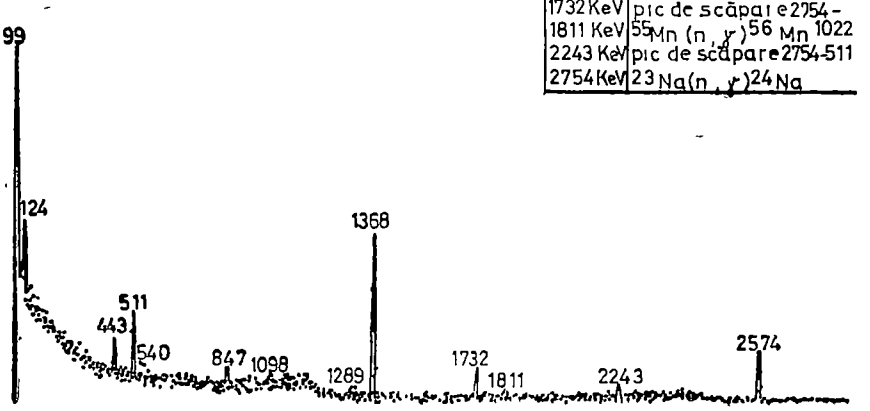

Energia	Reacția
124 KeV	$^{130}Ba(n,\gamma)^{131}Ba$
443 KeV	$^{127}I(n,\gamma)^{128}I$
511 KeV	pic de anihilare ^{24}Na
540 KeV	$^{127}I(n,\gamma)^{128}I$
847 KeV	$^{55}Mn(n,\gamma)^{56}Mn$
1368 KeV	$^{23}Na(n,\gamma)^{24}Na$
1732 KeV	pic de scăpare 2754-1022
1811 KeV	$^{55}Mn(n,\gamma)^{56}Mn$
2243 KeV	pic de scăpare 2754-511
2754 KeV	$^{23}Na(n,\gamma)^{24}Na$

Fig. 3.

Proba soluție LiCl
Cantitatea 5 ml, 2g LiCl / 40 ml H_2O
Timp de răcire 2,366 ore

Energia	Reacția
124 KeV	$^{130}Ba(n,\gamma)^{131}Ba$
216 KeV	$^{130}Ba(n,\gamma)^{131}Ba$
442 KeV	$^{127}I(n,\gamma)^{128}I$
511 KeV	$^{6}Li(n,\gamma)^{3}H$ $^{16}O(t,\gamma)^{18}F$
540 KeV	$^{127}I(n,\gamma)^{128}I$
847 KeV	$^{55}Mn(n,\gamma)^{56}Mn$
1368 KeV	$^{23}Na(n,\gamma)^{24}Na$
1642 KeV	$^{37}Cl(n,\gamma)^{38}Cl$
1732 KeV	pic de scăpare 2751-1022
2166 KeV	$^{37}Cl(n,\gamma)^{38}Cl$
2240 KeV	pic de scăpare 2754-511
2754 KeV	$^{23}Na(n,\gamma)^{24}Na$

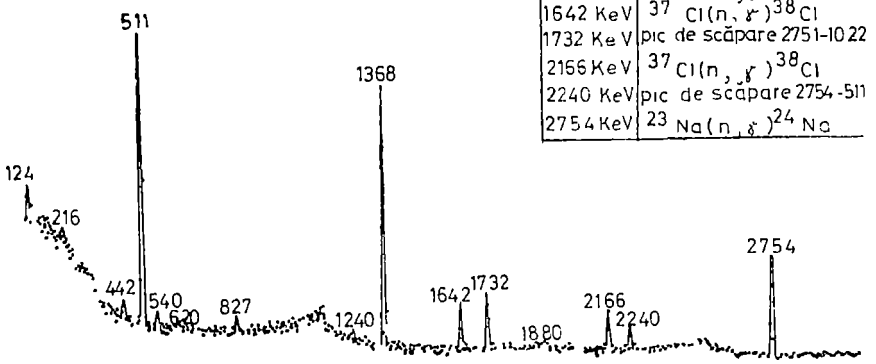

Fig 4

Proba soluție LiCl-reactiv chimic
Cantitatea 5 ml, 2g LiCl / 40 ml H_2O
Timp de iacire 3,5 ore

Energia	Reacția
443 KeV	$^{127}I(n,\gamma)^{128}I$
511 KeV	$^{6}Li(n,\gamma)^{3}H$ $^{16}O(t,\gamma)^{18}F$
847 KeV	$^{55}Mn(n,\gamma)^{56}Mn$
1297 KeV	$^{46}Ca(n,\gamma)^{47}Ca$
1368 KeV	$^{23}Na(n,\gamma)^{24}Na$
1642 KeV	$^{37}Cl(n,\gamma)^{38}Cl$
1732 KeV	pic de scăpare 2754-1022
2166 KeV	$^{37}Cl(n,\gamma)^{38}Cl$
2243 KeV	pic de scăpare 2754-511
2754 KeV	$^{23}Na(n,\gamma)^{24}Na$

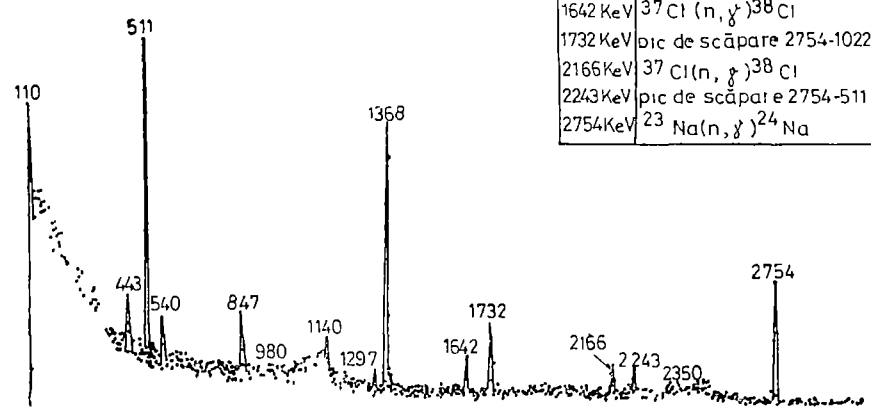

Fig 5.

Proba soluție LiCl Cantitatea 5 ml Timp de răcire 4,066 ore	Energia	Reacția
	443 KeV	$^{127}I(n,\gamma)^{128}I$
	511 KeV	$^{6}Li(n,\alpha)^{3}H$ $^{16}O(t,n)^{18}F$
	540 KeV	$^{127}I(n,\gamma)^{128}I$
	847 KeV	$^{55}Mn(n,\gamma)^{56}Mn$
	1368 KeV	$^{23}Na(n,\gamma)^{24}Na$
	1649 KeV	$^{37}Cl(n,\gamma)^{38}Cl$
	1732 KeV	pic de scăpare 2754-1022
	1810 KeV	$^{55}Mn(n,\gamma)^{56}Mn$
	2167 KeV	$^{37}Cl(n,\gamma)^{38}Cl$
	2243 KeV	pic de scăpare 2754-511
	2754 KeV	$^{23}Na(n,\gamma)^{24}Na$

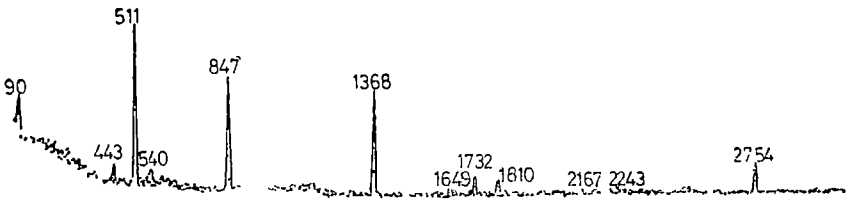

Fig. 6

Contribuția la picul de anihilare datorată ^{24}Na s-a estimat din activitatea picurilor de scăpare ca fiind de ordinul 60, ceea ce față de activități pe fotopic de ordinul 20 000—40 000 devine neînsemnată O altă interferență ar putea proveni de la reacția $^{18}O(p, n)\ ^{18}F$, care se produce cu protoni de recul în soluțiile apoase. Contribuția acestei reacții este neglijabilă ținînd cont că secțiunea eficace de formare a ^{18}F în apă prin iradiere cu neutroni este egală cu 0,1 mb și aceasta numai pentru o energie a neutronilor care lovesc protonii mai mare de 3,7 MeV [18], fiind vorba despre o reacție cu prag. Această metodă prezintă mari avantaje pentru cantități mici de litiu. La concentrații mari de ^{6}Li, curba de etalonare se abate de la liniaritate din cauza efectului de autoecranare [4, 19] Metoda este nedestructivă, cantitatea de ^{6}Li consumat în urma unor iradieri repetate fiind foarte mică [4], are specificitate izotopică absolută și este foarte sensibilă (cantitatea limită detectabilă de ^{6}Li fiind de $1{,}5 \cdot 10^{-3}$%). De asemenea, metoda se poate adapta la determinarea oxigenului pînă la urme de $7 \cdot 10^{-9}$ grame și la măsurarea unor straturi subțiri de oxizi.

*

Autorii mulțumesc prof dr doc V. Mercea și conf dr F Koch pentru sprijinul acordat la alcătuirea acestei lucrări

(Intrat în redacție la 19 octombrie 1977)

BIBLIOGRAFIE

1 T. Fiat, L. Dărăban, Studia Univ Babeş-Bolyai, Phys., 50 (1976).
2 J. Perdijon, *L'Analyse par activation*, Masson et C., Paris, 1967, p. 7.
3. H. R. Lukens, J Radional Chem., **1**, 4, 349 (1968)
4. M Wiernik, S Amiel, J Radioanal Chem., **5**, 1, 123 (1970).
5. E. Iwerson, W. S. Koski, F Rasetti, Phys Rev., **91**, 1229 (1953).
6. R Sher, J. J Floyd, Phys Rev, **102**, 242 (1956)
7. K Jantsch, Kernenergie, **4**, 846 (1961), **9**, 127 (1966); **9**, 348 (1966)
8. A K Valter et al, J èksp teor fiz, **40**, 1237 (1961)
9 S. Amiel, J Welwart, Analyt Chem, **35**, 4, 566 (1963)
10. L P Bilibin, A. A Lbov, I I. Naumova, At. Energ, **10**, 528 (1961).
11. R F. Bailey, D. A Ross, Analyt Chem, **35**, 7, 791 (1963).
12. H J Born, Angew. Chem, **72**, 559 (1960).
13 S S. Markowitz, P. D Mahohy, Analyt Chem., **34**, 329 (1962).
14. A G. Dutov, et al, Izv. Akad Uzb SSR, ser Fiz. mat. nauk., **6**, 76 (1966)
15 H. J. Born, P. Wilkniss, Intern J. Appl Rad and Isotopes, **10**, 133 (1961)
16 H. O. Banks, Jr., Nucleonics, **13**, 12, 62 (1955)
17 V F. Stepanenko et al, *Activationîi analiz a narodnom hoziaistve*, Izd „FAN", Uzb SSR, Taşkent, 1974, p. 109
18 H. L. Born, D C. Auman, Naturwiss., **51**, N7 (1964)
19. P. F. Zweifel, Nucleonics, **18**, 174 (1960).

THE LITHIUM-6 DETERMINATION STUDY BY INDIRECT ACTIVATION METHOD

(Summary)

A method for ^{6}Li isotopic concentrations determination by indirect activation according to the nuclear reactions $^{6}Li(n,\alpha)^{3}H$, $^{16}O(t, n)^{18}F$, is given

The authors also make an identification of the impurities from samples using the neutron activation analysis

STUDIA UNIV BABEŞ—BOLYAI, PHYSICA, 1, 1978

NOTE

IMAGE OF SOME RADIOACTIVE GRANULES WITH SOLID-STATE TRACK DETECTORS

F. KOCH

The track detectors or dielectric detectors are used for the study of the heavy particles, such as the α — particles or the fission fragments. P. B Price and R. M. Walker found already in 1962, [1], [2] that mica is suitable to record the fission fragments, then R. L. Fleischer realised how to use plastics for this and published a summary article in 1965 [4]. Recently the problem of studying some radioactive granules with this method appeared to determine the geological ages and the supposed new elements from halos. [5], [9]. G. M. Schmidt-Burbach determined with another method [6] that in the dosimetric problems at the particles with an activity of $3 \cdot 10^{-9}$ Ci and at a distance of 1 μm it appears a dose of 10^4 r/h. Investigations of this type were performed in Bucharest [8]. The general study of granules is in [7].

The following records represent the image of some U granules of 1—5mg (activity 10^{-10}Ci, 10^{18} atoms) and their fission fragment in the 2π geometry.

In figure 1 we represent the tracks of the α particles on celulose nitrat after an exposure of a day. It can be clearly seen that many particles reach the plate after a diffusion in air and therefore the form of the granules can't be distinguished

Figure 2 contains fission tracks on mica after a developing of 6—7 hours in HF of 40%. One can see the characteristic tomb tracks of the

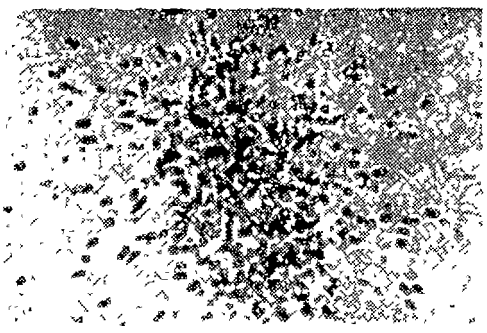

Fig. 1.

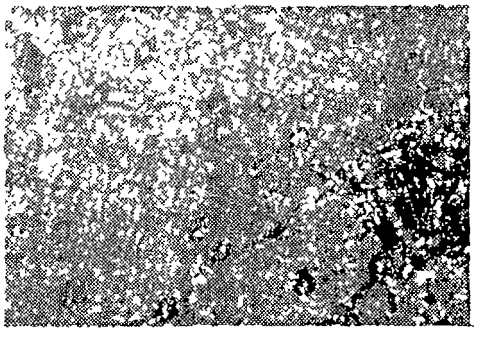

Fig. 2.

Fig 3

fragments. With an Am-Be neutron source of a 10^3n/cm^{2}s flux, after 2 days about 200 tracks appeared.

The track's study concludes the following : by an α decay and by the fission may appear the tearing off of some radioactive fragments from the granules, caused by the recoil effects in α-emission or by the pulverisation given by the fission fragments. In 2π geometry measurements it is possible that the effective mass of fission fragment involved in track detector and so the energy distribution between the two fragments is changed and this influences the detection probability. Anyway, it won't appear rings around the circular granules yet.

We found some rings in plastic track detectors (noticed by Biró T.) around some α-tracks (Fig. 3).

(Received January 29, 1977)

REFERENCES

1 P B Price, R M Walker, Phys Rev Letters, **8,** 217 (1962)
2 P B Price, R. M Walker, J Appl. Phys , **33,** 3407 (1962)
3 R L. Fleischer P. B , Price Science, **140,** 1221 (1963)
4. R L. Fleischer, P B Price R. M Walker, Ann Rev Nucl , Sc , **1,** (1965).
5 R V Gentry, T. A Cahill, et al , Phys. Rev Letters, **37,** 11 (1976)
6 G M Schmidt-Burbach, *Doctoral thesis*, Univ of Frankfurt/Main, 1969
7 N Pilpel, Endeavour, **XXX,** 77 (1971).
8 M Oncescu, Rev Roum Phys , **18,** 789 (1973)
9. F. Bosch, El Goresy, W Kratschmer, B Martin, B Povh, Phys. Rev Lett **37,** 1515, (1976).

IMAGINEA UNOR GRANULE RADIOACTIVE ÎNREGISTRATE CU DETECTORI DE CORP SOLID.

(Rezumat)

Radiaţiile α, precum şi fragmentele de frînare se înregistrează în jurul unor fragmente, granule radioactive, cu detectori S S N T D Cercetarea urmelor permite să observăm acţiunea aerului înconjurător, desprinderea unor aglomerări de substanţe de pe granule, rezultînd astfel un contur mult mai şters decît cel geometric.

STUDIA UNIV. BABEŞ—BOLYAI, PHYSICA, 1, 1978

STUDIU RES AL $(NH_4)_3AlF_6 : Ca$

O. COZAR, GH. ILONCA

Una dintre metodele de obţinere a centrilor paramagnetici este aceea a dopării unei substanţe cu ioni diferiţi de cei ai reţelei proprii [1]. În cazul de faţă se urmăreşte apariţia unor centrii paramagnetici în $(NH_4)_3AlF_6$ prin dopare cu ioni de Ca^{2+}.

Spectrul RES obţinut la temperatura camerei pe probe sub formă de pulbere constă din 7 linii, cele extreme fiind foarte slab rezolvate(fig. 1). Despicarea dintre liniile centrale este de 23,5 gauss, valoare comparabilă cu cea obţinută pentru despicările superhiperfine datorate nucleelor de fluor în cazul centrilor paramagnetici H_i^0 din $CaF_2 \cdot H$ [2]

Valoarea factorului g este de 2,0039. Întrucît aceasta este mai mare decît pentru electronul liber (2,0023), putem considera că avem de a face cu un centru paramagnetic format prin captare de goluri. Ionii Al^{3+} sînt substituiţi de Ca^{2+}, care pentru păstrarea neutralităţii locale captează un gol pozitiv. Prin interacţiunea acestuia cu cele şase nuclee de fluor echivalente $\left(I_F = \frac{1}{2}\right)$ rezultă 7 linii $(2nI + 1)$ de structură superhiperfină.

Hamiltonianul de spin caracteristic poate fi scris sub forma [3].

$$\hat{\mathcal{H}}_s = g\beta\vec{B} \cdot \vec{S} + \sum_\alpha \vec{I}_\alpha (a_\alpha + b_\alpha)\vec{S} \qquad (1)$$

unde a_α reprezintă interacţiunea izotropă de contact Fermi cu nucleele de fluor, iar b_α cea de tip dipolar.

D o y l e [4] a arătat că în astfel de cazuri se obţine o structură superhiperfină bine rezolvată atunci cînd constanta de interacţie a_α a primului strat de coordinaţie este mare în comparaţie cu toate celelalte constante de interacţie superhiperfină.

Deoarece spectrul obţinut (fig. 1) este bine rezolvat, considerăm că interacţia dipolară b_α poate fi neglijată. Cu aceasta, valorile proprii ale energiei sînt:

$$E = g\beta B m_s + m_s \sum_\alpha M_{I_\alpha} \cdot a_\alpha \qquad (2)$$

Dacă ţinem cont de regulile de selecţie pe care le satisfac tranziţiile RES, adică $\Delta m_s = \pm 1$ şi $\Delta M_I = 0$, obţinem următorul set de frecvenţe:

$$h\nu = g\beta B + \sum_\alpha M_{I_\alpha} \cdot a_\alpha \qquad (3)$$

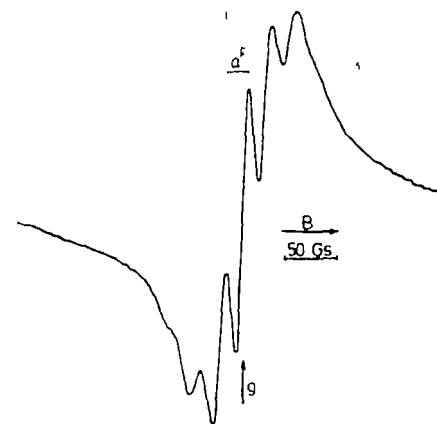

Fig 1 Spectrul R.E.S al $(NH_4)_3AlF_6$. Ca la temperatura camerei.

Folosind valorile experimentale a_α, putem calcula densitatea de probabilitate $|\Phi(0)|^2$ la nucleele de flour, după relaţia [3]:

$$a_\alpha = \frac{8\pi}{3} g\beta g_{I_\alpha}\beta_n |\Phi(0)|^2 \tag{4}$$

Se obţine astfel $|\Phi(0)|^2 = 0{,}10$ (Å^{-3}), ceea ce indică o localizare relativ mare a golului captat de ionul Ca^{2+}. Aceasta este comparabilă cu localizarea electronilor captaţi la formarea centrilor F din fluorurile alcaline NaF şi KF, unde s-a obţinut pentru $|\Phi(0)|^2$ valoarea 0,16 [4] şi respectiv 0,06 [5]. Ţinînd cont de aceste date, în cazul nostru rezultă o distanţă interatomică Ca—F de $\simeq$ 3,5 Å.

Probele au fost preparate la Center for Materials Research, Stanford University, California, S.U.A.

(Intrat în redacţie la 26 iulie 1977)

BIBLIOGRAFIE

1 C. Nicolau şi colab., *Rezonanţă electronică paramagnetică*, Ed. tehnică, Bucureşti, 1966.
2 Al. Nicula, O Cozar, Studia Univ. Babeş-Bolyai., ser. Phys., 2, 35 (1971).
3. J. Arends, Phys Stat. Solidi, **7**, 805 (1964).
4. W. T. Doyle, Phys. Rev., **131**, 555 (1963).
5. H. Seidel, Z. Phys., **165**, 218 (1961).

E.S.R. STUDY OF $(NH_4)_3AlF_6$ Ca

(Summary)

A paramagnetic center, due to a hole trapped at Ca^{2+} ion is presented. The probability density at the nearest-neighbour F^- nuclei is found to be about 0.10.

Întreprinderea Poligrafică Cluj, Municipiul Cluj-Napoca cd. 670/1978

În cel de al XXIII-lea an (1978) *Studia Universitatis Babeş—Bolyai* apare semestrial în specialităţile:

matematică

fizică

chimie

geologie—geografie

biologie

filosofie

ştiinţe economice

ştiinţe juridice

istorie

filologie

На XXIII году издания (1978) *Studia Universitatis Babeş—Bolyai* выходит два раза в год со следующими специальностями:

математика

физика

химия

геология—география

биология

философия

экономические науки

юридические науки

история

филология

Dans sa XXIII-e année (1978) *Studia Universitatis Babeş—Bolyai* paraît semestriellement dans les spécialités:

mathématiques

physique

chimie

géologie—géographie

biologie

philosophie

sciences économiques

sciences juridiques

histoire

philologie

Abonamentele se fac la oficiile poştale, prin factorii poştali şi prin difuzorii de presă, iar pentru străinătate prin ILEXIM, Departamentul Export-Import Presă, P.O. Box 136—137 telex 11226, Bucureşti, str. 13 Decembrie nr. 3

Lei 10